香港氣象學會

HONG KONG METEOROLOGICAL SOCIETY

Bulletin

Volume 17, 2007
ISSN 1024-4468

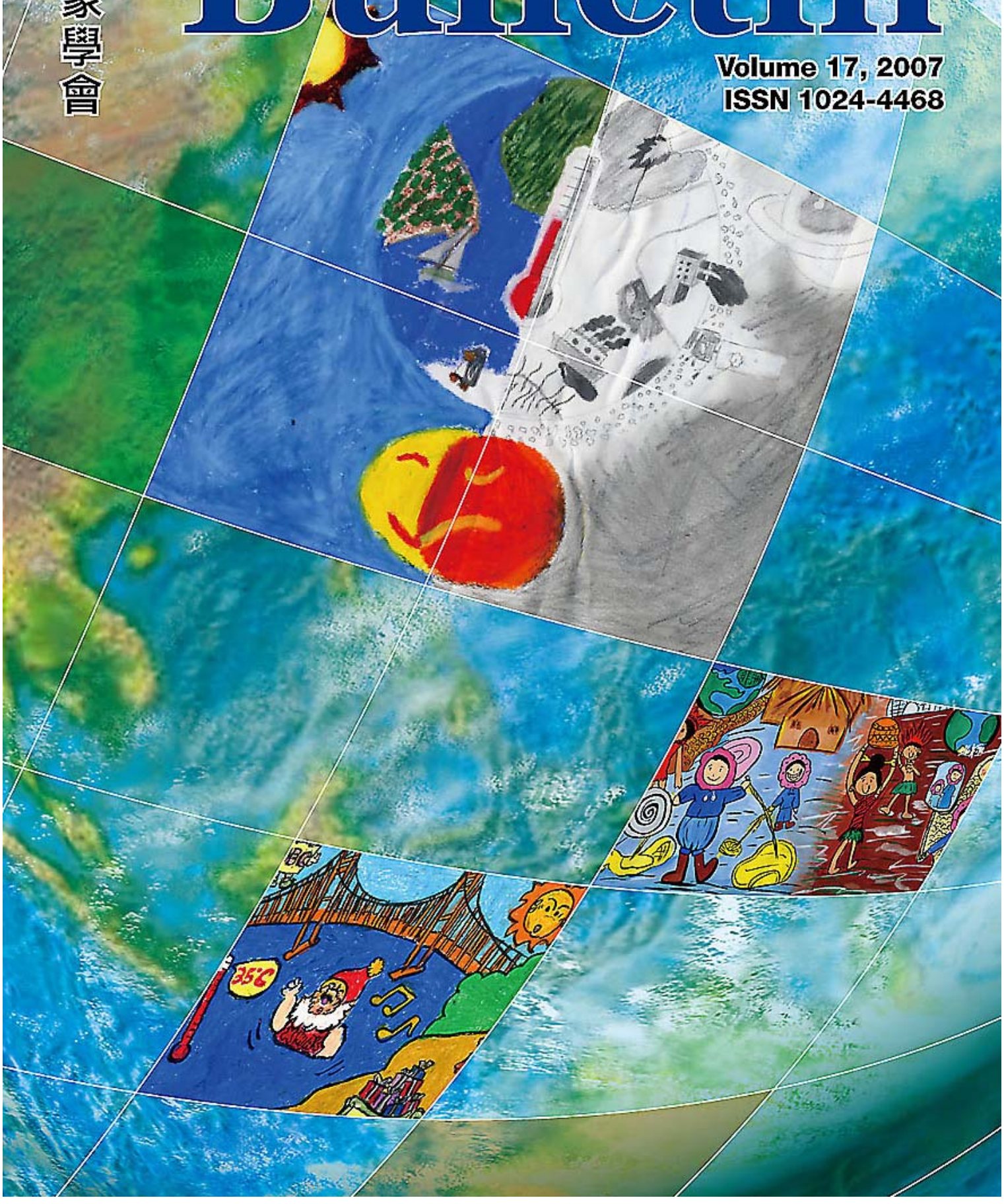

ISSN 1024-4468

The Hong Kong Meteorological Society Bulletin is the official organ of the Society, devoted to articles, editorials, news and views, activities and announcements of the Society.

Members are encouraged to send any articles, media items or information for publication in the Bulletin. For guidance see the information for contributors in the inside back cover.

Advertisements for products and/or services of interest to members of the Society are accepted for publication in the BULLETIN.

For information on formats and rates please contact the Society secretary at the address opposite.

Views and opinions expressed in the articles or any correspondence are those of the author(s) alone and do not necessarily represent the views and opinions of the Society.

The mention of specific products and/or companies does not imply there is any endorsement by the Society or its office bearers in preference to others which are not so mentioned.

SUBSCRIPTION RATES

Institutional rate:	HK$ 300 per volume
Individual rate:	HK$ 150 per volume

Published by

The Hong Kong Meteorological Society
c/o Hong Kong Observatory
134A Nathan Road
Kowloon, Hong Kong

Homepage
http:www.meteorology.org.hk/index.htm

Contents

Editorial

In recent years, the general public is paying more and more attention to climate change issues. Our Society also contributes by hosting various activities like painting and web page design competitions and public lectures to introduce the topic to the general public. These form features in the current issue of the Society Bulletin. We also have three papers in this issue related to climate change.

The first paper by Prof. Lau Ngar-Cheung describes the essence of the scientific findings of Intergovernmental Panel on Climate Change (IPCC) Fourth Assessment Report. The Chinese version of this article was published in the "Twenty-First Century" journal of the Chinese University. The second paper by Y.K. Leung, M.C. Wu, K.K. Yeung and W.M. Leung of the Hong Kong Observatory was also related to IPCC report and gives details on temperature projections in Hong Kong. The third paper by M.C. Wu, K.H. Yeung and Y.K. Leung of the Observatory attempts to find out changes in the East Asian winter atmospheric circulation against the background of global warming. The fourth paper by C.K. Ho, J.K.W. Chan and K.C. Tsui and the fifth paper by L.S. Lee and M.Y. Leung, all from the Observatory, explains respectively solar radiation trends and ultraviolet index of Hong Kong. The sixth and seventh papers are also from the Observatory – C.C. Lam introduces the characteristics of the Southeast Monsoon in Hong Kong while P.W. Chan and C.M. Shun talk about visibility at the Hong Kong International Airport. The eighth paper by Dr. Mickey Man-Kui Wai is the last of a sequel about the Tropical Cyclone Warning Systems in Hong Kong.

Scientific Basis of Climate Change

LAU NGAR-CHEUNG, Geophysical Fluid Dynamics Laboratory/NOAA, Princeton University Princeton, New Jersey USA

Prologue

Our awareness of possible human impacts on the earth's climate system dates back to the early 19th century. In 1827, the renowned French mathematician Jean-Baptiste Fourier recognized that the atmosphere acts like a 'glass vessel' by trapping heat energy derived from sunlight. This idea later evolved into the concept of 'greenhouse effect' as the principal cause for global warming. The marked increase in the burning of fossil fuels (mainly coal and petroleum) since the Industrial Revolution has led to emissions of large amounts of carbon dioxide (CO2) to the atmosphere. In 1896, the Swedish chemist Svante Arrhenius first noted that the rising level of this gas could warm our climate. Systematic efforts to monitor the atmospheric concentration of CO2 and various indicators of the global environment (such as temperature, precipitation, ice cover, etc.) were launched in the 20th century. The emerging scientific evidence has caused sufficient concern that the Massachusetts Institute of Technology (MIT) sponsored a month-long study in the summer of 1970. More than forty eminent scientists and professionals contributed their knowledge on the emission rates, pathways and global impacts of various pollutants[1].

1. The IPCC Process

Through coordinated international efforts, our understanding of the earth's climate system and the potential impacts of human activities has expanded tremendously since the MIT study. The series of assessments performed by the Intergovernmental Panel on Climate Change (IPCC) represent the most comprehensive and authoritative synthesis of our knowledge of these issues. The IPCC was established in 1988 by the United Nations (UN) Environment Programme and the World Meteorological Organization. The task of this body is to provide the world community with objective and transparent advice on the technical and societal dimensions of climate change. This panel consists of three working groups, which are devoted to scientific information, socio-economic impacts, and formulation of response or mitigation strategies. The IPCC does not conduct research on its own, but its participants are actively engaged in a broad range of climate-related investigations at their home institutions. At intervals of 5-6 years, the IPCC has published four successive assessment reports, in 1990, 1995, 2001 and 2007. Vigorous procedures have been established for the preparation of these documents. The individual chapters were drafted by teams of experts familiar with the subject matter. These preliminary versions were subjected to a two-stage review, firstly by other experts, and secondly by both experts and governments. The final reports were accepted at plenary sessions attended by the contributing authors and government representatives. These participants also scrutinized every word in the Summary for Policymakers, before approving it for public release.

The IPCC assessment reports, which comprise contributions from each of the working groups, represent major milestones in international cooperation to address global issues related to climate change. The findings of the first assessment report served as the basis for negotiating the UN Framework Convention on Climate Change (UNFCCC), which was opened for signature at the 1992

[1] The findings of this study have been summarized in the document *Man's Impact on the Global Environment: Assessment and Recommendations for Action.* Report of the Study of Critical Environmental Problems. MIT Press, 1970.

UN Conference on Environment and Development in Rio de Janeiro. The second assessment report provided the impetus for the Kyoto Protocol, which was negotiated in 1997 and commits the signatory nations to specific targets of reductions in their emissions of CO2 and other greenhouse gases. The updated information in the third assessment report has been used on a routine basis by the annual Conference of Parties to the UNFCCC.

The fourth assessment report (AR4) of IPCC by working groups I, II and III was released in February (Paris), April (Brussels), and May (Bangkok) of 2007, respectively. This state-of-the-art exposition of our knowledge of climate change is the product of the broadest collaborations within the research community thus far. As an illustration of the immensity of the efforts involved, the report of working group I (WGI, on physical science basis) was jointly written by 150 lead authors and 450 contributing authors, who were nominated by 40 governments. The drafts of these authors were examined by more than 600 reviewers, who submitted 30,000 comments. Every comment has been addressed by the authors to the reviewer's satisfaction. Finally, the precise wording of the Summary for Policymakers was debated and polished by 300 representatives from 113 countries.

The full AR4 report of WGI is a voluminous document with a total length of almost a thousand pages. Its 11 chapters cover the full range of scientific issues pertaining to climate change. An attempt is made in this short article to summarize those findings that are of most interest to the readership of the Bulletin. Specifically, this overview is mainly concerned with the increasing levels of atmospheric constituents that have climatic implications, observed changes in different components of the climate system, efforts aimed at linking these changes to human activities, and projections of future climate changes based on the output from an ensemble of model simulations. All numerical data cited here are extracted from the AR4 report of WGI. Readers who wish to explore the pertinent issues in greater depth are urged to refer to the original AR4 documents[2].

2. Anthropogenic Drivers of Climate Change

The fundamental physical principles of the greenhouse effect and its role in climate change are rather simple. In brief, our planet receives its energy from the sun, which emits most of its radiation in the visible portion of the light spectrum. In order to achieve a state of equilibrium, this solar input is balanced by the emission of light energy from the earth back to space. This energy loss from the earth is mostly attained by radiation in the 'infrared' portion of the spectrum, due to its much lower temperature as compared to the sun. Certain gaseous species in the earth's atmosphere act differently on the visible and infrared radiation: they are transparent to the incoming visible sunlight, but intercept the outgoing infrared rays and re-emit them back to the earth's surface. Hence these atmospheric constituents serve a function analogous to that of the glass casing of a greenhouse (as noted by Fourier), which allows the sunshine to warm its interior, but prevents the escape of energy from that structure through blockage of heat transfer to the ambient environment. It is therefore anticipated that increased loading of the 'greenhouse gases' in the earth's atmosphere will lead to rising temperatures in a globally averaged sense. Although this basic mechanism is well understood, active research continues on many aspects of the consequences of greenhouse warming. The scientific community still faces formidable challenges in its attempts to quantify the details of greenhouse responses in various geographical regions. These difficulties are primarily linked to the complexity of highly interactive processes operating in our climate system. Such interactions occur on various time and space scales in the atmosphere, ocean, cryosphere (e.g., continental and sea ice),

[2] The entirety of the IPCC AR4 report of WGI, including the Summary for Policymakers, Technical Summary and the 11 individual chapters, can be viewed at, or downloaded from, the electronic website http://www.ipcc.ch

and land surface (e.g., vegetation cover, groundwater storage, river discharge), as well as within the hydrological cycle (e.g., cloud formation and precipitation).

The most important greenhouse gases of anthropogenic origin are CO2, methane and nitrous oxide. The variations of atmospheric concentrations of these gases during the past 2000 years are summarized in Fig. C1-1 (COLOUR PLATES). The primary sources of CO2 are consumption of fossil fuel [amounting to 6.4 billion metric tons of carbon (GtC) per year in the 1990s and 7.2 GtC per year in 2000-2005] and land use change due to deforestation and biomass burning (about 1.6 GtC per year in the 1990s). These inputs are accompanied by an increase of the global atmospheric CO2 concentration from the pre-industrial (circa 1750) level of 280 parts per million (ppm) to the 2005 level of 379 ppm, which far exceeds the range of natural variability over the past 650,000 years (180-330 ppm), as estimated from ice-core records. The contemporary rate of CO2 increase is 1.9 ppm per year. The dominant human sources of methane are agricultural activities and use of fossil fuel, which contribute to the observed rise in concentration of this gas from the pre-industrial level of 715 parts per billion (ppb) to 1774 ppb in 2005, which also stands far beyond the range of natural fluctuations (320-790 ppb). The anthropogenic origin of nitrous oxide, mostly associated with agricultural practices, contributes to about one-third of the observed increase in the atmospheric level of this gas from the pre-industrial value of 270 ppb to 319 ppb in 2005. In addition to the three gases noted above, tropospheric ozone (which results from emissions of nitrogen oxides and carbon monoxide, and their subsequent chemical transformations) and various halocarbons (mostly found in industrial solvents, refrigerants and plastics) are also known to have warming effects on the earth's climate.

The AR4 report has published quantitative measures of the radiative effects of different greenhouse gases, so as to facilitate assessments of their relative importance. These 'impact factors' are formulated in terms of the time rate of perturbed energy flow through a surface of unit area due to the presence of a given atmospheric constituent at the concentration level detected in 2005. Such comparisons indicate that the CO2 is the strongest contributor to greenhouse warming, with an impact factor of 1.66 watts per square meter. This effect is comparable to the warmth felt by a person standing at a distance of about 1.5 m from a 40-watt electric light bulb. The warming effect of CO2 may also be contrasted with the total direct energy flow rate from the overhead sun, which has a much larger magnitude of 1380 watts per square meter. The corresponding magnitudes of the warming due to methane, nitrous oxide, tropospheric ozone and halocarbons are 29, 10, 21 and 20% of the CO2 impact as cited above.

In addition to the emission of various greenhouse gases, human activities have also led to the injection of increasingly large amounts of particulate matter into the atmosphere. These substances, which exist in solid, liquid, or mixed solid-liquid forms, are sufficiently light to be suspended in air, and are collectively referred to as 'aerosols'. Their main ingredients are sulfates, nitrates, various forms of carbon, and dust. The notable increase in the frequency of hazy skies in many population centers of the world (including Hong Kong) during recent years may largely be attributable to elevated levels of these atmospheric aerosols. Such trace constituents influence the climate system in multiple ways. Their most direct effect is to reflect a larger portion of the incoming sunlight back to space, thus reducing the amount of solar energy arriving at the earth's surface, and thereby lowering its temperature. Hence this cooling effect partially offsets the temperature increase due to the greenhouse gases. It is estimated that the magnitude of the aerosol-induced direct cooling is about 30% of the warming associated with CO2. The aerosols also participate in nucleation processes that lead to cloud formation. Increased aerosol levels could enhance the reflectivity of clouds, which

results in additional cooling of the earth's surface. This indirect effect could cancel about 42% of the warming associated with CO2. The magnitudes of both the direct and indirect aerosol effects are still subject to large uncertainties.

3. Observed Climate Changes in the Recent Past

Painstaking efforts have been made to reconstruct the recent climate history of the earth. These investigations are hampered by many obstacles. Most components of the climate system (the atmosphere and ocean in particular) exhibit a high degree of internal (or 'natural') variability, which is present even when no changes in external conditions are applied. The turbulent behavior of these subsystems introduces a substantial level of noise to the climate records, thus leading to considerable difficulties in detecting various response signals of interest. The amplitude of such background noise is particularly high when climate variations over smaller geographical regions are considered. Moreover, the observational networks for monitoring past climate changes is far from ideal, with prominent data gaps in both space and time. Such inhomogeneities in data coverage complicate the estimation of many standard indicators of climate change, which often entail the computation of averages over large spatial domains (e.g., a certain continent, ocean basin, or the entire globe) during extended periods of time (e.g., a century or longer). Changes in measurement techniques (e.g., thermometer readings versus temperatures inferred from satellite platforms) also lead to artificial discontinuities in the data records, which can only be partially resolved through careful cross-calibrations among different instruments.

Notwithstanding the afore-mentioned challenges, much progress has been made in documenting the evolution of critical climate indices based on the existing observational records. Of particular note are the following long-term trends:

- The globally averaged surface temperature has increased by 0.74°C during the 1906-2005 period. The warming trend has undergone noticeable acceleration in the course of the 20th century, with the trend value for the last 50 years being double that for the entire century (see Fig. C1-2 in COLOUR PLATES). Among the 12 years in the most recent period (1995-2006), 11 years rank among the warmest years in the instrumental temperature record commencing in 1850. Similar warming rates are detected during recent decades in the atmospheric layer extending to several kilometers above the earth's surface. Warming has also occurred within the global oceans, with rising temperatures being observed at depths of at least 3000 m.

- The extent of snow and ice cover in land regions, including mountain glaciers and ice caps, has decreased. Losses from the ice sheets of Greenland and Antarctica through increased ice flow to the oceans and excessive melting have been detected.

- The global sea level has risen by 0.17 m during the 20th century. This rising trend has noticeably accelerated during the 1993-2003 period. Within that decade, thermal expansion of sea water due to increasing temperatures accounts for 57% of the sea level rise, whereas the contributions from melting glaciers/ice caps and from the Greenland/Antarctica ice sheets are 28 and 15%, respectively.

On the basis of this observational evidence, as well as their mutual consistency, the AR4 report characterizes the recent warming of the climate system as 'unequivocal'. These findings are further buttressed by comparing the above instrumental climate records with indicators of the climate history dating back to the more distant past. The latter information has been inferred from proxy data such as

tree-ring widths and ice cores. Such paleoclimatic studies suggest that the warmth of the past half century exceeds any other 50-year period in at least the past 1300 years. During the last prominent warm period about 125,000 years ago, the 3-5°C temperature increase over the polar regions was accompanied by a global sea level rise of 4-6 m, with the Greenland ice sheet and other Arctic ice fields contributing to no more than 4 m of that signal.

Besides the global measures described above, the following climate changes on smaller regional scales are also noteworthy:

- Warming of the Arctic basin has proceeded at a rate which is two times that of the global average. Since 1974, the sea ice extent in this region has shrunk at a rate of 7.4% per decade during the summer season. In the past two decades, the temperature of the permafrost layer (long-lasting frozen soil) in this region has risen by as much as 3°C. The enhanced warming in high-latitude regions is in part the consequence of a positive feedback loop: greenhouse warming accelerates the melting of ice and snow; removal of the snow or ice cover leads to reduction in the degree of reflectivity of the land and ocean surface; the increased absorption of the incoming solar radiation results in still further warming, thus reinforcing the original perturbation that initiated this chain of processes, and amplifying the changes in subsequent iterations of the loop .

- Century-long precipitation trends have been observed in many regions. Of special interest to the readers of the *Bulletin* are the increased precipitation over parts of northern and central Asia, and decreased precipitation over parts of southern Asia. Droughts with stronger severity and longer duration have occurred in the past three decades, especially in the tropical and subtropical zones. Frequency of heavy precipitation events has increased over land areas. These secular precipitation changes are accompanied by perturbations of wind patterns, which are in turn linked to altered surface conditions of the oceans and continents in response to rising levels of greenhouse gases and aerosols.

- In association with the general rising temperature trend, extremely hot episodes (such as prolonged heat waves) have become more frequent, whereas cold events have become less frequent.

- Observational evidence indicates an increase in activities of intense tropical cyclones (hurricanes and typhoons) over the North Atlantic in recent decades. This enhanced degree of storminess is coincident with rising sea surface temperature. The resulting increases in evaporation and water vapor content in the atmosphere lead to stronger latent heat release in the tropical convective zones, thereby promoting the formation and growth of cyclones.

4. Attribution of the Recent Climate Changes to Anthropogenic Causes

The extent to which the myriad signals of climate change in the recent past may be attributed to anthropogenic emissions of greenhouse gases and aerosols has been investigated extensively. A valuable tool in such studies are the climate models developed at various participating institutions, including research centers in China, Japan and Korea. In essence, these models are very complex computer algorithms incorporating the physical laws and mathematical equations that govern the mechanisms operating in, and interactions among, various components of the climate system. They provide simulations of a large variety of phenomena and processes, such as atmospheric and oceanic motions, flow of radiative energy at different wavelengths, cloud cover and precipitation, energy and

momentum transfers at air-sea and air-land interfaces, vegetation, ground hydrology, and dynamics of land and sea ice. Some of the more comprehensive models encompass the exchange and transport of trace constituents in various atmospheric, hydrospheric and biospheric reservoirs. Marching (or 'integrating') these models forward in time yield detailed information on the three-dimensional structure of an extensive suite of physical variables (including winds and ocean currents, temperature, pressure, atmospheric humidity, oceanic salinity, etc.), with typical grid spacings of 50-500 km and 1 km in the horizontal and vertical directions, respectively, and on the temporal development of these fields, at intervals of minutes or hours. The speed and memory requirements of the more advanced climate models can only be accommodated by some of the most powerful electronic computers in the world. In spite of the tremendous resources invested in the development of these models, there is still considerable room for improvement in the simulation of various facets of the climate system. Model-based findings must therefore be interpreted with such imperfections in mind.

Since the model settings could be adjusted at will to correspond to various climate 'scenarios' with specified levels of greenhouse gases and aerosols, these models are well suited for a wide range of studies on climate change. Two suites of model experiments are especially relevant to the identification of causes for the observed climate change. These integrations extend from the early 20th century to the present. In the course of both experiments, the year-to-year variations of certain sets of conditions are prescribed. For the first suite, only the influences (or 'forcings') due to naturally occurring processes are considered. The time sequence of such forcings primarily reflects the variations of two principal drivers of natural variability as observed during the past century: solar activity and volcanic eruptions. Changes in energy input to the climate system from the sun are modulated mostly by the sunspot cycle and fluctuations in the earth's orbit around the sun. Sporadic volcanic eruptions at varying sites lead to injections of dust particles to the atmosphere, which reflect more sunlight back to space, thus resulting in cooling at the earth's surface. The second suite of experiments entails the insertion of conditions with both natural and human origins in the climate models. The anthropogenic forcings are deduced from the progression of estimated atmospheric loadings of greenhouse gases and aerosols during the past 100 years (e.g., see Fig. C1-1). This pair of experimental designs has been implemented using different climate models. For some of the models, the suite of integrations is repeated several times by initiating the integrations with distinct sets of conditions, but subjecting the models to the identical sequence of forcings. Ensemble averages over the output from these multiple, independent realizations allow for a more reliable assessment of the sensitivity of individual models to climate forcings.

Time series of the range of model responses in surface temperature to natural forcings only, and to the sum of natural and anthropogenic forcings, are shown using blue and red shaded bands, respectively, in Fig. C1-3 (COLOUR PLATES). The black curves in the individual panels indicate the corresponding observed temperature variations. Results are displayed for each of the continents except Antarctica. It is apparent from Fig. C1-3 that, for all continental sites considered here, none of the model simulations subjected to natural forcings only (see blue bands) is capable of reproducing the observed warming trends since the mid-20th century. On the other hand, the observational data (black curves) lie well within the envelope of model responses to the combination of natural and anthropogenic forcings (see red bands). These results hence offer convincing evidence on the crucial role of human activities in the warming trend as observed in recent decades. Analogous comparisons between the simulations for 'natural only' and 'natural plus anthropogenic' forcings have also been performed for other climate indices besides surface temperature. This exercise indicates that the observed changes in oceanic temperature, sea level, frequency of extreme precipitation and temperature episodes, wind patterns, and tropical cyclone activity are to varying degrees attributable

to human influences. Model experiments have also been conducted to assess the contributions of greenhouse gases and aerosols separately. These additional integrations confirm that the warming effects of greenhouse gases are partially offset by the cooling due to aerosols. Furthermore, detailed diagnoses of the output from these or other experiments have enhanced our scientific understanding of the physical mechanisms linking various forcings to specific climate responses.

5. Projections of Future Climate Changes

The computer models used in retrospective simulations of the climate of the past century (see previous section) may also be deployed as a prediction tool for making projections of climate changes in the future. In the latter application, the climate models are initiated at near-present conditions, and are marched through the 21st century and beyond. In the course of such experiments, the time evolution of the atmospheric levels of greenhouse gases and aerosols are set according to different emission 'storylines' or 'scenarios'. These scenarios are constructed using various assumptions on future economic development, population pattern, relative mix of fossil and non-fossil energy uses, and degree of convergence among regions in economic structures and environmental policies. Results for the following three scenarios will be highlighted:

- B1 ('low'): rapid change toward a service and information economy; with global population peaking in mid-21st century, and declining thereafter; emphasis on global solutions to socio-economic and environmental sustainability; introduction of clean and resource efficient technologies; equivalent CO2 concentration in 2100 is estimated at 600 ppm.

- A1B ('balanced'): rapid economic growth; same population trends as B1; increased cultural and socio-economic convergence among regions; balanced mix of usage of fossil and non-fossil fuels; equivalent CO2 level in 2100 is about 850 ppm.

- A2 ('high'): regionally oriented and fragmented economic and technological development; continuously increasing population; emphasis on self reliance and preservation of local identities; equivalent CO2 loading reaches 1250 ppm in 2100.

The reliability of the model projections is dependent on the accuracy of forcings associated with these scenarios. The lack of measurements of the initial (i.e., present-day) conditions of some slowly-varying components of the climate system (e.g., ocean, land and cryosphere), as well as deficiencies of the model themselves, also introduce uncertainties to the model projections. Notwithstanding these obstacles, model projections made in the previous three IPCC assessments for the period from 1990 to present are in general agreement with the observational data that have become available after the projections were made. This verification exercise enhances the credibility of the projections for the near future.

Projections of the various global measures of climate changes, as deduced from multiple simulations using a large number of participating models, may be summarized as follows:

- The total increase in globally averaged surface temperature during the 21st century is estimated to be 1.8, 2.8 and 3.4°C for the B1, A1B and A2 scenarios, respectively (see blue, green and red curves in Fig. C1-4 in COLOUR PLATES). During the next two decades, the warming trend is about 0.2°C per decade for all scenarios. Even if the anthropogenic forcings were held fixed at the levels in year 2000, the temperature rise would still proceed at a rate of about 0.1°C per decade in the coming two decades (see orange curve in Fig. C1-4), due

mainly to the slow response of the oceans. If the forcings were stabilized in year 2100 at the B1 or A1B levels, a further warming of about 0.5°C would still occur by year 2200 (see green and blue curves for time periods beyond 2100).

- The projected total rise in sea level in the 21st century lies within the ranges of 0.18-0.38, 0.21-0.48 and 0.23-0.51 m for the B1, A1B and A2 scenarios, respectively. If anthropogenic forcings were stabilized at the A1B levels in 2100, thermal expansion of seawater would continue due to slow penetration of heat to the deep ocean. This delayed effect could lead to a further rise of sea level by 0.3-0.8 m by 2300. Complete elimination of the Greenland ice sheet after a long period of sustained warming could result in an additional sea level rise of about 7 m. An elevation of sea level of that magnitude will inundate many low-lying areas along the eastern and southern coasts of China, including those neighboring the population centers of Hong Kong-Guangzhou, Shanghai and Tienjin.

- Due to the long lifetime of CO2 in the atmosphere (as much as 200 years), and the slowness of oceanic responses to the greenhouse effect, the rises in temperature and sea level due to both past and future human emissions of CO2 will be sustained for longer than a millennium from present.

Beyond the global averages quoted above, the model experiments also provide data on the geographical distributions of the projected changes. The patterns of increases in the surface temperature during the decades of 2020-2029 and 2090-2099, as estimated by averaging the output from several models based on the B1, A1B and A2 scenarios, are displayed in Fig. C1-5 (COLOUR PLATES). The general character of the patterns for various scenarios is similar to each other. It is evident from the charts for the 2090-2099 era that the amplitude of the model responses increases progressively from the 'low' scenario B1 to the 'balanced' and 'high' scenarios A1B and A2. Due to the larger heat capacity of seawater as compared to land surfaces, the temperature rise over continents is noticeably higher than that over oceans. The most acute warming is projected over the Arctic region and the high-latitude zones of Eurasia and North America, primarily due to the positive feedback chain linking greenhouse warming, ice- and snow-melt, decrease in surface reflectivity, and increase in absorption of sunlight (see Section 3). The weak warming over the Southern Ocean and parts of the North Atlantic is due to the special structure of the oceanic circulation in those regions, which is conducive to conditions that tend to oppose greenhouse-induced warming. Time series of projected temperature change in various continents for the 2001-2050 period of the A1B scenario are also shown in Fig. C1-3 (see yellow bands). The projected trends over all six continents clearly rise above the estimated level of variability due to natural causes (indicated by green bars).

The projections shown in Fig. C1-5 indicate a warming of 2-4°C over most parts of China by the end of the 21st century. An appreciation of the climatic impacts in this region may be gained by comparing the current climatological data for various Chinese cities. With a temperature rise of the magnitude as cited above, the annual mean temperature in Qingdao a century from now will be approximately equal to that in present-day Shanghai. Analogously, the future summertime temperature in Harbin will approach that in contemporary Beijing; whereas winters in Fuzhou will be similar to those in today's Guangzhou.

The patterns of the anticipated precipitation change during the 21st century for the December-January-February and June-July-August seasons, as obtained from averages of the output from several models for the A1B scenario, are illustrated in Fig. C1-6 (COLOUR PLATES). Stippling indicates those features for which different models exhibit strong agreement. A majority of

the models project increased precipitation in high-latitudes by 10% or more. This response is partly due to the poleward shifts in the strong eastward wind belt and in the trajectories of extratropical storms, and to enhanced warming in these regions (see Fig. C1-5), which allows the local air masses to hold more water vapor. Also evident in Fig. C1-6 are the narrow zone of positive rainfall changes near the equator, and broader belts of reduced precipitation over the subtropics of both hemispheres. These features may be related to alterations in the intensity and spatial extent of large-scale atmospheric circulation cells over these regions in response to greenhouse warming. The most noteworthy signal in the Chinese sector is the precipitation increase over northern China, especially during the winter season.

In addition to the temperature and precipitation changes highlighted in Figs. C1-5 and C1-6, the models also project further contraction of snow cover, continued shrinking of the sea ice in both the Arctic and the Antarctic (to such an extent that Arctic sea ice may disappear completely during late summer at the end of this century), still more frequent events of extreme high temperatures and precipitation amounts, and increased intensity of tropical cyclones.

The model projections indicate that, as our climate warms, the uptake of atmospheric CO2 by the oceanic and land reservoirs is reduced. As a result, a larger fraction of the emitted CO2 will stay in the atmosphere. It is estimated that this feedback between climate change and the earth's carbon cycle could lead to an additional warming of more than 1°C by 2100.

Climate scientists have long been concerned with the future course of a massive oceanic circulation loop in the Atlantic basin. Historical climate records suggest that variations in the intensity of this current system could be accompanied by abrupt climate changes in different parts of the globe. It has been speculated that greenhouse warming could reduce the northward flow of warm waters near the surface of the North Atlantic, thereby leading to cooling of northern Europe and parts of the Arctic basin. Model projections performed for the AR4 report indicate that the slowing-down of the Atlantic circulation loop in the 21st century will be rather modest (by about 25%), and the attendant cooling tendencies will be more than compensated by the general warming trend due to the greenhouse effect.

6. Certainties and Unknowns

Comparison between the findings presented in AR4 and the previous three IPCC reports reveals that substantial progress has been achieved in our scientific understanding and prediction capability of climate change. Such advances are made possible by the availability of more extensive observational and model-generated datasets, more incisive diagnoses and intercomparisons of the information contained therein, improved model simulations of the pertinent processes, and more definitive measures of the reliability of the projected climate changes based on the range of responses in multiple models. These developments have led to increased confidence in some of the conclusions highlighted in AR4, and in some of the quantitative estimates of past and future climate changes. For instance, the report is *virtually certain* (i.e., with more than 95% probability of being correct) that the warming trend will continue in the 21st century, and that the observed global climate change of the past 50 years cannot be solely attributed to natural forcings. It also claims with a *very high degree of confidence* or regards as *very likely* (i.e., with more than 90% probability of being correct) the following results:

- The observed temperature rise since the mid-20th century is due to observed increase of greenhouse gas emissions from human activities. The projected warming and other changes in

the climate system in the 21st century will be larger than those observed in the 20th century.

- In the post-1960 era, frequency of cold days and nights has decreased, whereas frequency of warm days and nights have increased. Frequency of warm spells and heat waves is projected to increase in the 21st century.

- Frequency of heavy precipitation events over most areas, as well as total precipitation amounts in high-latitude zones, are projected to increase in the 21st century.

- Losses from the Greenland and Antarctica ice sheets have contributed to the rise of sea level during 1993-2003.

Despite the considerable expansion of our scientific knowledge of climate change, large uncertainties remain in several aspects of this complex problem. More accurate and reliable assessments in the future will depend on progress along the following avenues of research:

- The magnitudes and spatial distribution of the cooling due to direct and indirect effects of aerosols (see Section 2) are still poorly known. The estimated upper bound of globally averaged cooling is larger than the lower bound by a factor of 9 and 6 for the direct and indirect (related to cloud reflectivity) effects, respectively. These broad ranges of the possible climate responses to aerosol forcing reflect our limited understanding of the interactions between aerosols, radiative transfer and various cloud processes.

- Our understanding is still lacking on the impacts of greenhouse warming on various cloud-related characteristics (e.g., cloud type, altitudes of cloud top and cloud base, reflectivity and absorptivity of radiative energy, form and intensity of precipitation, etc.) in different geographical locations, and the manner in which the cloud and precipitation changes are coupled with the ambient atmospheric circulation.

- The nature of the processes contributing to the surface mass balance of land ice, as well as the dynamical mechanisms related to ice flow, are critical for projecting the future states of the Greenland and Antarctic ice sheets, which in turn have a strong impact on the magnitude of sea level changes.

- The need for information on regional details of climate change calls for continued efforts to understand and project climate responses to various forcings on small spatial scales. Such efforts entail a fuller understanding of the interactions between the climate processes on a local context, and experimentation with climate models with increasing spatial resolution.

- The implications of climate change on the statistical behavior of weather phenomena (such as the distribution of probability of events in various categories of severity) at different locations need to be assessed in greater detail. Such investigations provide information on the shifts in frequency and intensity of extreme weather episodes (e.g., floods, dry spells, heat waves, severe tropical storms) associated with climate change, which have stronger socio-economic consequences than shifts in the longer-term averages (e.g., monthly and seasonal means).

Epilogue

The much greater breadth and depth of the IPCC assessment reports, as compared with the MIT

study mentioned at the beginning of this article, is testimony to the maturation of climate science during the past several decades. Such scientific advances have greatly heightened the awareness of human impacts on our environment, to the extent that global climate change issues are now brought to the forefront of the political agendas of world governments. The notion that human-induced climate change is one of the most critical issues facing humanity in the 21st century has gained increasing acceptance. In recognition of the efforts of IPCC to disseminate the knowledge on climate change, this panel was named as a co-recipient of the 2007 Nobel Peace Prize.

The excitement and potency of various climate issues, as conveyed in the comprehensive and thorough IPCC documents, will hopefully motivate more scientists to join in this effort. In view of the strong cross-disciplinary nature of this field, preparations of these future climate scientists necessitate educational infrastructures that span across traditional academic boundaries. The global nature of various climate issues also requires the nurturing of broad world views and a strong spirit of international cooperation among the scientists in this endeavor.

It is worth noting that, in order to ensure freshness and independence of the findings and viewpoints expressed in the report of WGI of AR4, three quarters of it 150 lead authors have not been involved in the preparation of previous reports, and one-third of them received their last academic degree within the past decade. In effect, the torch of climate change research has been passed to a younger generation of scientists. There is much optimism that, when the time comes to compile the fifth assessment report, probably in about 2013, yet another cohort of even younger and well-trained climate scientists will step up to the challenge of presenting to the world the best possible assessment of the current and future course of the Earth's climate system.

Acknowledgment

The Chinese version of this article has appeared in the August 2007 issue of the Twenty-First Century Bimonthly, published by the Institute of Chinese Studies, Chinese University of Hong Kong. Permission by the editors of the above journal to publish this paper in its present form is gratefully acknowledged.

Temperature projections in Hong Kong based on IPCC Fourth Assessment Report

Y.K. Leung, M.C. Wu, K.K. Yeung and W.M. Leung, Hong Kong Observatory, Hong Kong, China

1. Background

In the past several years, the Hong Kong Observatory (HKO) has carried out a series of studies on climate change in Hong Kong. One such study is on temperature projections based on the projections made in the Intergovernmental Panel on Climate Change (IPCC) Third Assessment Report (AR3) (IPCC, 2001). Since then, new methodologies, new models, expanded data sets, and new findings have emerged. These are reflected in the IPCC Fourth Assessment Report (AR4) published in 2007 (IPCC, 2007).

In view of the new assessment in AR4, the temperature projections in Hong Kong need to be revised. As urbanization also contributes to the rise in Hong Kong's temperature, the re-assessment will also take into account this effect. This paper outlines the methodology and presents some salient results.

2. Data and Methodology

2.1 Data

In IPCC AR4, the Special Report on the 6 Emission Scenarios (SRES) for greenhouse gas employed in IPCC AR3 is still adopted. The 6 scenarios from low to high emission are B1, A1T, B2, A1B, A2 and A1FI (Fig. C2-1 in COLOUR PLATES). Higher resolution and more sophisticated global climate models are developed since IPCC AR3. 16 (7 in AR3) gridded model temperature data for 3 scenarios, viz. B1, A1B and A2 (6 in AR3) are available from AR4 (Table 2-1). Unlike AR3, maximum and minimum temperatures of most models as well as the gridded data of the remaining 3 scenarios, viz. A1T, B2 and A1FI, are not available on the internet for public access in AR4.

2.2 Methodology

Fig. C2-2 (COLOUR PLATES) shows the schematic diagram for the methodology. In essence, the projected temperature utilises the forecasts of global climate models forced with different greenhouse gas emission scenarios. The global climate models and the greenhouse gas emission scenarios used are those in IPCC AR4.

2.2.1 Downscaling

Statistical downscaling is a commonly employed technique to obtain local and regional scale climate projections from global climate forecasts. Statistical downscaling demands less on computational resources (Benestad 2001) and has a skill on a par with the dynamical approach (Murphy 1999). Regression is often used in statistical downscaling (Wilby et al. 2005). This is also the technique used by HKO in 2004 to project Hong Kong's temperature to the end of this century (Leung et al. 2004a) and in this paper. The temperature projections for southern China is downscaled to Hong Kong based on past temperature regression relationship between southern China and Hong Kong.

Country	Originating Centre	Model	A1B	A2	B1
Norway	Bjerknes Centre for Climate Research	BCM2		■	■
Canada	Canadian Center for Climate Modeling and Analysis	CGMR	■		
France	Centre National de Recherches Meteorologiques	CNCM3	■	■	■
Australia	Australia's Commonwealth Scientific and Industrial Research Organization	CSMK3		■	■
USA	Geophysical Fluid Dynamics Laboratory	GFCM20	■	■	■
	Goddard Institute for Space Studies	GIAOM	■		■
	National Centre for Atmospheric Research	NCCCSM	■	■	■
		NCPCM	■	■	
UK	UK Meteorological Office	HADCM3	■	■	■
		HADGEM	■	■	
Japan	National Institute for Environmental Studies	MIHR	■		■
		MIMR	■	■	■
	Meteorological Research Institute	MRCGCM	■	■	■
Korea, Germany	Meteorological Research Institute of KMA,	ECHOG	■	■	
	Meteorological Institute, University of Bonn,				
	Model and Data Groupe at MPI-M				
Germany	Max-Planck-Institut for Meteorology	MPEH5	■	■	■
Russia	Institute for Numerical Mathematics	INCM3	■		■

■ Available

Table 2-1 Model data availability in IPCC AR4

2.2.2 Relationship between temperature in southern China and Hong Kong with urbanization effect removed

For southern China, Empirical Orthogonal Function (EOF) analysis on 28 stations showed that there was generally warming mode over southern China from 1951 to 2000 (Leung et al. 2004a). Part of this warming is caused by urbanization (Guangdong Meteorological Bureau 2007). Unfortunately, quantitative assessment of the urbanization effect has not been made as no rural stations can be identified in southern China (Zhou et al. 2004).

This paper makes use of the past NCEP re-analysis temperature data instead of the observed data from southern China weather stations to correlate with Hong Kong's temperature. NCEP re-analysis data is relatively free from urbanization or land use effect because surface temperature observations are not used directly (Kalnay and Cai 2003). Instead, atmospheric vertical soundings of wind and temperature strongly influence the data (Kalnay et al. 1996). The trend for the NCEP temperature data is 0.03˚C per decade, smaller than the 0.11˚C per decade for the mean temperature of the 28 stations in southern China during the same period of 1951 to 2001.

The magnitude of urbanization effect on temperature is taken as the temperature of the urban station minus that of a typical rural station of the region (e.g. Sakakibara and Owa 2005). In Hong Kong, the HKO Headquarters (HKO Hq) is chosen as the urban station. In a previous study (Leung et al. 2004b), Ta Kwu Ling (TKL) and Lau Fau Shan (LFS) were taken as the typical rural stations. Temperatures of the island stations such as Cheung Chau and Waglan Island were found substantially modulated by the relatively more complicated variation of temperature of the near-shore waters, hence the island stations had not been used as rural stations (Sakakibara and Owa 2005).

At LFS, changes in the environment were observed near the site in the past few years. The grassland in the vicinity of LFS was converted into concrete surface for stacking up cargo containers. Also, there had been continuous new town developments at Tin Shui Wai which is about 1 km away. In contrast, there is no significant change in the immediate environment for TKL although the rapid urban development in the nearby city of Shenzhen cannot be completely ignored.

A plot (Fig. C2-3 in COLOUR PLATES) of diurnal cycle of the temperature difference between HKO Hq and some chosen stations shows similarity between LFS and those "suburban" stations (Shatin, Tuen Mun, Hong Kong South). This is in stark contrast to that of TKL, which shows most characteristics of a rural station. This paper therefore takes TKL as a rural station.

Fig. 2-4 shows a trend of the annual mean temperature difference between HKO Hq and TKL (Tu-r) by linear regression. Since the data period is relatively short and there is large year-to-year variation in Tu-r, the trend derived is found statistically not significant at 5%. As such, the trend derived this way is not suitable for estimating long-term urbanization effect. Similar to Choi et al. (2003), this paper uses the method of differencing period means to estimate the long-term urbanization effect and to obtain the de-urbanized temperature by removing this urbanization effect. The mean value of Tu-r for the 18 years data period (1989-2006) is 0.81˚C. In its early establishment in the late nineteen century, the HKO Hq was in a countryside setting surrounded by extensive paddy fields (Doberck 1885). The mean value of Tu-r for the 18 years data period (1885-1902) can be assigned a "0" value. The average rate of urbanization between 1885 and 2006 is computed to be 0.08˚C per decade (0.81˚C divided by the 10.4 decades between 1894 and 1998, Year 1894 and Year 1998 being the mid-point years of the two periods 1885-1902 and 1989-2006 respectively). The temperature in Hong Kong without urbanization (de-urbanized temperature) is then taken as the HKO Hq temperature minus the corresponding urbanization contribution.

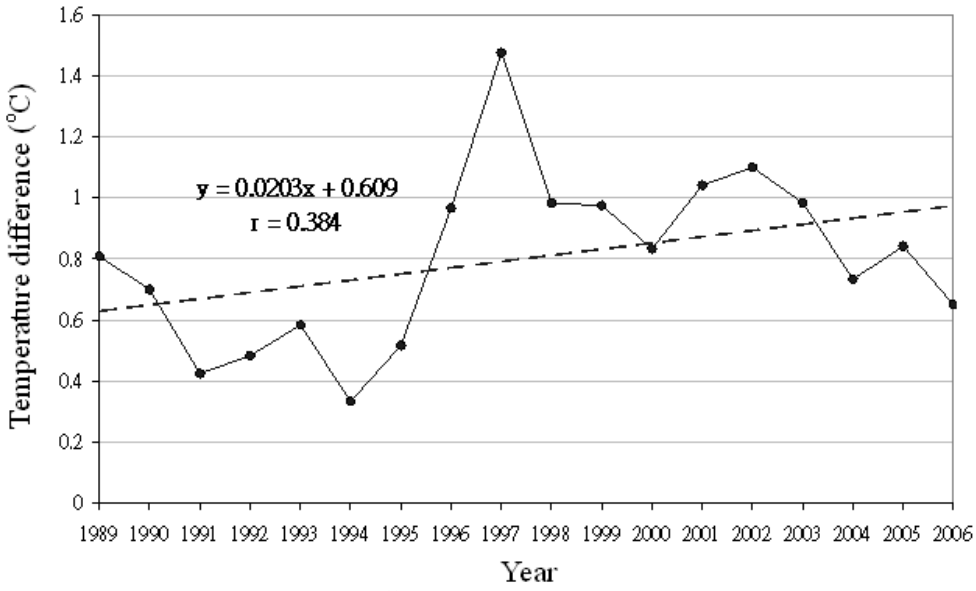

Fig. 2-4 Annual temperature difference between HKO Hq and TKL (1989-2006).

The rate of 0.08˚C per decade is comparable in order of magnitude with that in other large cities (population of over 0.5 million) of China where 0.05˚C per decade between 1961 and 2000 was found (Hua et al. 2007). In Beijing area, the trend was 0.16˚C per decade between 1961 and 2000 (Chu and Ren 2005). For London, about 1˚C of the temperature change between 1878 and 1968

could be attributed to urbanization (Moffit 1972), i.e. a trend of 0.11˚C per decade while between 1962 and 1989, the trend was 0.07˚C per decade in summer (Lee 1992). In the United States, the mean trend for 50 large metropolitan areas between 1951 and 2000 was 0.05˚C per decade (Stone 2007).

The above describes our first attempt at quantifying the long-term urbanization effect on air temperature in Hong Kong. Further refinements might follow on the basis of further studies on air temperature.

Regression between temperature anomalies (with reference to the mean temperature of 1980-1999, period also chosen by IPCC AR4 for computation of climatological normal) in southern China and Hong Kong is carried out from the NCEP re-analysis data and de-urbanized HKO Hq data for the past 55 years from 1951 to 2006. The projected temperature data for southern China derived from the IPCC AR4 global model data are then fed into the regression relationship to get the temperature projections in Hong Kong without urbanization effect.

2.2.3 Projections on urbanization effect

In the lack of information on the future change to the end of the century in urban planning, land use, population etc. that will have an influence on temperature, this study makes use of two assumptions for the future urbanization projections: (i) constant rate of change of urbanization as mentioned in paragraph 6 of Section 2.2.2, and (ii) urbanization frozen at 2006, the time of the latest available data when this assessment is made.

Since the urbanization effect will unlikely go up forever, the former provides the upper bound while the latter the lower bound for the urbanization effect on temperature in the future. The actual future urbanization effect may lie within these boundaries. This is consistent with the future population trend as discussed below.

A plot of the logarithm of the population (Fig. C2-5 in COLOUR PLATES, data from Census and Statistics Department, and also Planning Department) from 1885 to 2006 with prediction extending to 2036 shows a rather linear trend up to 1980s. The rate of change gradually decreases thereafter and is projected to remain so into the future. Empirically, some researcher (e.g., Karl et al. 1988) suggested that Tu-r may be linearly correlated with the logarithm of the population. If this is the case, Tu-r will exhibit a generally linear trend in the past and its rate of change gradually decreases in the future similar to the logarithm of the population.

2.2.4 Temperature projections incorporating urbanization effect

The urbanization effect mentioned in Section 2.2.3 is added to the temperature projections without urbanization effect in Section 2.2.2 to give the final temperature projections in Hong Kong.

2.2.5 Scaling for other 3 SRES scenarios

As mentioned in Section 2.1, only gridded model data from the three SRES scenarios B1, A1B and A2 are available. Following Carter et al. (2000), scaling method is used to estimate the temperature projections in 2090-2099 for the other three SRES scenarios A1T, B2 and A1FI. In essence, the method assumes that the ratio in regional temperature projections under two different emission scenarios is equal to their global temperature projections ratio.

To find the temperature anomaly in Hong Kong under A1FI, we apply the formula:

> *Temperature anomaly in Hong Kong under A1FI : Temperature anomaly in Hong Kong under A2 = Global temperature anomaly under A1FI : Global temperature anomaly under A2.*

The reason to use A2 rather than B1 or A1B to scale A1FI is that the carbon dioxide emission profile for A1FI is closer to A2 than B1 or A1B (see Fig. C2-1). Similarly, B1 is used to scale both A1T and B2.

For 2090-2099, the global temperature anomalies under all the six SRES scenarios are available from IPCC AR4 final report, and hence the temperature anomalies in Hong Kong under the three scenarios A1T, B2 and A1FI can be computed.

To indicate somehow the degree of accuracy of the above scaling methodology, we can use A1B or B1 to scale A2 and then compare the scaling results with the results obtained by downscaling. The carbon dioxide emission profile for A2 is closer to A1B than B1 (see Fig. C2-1). In the case of using A1B to scale A2, the mean temperature anomaly for A2 in 2090-2099 is 6.21˚C, 7.8% higher than the 5.76˚C obtained from downscaling. This deviation of 7.8% is smaller than the 21.7% when B1 is used to scale A2.

2.2.6 Projections of cold days, hot nights and very hot days

In Leung et al. (2004a), the projected number of cold days in winter, hot nights and very hot days in summer are based on the regression relationships in the past between these parameters and the minimum/maximum temperature at HKO Hq respectively. Since gridded projected minimum and maximum temperature data in most models used in AR4 are not available (see Section 2.1), mean temperature data are used instead for generating the regression relationships.

3. Results

Fig. C2-6 (COLOUR PLATES) shows as an example the projected temperature change for southern China in the model BCM2 under the SRES scenario B1 for 2050-2059 and 2080-2089 (relative to 2000-2009). Temperatures are on a rising trend in southern China.

Fig. 2-7 to 2-10 show respectively the scatter diagrams of temperature regression relationship between southern China and Hong Kong, and the parameters in Section 2.2.6 with temperature at HKO Hq. The correlation coefficients are all statistically significant at 5%. The correlation coefficients between the mean temperature and the number of cold days in winter, hot nights and very hot days in summer are 0.90, 0.78 and 0.56 respectively. Comparing with the correlation coefficients using maximum and minimum temperatures with the number of cold days in winter, hot nights and very hot days in summer, i.e. 0.90, 0.83 and 0.65 respectively, the present assessment have roughly the same or slightly lower correlation.

The theoretical temperature projections in Hong Kong in which the urbanization effect has been removed are given in Fig. C2-11 (COLOUR PLATES). In the figure, the decadal mean temperature of the model ensemble under the scenarios B1, A1B and A2 are shown respectively. For 2090-2099, the model ensemble means as well as the range under each of the 6 scenarios are also given. The results of temperature projections incorporating two scenarios of urbanization viz. (a) urbanization

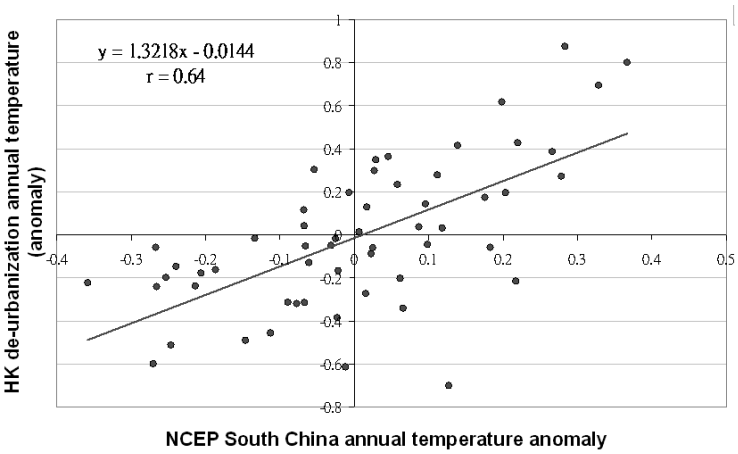

Fig. 2-7 Temperature regression relationship between southern China and Hong Kong (1951-2006).

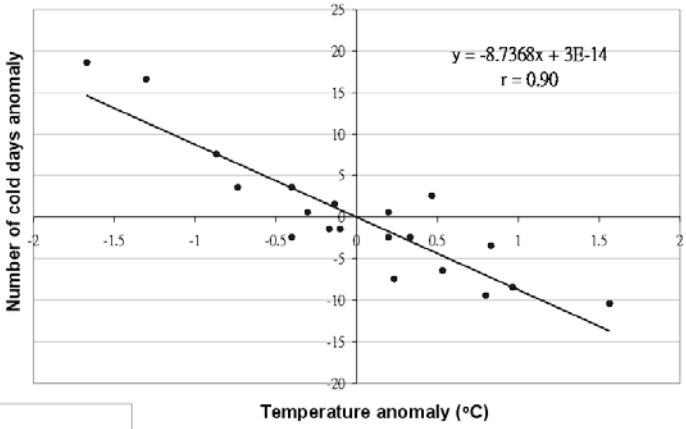

Fig. 2-8 Regression relationship between the number of cold days in winter and winter mean temperature (1980-1999).

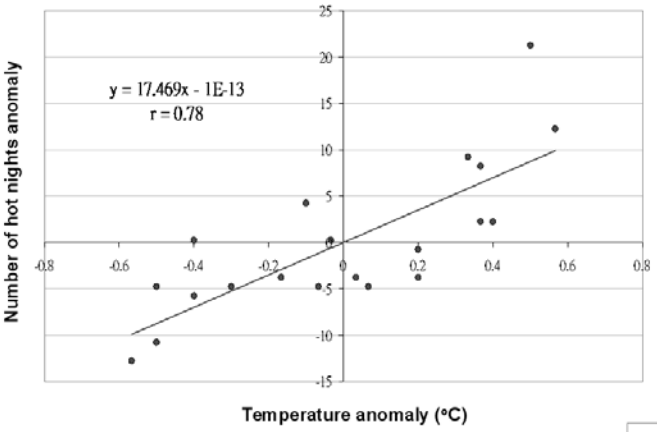

Fig. 2-9 Regression relationship between the number of hot nights in summer and summer mean temperature (1980-1999).

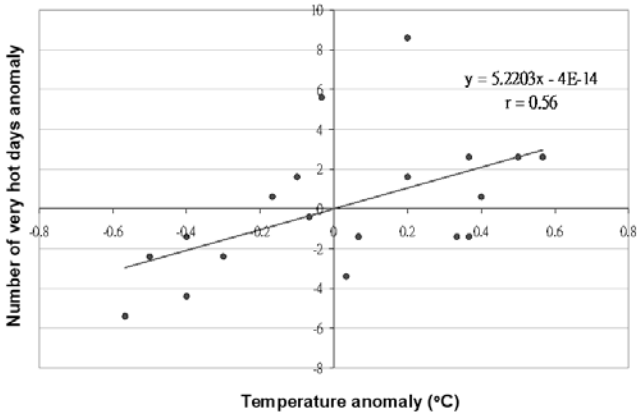

Fig. 2-10 Regression relationship between the number of very hot days in summer and summer mean temperature (1980-1999).

frozen at 2006 and (b) constant urbanization rate, are shown in Fig. C2-12 and C2-13 in COLOUR PLATES respectively. It should be noted that both scenarios are not likely to happen but may serve as the lower and upper bounds for this assessment. The truth most probably would be somewhere in between (see Section 2.2.3).

The projections for the number of cold days in winter, the number of hot nights and very hot days in summer for the two scenarios on future urbanization are shown respectively in Fig. C2-14, C2-15 and C2-16 in COLOUR PLATES.

In Fig. C2-12 to C2-16, for the purpose of presenting the result in a time scale in units of decades, the decadal mean of two periods, viz. 1940-1949 and 2000-2009, require special treatment: (i) the 3-year mean for 1947-1949 is used instead of the true decadal mean for 1940-1949 since data from 1940-1946 are not available owing to the Second World War; (ii) the mean derived from the actual observations in 2000-2006 together with the downscaled model values for the period 2007-2009 is used to represent the decadal mean for 2000-2009 because data for 2007-2009 are not yet available.

Parameter	**1980-1999 mean**	**2090-2099**			
		Urbanization frozen at 2006		**Constant urbanization rate**	
Temperature (°C)	23.1	Range:	24.5-31.5	Range:	25.1-32.3
		Best estimate:	26.1-29.1	Best estimate:	26.8-29.9
		Ensemble mean:	27.5	Ensemble mean:	28.3
Hot nights (nights)	14.8	Range:	22.0-59.9	Range:	29.4-68.7
		Best estimate:	29.5-45.3	Best estimate:	37.0-54.0
		Ensemble mean:	36.9	Ensemble mean:	45.4
Very hot days (days)	7.4	Range:	9.6-20.9	Range:	11.8-23.5
		Best estimate:	11.8-16.5	Best estimate:	14.0-19.1
		Ensemble mean:	14.0	Ensemble mean:	16.6
Parameter	**1980-1999 mean**	**The decade when cold days vanish**			
		Urbanization frozen at 2006		**Constant urbanization rate**	
Cold days (days)	14.4	2040-2049		2030-2039	

Table 2-2. Projections of temperature, number of cold days in winter, hot nights and very hot days in summer

Table 2-2 summarizes the projected results in 2090-2099 for temperature and the number of hot nights and very hot days in summer under the two different projections on urbanization effect: urbanization frozen at 2006 and constant urbanization rate. Similar to IPCC AR4, best estimates in the table refer to the range of model ensemble for the scenario B1 to the scenario A1FI. The table also gives the estimated decade that there would be no more cold days in Hong Kong. A comparison of the results based on AR4 with the previous results of AR3 can be found in Table 2-3.

Compared with 1980-1999, the temperature rise is projected to be 4.4˚C in 2090-2099 for the case of urbanization frozen at 2006 and 5.2˚C for the case of constant urbanization rate, both are higher than the 3.4˚C in the previous result using AR3. The higher temperature rise in the present assessment is attributed mainly to the higher projected temperature given by the models in AR4 and the inclusion of the urbanization effect.

Parameter	2090-2099					
	AR4				AR3	
	Urbanization frozen at 2006		Constant urbanization rate			
Temperature (°C)	Range:	24.5-31.5	Range:	25.1-32.3	Range:	24.4-28.8
	Ensemble mean:	27.5	Ensemble mean:	28.3	Ensemble mean:	26.5
Hot nights (nights)	Ensemble mean:	36.9	Ensemble mean:	45.4	Ensemble mean:	30
Very hot days (days)	Ensemble mean:	14.0	Ensemble mean:	16.6	Ensemble mean:	24
Parameter	The decade when cold days vanish					
	AR4				AR3	
	Urbanization frozen at 2006		Constant urbanization rate			
Cold days (days)	2040-2049		2030-2039		2090-2099	

Table 2-3. Comparison of the results on the projection of temperature, number of cold days in winter, hot nights and very hot days in summer based on AR4 with that of the previous results based on AR3

Cold days will vanish in 2040-2049 if urbanization is frozen at 2006 level but this would take place even earlier in 2030-2039 for the case of constant urbanization rate. Both are half a century or more earlier than that predicted in the previous assessment (2090-2099). The earlier realization of "no cold days" in the present assessment compared with the previous one is consistent with the higher projected temperature.

The number of hot nights per summer is projected to increase from 15 nights in 1980-1999 to 37 nights and 45 nights respectively in 2090-2099 for the case of urbanization frozen at 2006 and constant urbanization rate. In both cases, the number of hot nights in 2090-2099 is higher than 30 nights predicted in the previous assessment. The present assessment also predicts that there would be 30 hot nights per summer by 2070-2079 if urbanization is frozen at 2006; and by 2050-2059 if constant urbanization rate is assumed. Both are decades earlier than that predicted in the previous assessment (2090-2099). Again such predictions are consistent with the higher projected temperature.

The number of very hot days per summer is projected to increase from 7 in 1980-1999 to 14 and 17 respectively in 2090-2099 for the case of urbanization frozen at 2006 and constant urbanization rate. In both cases, the number of very hot days in 2090-2099 is lower than 24, the value predicted in the previous assessment. The projected number of very hot days is computed as the projected anomaly obtained from regression equation plus the number of very hot days in the reference period. The relatively smaller number of very hot days (i.e. 7) in the reference period 1980-1999 in the present assessment compared with 12 in the 1961-1990 used in the previous assessment contributed to the smaller projected number of very hot days.

4. Conclusion

Temperature projections for the 21st Century for Hong Kong by downscaling the global climate model projections of the Intergovernmental Panel on Climate Change (IPCC) Fourth Assessment Report were made. With respect to the 1980-1999 climatological mean, Hong Kong temperature is projected to rise by 4.4˚C in 2090-2099 for the case of urbanization frozen at 2006 and 5.2˚C for the

case of constant urbanization rate, both are higher than the 3.4˚C in the previous result based on the projections made in the IPCC Third Assessment Report.

Cold days will vanish in 2040-2049 if urbanization is frozen at 2006 level but this would take place even earlier in 2030-2039 for the case of constant urbanization rate. The number of hot nights per summer is projected to increase from 15 nights in 1980-1999 to 37 nights and 45 nights respectively in 2090-2099 for the case of urbanization frozen at 2006 and constant urbanization rate. The present assessment also predicts that there would be 30 hot nights per summer by 2070-2079 if urbanization is frozen at 2006; and by 2050-2059 if constant urbanization rate is assumed. The number of very hot days per summer is projected to increase from 7 in 1980-1999 to 14 and 17 respectively in 2090-2099 for the case of urbanization frozen at 2006 and constant urbanization rate.

Acknowledgement

The authors would like to thank colleagues of the Hong Kong Observatory Ms. Y.Y. Cheng and Mr. Y.H. Lau for their assistance in data extraction and compilation, and to Mr. C.Y. Lam for his invaluable advice.

Reference

Benestad, R., 2001: A comparison between two empirical downscaling strategies. *International Journal on Climatology,* **21**, 1645-1668.

Carter, T.R., M. Hulme, J.F. Crossley, S. Malyshev, M.G. New, M.E. Schlesinger, and H. Tuomenvirta, 2000: Climate Change in the Century - Interim Characterizations based on the New IPCC Emissions Scenarios. *The Finnish Environment*, **433**, Finnish Environment Institute, Helsinki. 148 pp.

Choi, Y., H-S Jung, K-Y Nam and W.T. Kwon, 2003: Adjusting urban bias in the regional mean surface temperature series of South Korea, 1968-99. *International Journal on Climatology,* **23**, 577-591.

Chu, Z. and G. Ren, 2005: Change in urban heat island magnitude and its effect on mean air temperature record in Beijing region. *ACTA Meteorologica Sinica,* **63(4)**, 534-540 (In Chinese).

Doberck, W, 1885: Annual Departmental Report. *Observations and researches made at the Hong Kong Observatory in the year 1885.* Hong Kong Observatory.

Guangdong Meteorological Bureau, 2007: *Guangdong Assessment Report of Climate Change.* 27 pp (In Chinese).

Hua, L. J., Z. G. Ma and W.D. Guo, 2007: The impact of urbanization on air temperature across China. *Theoretical and Applied Climatology,* DOI 10.1007/s00704-007-0339-8.

IPCC, 2001: *Climate Change 2001: The Science of Climate Change. Contribution of the Working Group I to the Third Assessment Report of the Intergovernmental Panel on Climate Change* [Houghton, J.T., Y. Ding, D.J. Griggs, M. Noguer, P.J. van der Linden, X. Dai, K. Maskell, C.A. Johnson (eds.)]. Cambridge University Press, Cambridge, United Kingdom and New York, NY,

USA, 881 pp.

IPCC, 2007: *Climate Change 2007: The Physical Science Basis. Contribution of the Working Group I to the Fourth Assessment Report of the Intergovernmental Panel on Climate Change* [Solomon, S., D. Qin, M. Manning, Z. Chen, M. Marquis, K.B. Averyt, M. Tignor and H.L. Miller (eds.)]. Cambridge University Press, Cambridge, United Kingdom and New York, NY, USA, 996 pp.

Kalnay, E., and Coauthors, 1996: The NCEP/NCAR 40-year reanalysis project. *Bulletin of American Meteorological Society*, **77**, 437-471.

Kalnay, E., and M. Cai, 2003: Impact of urbanization and land-use change on climate. *Nature*, **423**, 528-531.

Karl, T.R., H.F. Diaz and G. Kukla, 1998: Urbanization: Its detection and effect in the United States climate record. *Journal of Climate*, November 1988 Volume 1, 1099-1123.

Lee, D.O., 1992: Urban warming? – An analysis of recent trends in London's urban heat island. *Weather*, **47**, 50-56.

Leung, Y.K., E.W.L. Ginn, M.C. Wu, K.H. Yeung and W.L. Chang, 2004a: Temperature projections for Hong Kong in the 21st Century. *Bulletin of Hong Kong Meteorological Society,* **4**, No.1/2, 21-48.

Leung, Y.K., K.H. Yeung, E.W.L. Ginn and W.M. Leung, 2004b: Climate Change in Hong Kong. *Hong Kong Observatory Technical Note,* **107**, 41pp.

Moffit, B.J., 1972: The effects of urbanisation on mean temperatures at Kew Observatory. *Weather,* **27**, 121-129.

Murphy, J.M., 1999: An evaluation of statistical and dynamical techniques for downscaling local climate. *Journal of Climate*, **12**, 2256-2284.

Sakakibara, Y. and K. Owa, 2005: Urban – rural temperature differences in coastal cities: Influence of rural sites. *International Journal of Climatology*, **25**, 811-820.

Stone, B. Jr., 2007: Urban and rural temperature trends in proximity to large US cities: 1951-2000. *International Journal of Climatology*, **27(13)**, 1801-1807.

Wilby, R.L., S.P. Charles, E. Zorita, B. Timbal, P. Whetton and L.Mearns, 2005: *Guidelines for use of climate scenarios developed from statistical downscaling methods.* 27pp.

Zhou, L., R.E. Dickinson, Y. Tian, J. Fang, Q. Li, R.K. Kaufmann, C.J. Tucker, and R.B. Myneni, 2004: Evidence for a significant urbanization effect on Climate in China. *Proceedings of the National Academy of Sciences*, **101**, 9540-9544.

Some Characteristic on the Apparent Changes in East Asian Winter Atmospheric Circulation

M.C. Wu, K.K. Yeung and Y.K. Leung, Hong Kong Observatory, Hong Kong, China

Abstract

Against the background of global warming, this study attempts to find out if there has been any change in the East Asian winter atmospheric circulation in the last several decades by examining the trends of the characteristics of its eight components and their correlations. These eight components were the monsoon surges, the Siberia-Mongolia high, the Aleutian low and the equatorial monsoon trough in the lower troposphere; the western North Pacific subtropical high, the Eurasian westerlies and the East Asian trough in the mid-troposphere; and the subtropical jet aloft.

Trends are noted in the characteristics of all the components studied except the strength of the subtropical jet, indicating an apparent change in the atmospheric circulation pattern. With the exception of the intensifying Aleutian low, all trends found are consistent with the observed rising winter temperatures in southern China which has been attributed in part to global warming.

Moving correlation analysis with a 29-year sliding window applied to time series showed that the degree of correlation between the Eurasian westerlies index and the three different subtropical high indices is declining. This decreasing covariability between the tropical circulation (i.e., the subtropical high) and the mid-latitude circulation (i.e., the Eurasian westerlies) is another indication of the climatic change in the East Asian winter atmospheric circulation. Whether such changes were due to global warming requires further investigation.

Keywords

Global warming, East Asian winter atmospheric circulation, Trend, Covariability

1. Introduction

The Intergovernmental Panel on Climate Change (IPCC) has recently concluded that global warming is unequivocal [IPCC, 2007]. Observed to occur concurrently are changes in the regional climate in different parts of world. The trends of regional temperature variations are important aspects of the baseline against which the potential effects of climate change should be assessed [IPCC, 1998].

A rising trend has been found in the winter temperature in Hong Kong between 1947 and 2003 [LEUNG et al, 2004a,b]. At the regional scale, LIANG et al [1999] suggested that both global warming and local urbanization effects are among the reasons for the winter warming in the Guangdong Province of China, and WANG et al [2003] described the warming over southern China as a whole. From the perspective of regime shifts, WU et al [2006] related the recent rise in winter temperature in Hong Kong, as part of a regional phenomenon, with the weakening of the East Asian winter monsoon. Many model simulations have suggested a weakening of the East Asian winter monsoon under global warming [HU et al, 2000; BRANDEFLT, 2006; HORI et al, 2006 among others].

This study attempts to find out if there has been any change in the East Asian winter atmospheric circulation in the last several decades (1958-2005) by examining the trends of the characteristics of

its major components and their correlations. Their relationships with the winter temperature in Hong Kong are examined. Finally, the modulating effects of the Arctic Oscillation (AO) and the Pacific Decadal Oscillation (PDO) on the East Asian winter atmospheric circulation are also analyzed [GONG et al, 2001; JHUN et al, 2004; CHAN et al, 2005].

2. Data and Methodology

2.1 Data and definitions

Northern Hemisphere (NH) winter surface temperature anomaly data (December to February, DJF) are obtained from the National Climatic Data Center of NOAA (http://lwf.ncdc.noaa.gov/). Global atmospheric and sea surface temperature (SST) data in 1958-2005 comes from the monthly reanalysis of the National Centers for Environmental Prediction and the National Center for Atmospheric Research (NCEP-NCAR) [KALNAY et al, 1996]. NCEP-NCAR data prior to 1958 are not used because the quality is low [TRENBERTH et al, 2000]. In the computation of indices related to sea level pressure (SLP), Trenberth's monthly gridded northern hemisphere SLP data [TRENBERTH et al, 1980] are used (http://dss.ucar.edu/).

Winter temperatures of Hong Kong are computed from hourly temperatures recorded at the Hong Kong Observatory Headquarters. In the present study, temperature variation in Hong Kong is taken as a proxy for that of southern China because of the very high correlation between the two [LEUNG et al, 2004b].

Values of the Pacific Decadal Oscillation (PDO) index and the Arctic Oscillation (AO) index are obtained from the Joint Institute for the Study of the Atmosphere and Ocean of the University of Washington (http://jisao.washington.edu/) and the Climate and Global Dynamics Division of the Earth and Sun Systems Laboratory at NCAR (http://www.cgd.ucar.edu/) respectively. Values of the El Nino-Southern Oscillation (ENSO) index is calculated from the monthly SST in Nino region 3.4 (5°N-5°S, 170-120°W) data from the Climate Prediction Center of NOAA (http://www.cpc.noaa.gov/).

Published data from the National Climate Center (NCC) of the China Meteorological Administration (CMA) are also used, including values of the Subtropical High indices, the Eurasian Westerlies index and the East Asian Trough (position) index.

Eight major components of the East Asian winter monsoon have been identified [WU, 2003], namely the monsoon surges, the Siberia-Mongolia high, the Aleutian low and the equatorial monsoon trough in the lower troposphere; the western North Pacific subtropical high, the Eurasian westerlies and the East Asian trough in the mid-troposphere; and the subtropical jet aloft. Table 3-1 summarizes the definitions of the related indices and the data used in their computation.

2.2 Methods

In this study, the trend in a time series and its statistical significance are assessed using the non-parametric Mann-Kendall (MK) test. Since the MK test gives only the significance and the direction of the trend but not the trend itself, the non-parametric Sen's slope estimator [SEN, 1968] is used to obtain the magnitude of the trend. Both MK test and the Sen's slope estimator have the advantage of not being predicated upon the normal distribution, while able to be applied to data with linear or non-linear trends, and insensitive to outliers [SNEYERS, 1990; FU et al, 1992]. However,

for simplicity, trends of surface temperature, SLP, 500 hPa geopotential height and 200 hPa zonal wind for different grid points in NH are determined using linear regression analysis [EASTERLING et al, 1997].

Table 3-1 Definitions of indices characterizing the eight components of the East Asian winter monsoon

Component		Index	Definition of the indices and data used
Lower troposphere	Winter monsoon surge	WMI	Defined by YOUN [2005] as standardized SLP difference between (40°N, 135°E) and (45°N, 95°E) averaged for DJF and is calculated using Trenberth's SLP data. The more negative the WMI the stronger is the monsoon.
	Siberia-Mongolia high	SMH	Defined as SLP averaged over (45-55°N, 95-100°E)[1] and is calculated using Trenberth's SLP data. Larger value indicates a stronger Siberia-Mongolia high.
	Aleutian low	ALPI	The mean area (km^2) with SLP ≤1005 hPa [BEAMISH et al,1997]. A positive ALPI reflects a strong Aleutian low. Values of ALPI are downloaded from Fisheries and Oceans Canada at http://www.pac.dfo-mpo.gc.ca/.
	Equatorial monsoon trough	EMT	The outgoing longwave radiation (OLR) averaged over the region (10°S-10°N, 100-160°E). Larger values represent weaker convection and a weaker monsoon trough. NCEP-NCAR reanalysis data are used to calculate the values of this index.
Mid-troposphere	Subtropical high	SH_I	The intensity of the subtropical high. Data from NCC[2].
		SH_R	The ridge line position of the subtropical high. An increasing value refers to a northward shift of the subtropical high. Data from NCC.
		SH_W	The western position of the subtropical high. An increasing value refers to a eastward shift of the subtropical high. Data from NCC.
	Eurasian westerlies	EAW	It denotes the mid-latitude circulation condition in the Eurasia sector (45-65°N, 0-150°E). A positive value corresponds to the dominance of zonal flow in Eurasia. Data from NCC.
	East Asian trough	EAT	The longitudinal position of the East Asian trough. Data from NCC.
Aloft	Subtropical jet	JET	The areal average of the 200-hPa zonal wind over (30-35°N, 130-160°E) as defined by YANG et al [2002]. A larger value represents a stronger subtropical jet. NCEP-NCAR reanalysis data are used to calculate the values of this index.

[1] Region defined by WU et al [1997] to represent the Siberia-Mongolia high but using 1000 hPa geopotential height.
[2] See ZHAO [1999] for the detailed definitions of NCC indices.

Moving correlation analysis [KUZNETS, 1928] with a 29-year sliding window is used to examine the temporal variability in the relationship between any two indices [MCCABE et al, 2006]. Unless otherwise stated, spearman rank correlation [WILKS, 1995] is used to minimize outlier influence, although Pearson's correlation produces essentially the same results.

The empirical orthogonal function (EOF) technique [von STORCH et al, 1999] is used to highlight the coherent modes of variability in NH winter atmospheric circulation, which are compared with the linear trends. The cumulative summation (CUSUM) technique is used to determine changes in the trend of a time series, to identify periods of regime reversal and to see whether changes in trends tend to match up across indices [HARE, 1996; LEUNG et al, 2005]. It is defined as the accumulating sum of anomalies (from the overall mean) of all preceding values.

3. Results

3.1 Overall changes in Northern Hemisphere winter atmospheric circulation

Fig. 3-1 compares the pattern of the linear trend describing the overall change and the pattern of the first EOF (i.e., EOF 1) of NH winter surface temperature in the period 1958-2005. The similarity between the two indicates that the trend dominates the variability of NH winter temperature as a whole. It is also noted that the temporal score or principal component (PC) of the first EOF exhibits an increasing trend (not shown) suggesting that warming is the key feature of NH in this period. The north-south SLP gradient (Fig. 3-2a) and the East Asian trough in the vicinity of Japan (Fig. 3-2b) have been weakening, indicating a weakening of the East Asian monsoon. These changes are also found to be consistent with their respective leading mode of variability (Fig. 3-3a,b) with positive trends in the associated PCs.

Aloft, the most prominent features of the spatial trend of the 200 hPa zonal wind are the northward displacement and eastward extension of the subtropical jet (Fig. 3-2c). No significant trend is found in the first two EOFs (i.e., EOFs 1 and 2) of the 200 hPa zonal wind. Both the third and fourth EOFs have significant positive trends in the corresponding PCs, suggest a weakening (EOF 3) and an eastward shift (EOF 4) of the subtropical jet. These findings also suggest a weakening of the winter monsoon circulation over East Asia. Changes in the major components of the East Asian winter atmospheric circulation are examined in more details below.

3.2 Trends in components of the East Asian winter atmospheric circulation

Significant trends (at 5% level) are found in the indices of all the components studied except the strength of the subtropical jet (JET) aloft (Table 3-2), indicating a remarkable change in the East Asian winter atmospheric circulation particularly in the lower troposphere. Converting the trends to a common scale expressed in terms of a fraction of the standard deviation (Stdev) allows comparison of trends of different indices. It is found that the trend is most prominent in the Siberia-Mongolia high (SMH) in the lower troposphere and the East Asian trough (EAT) in the mid-troposphere respectively. The ratio of the standard deviation to the trend provides a measure of the time required for the trend to give a change equivalent to one standard deviation, and it ranges from ~ 20 to ~40 years for different indices.

Table 3-3 summarizes the change of each component of the East Asian winter monsoon circulation as revealed by the trend of the corresponding index. The average of Hong Kong's winter temperature corresponding to the 10 largest values of each index is compared with that corresponding to the 10 lowest values of the index to see how the winter temperatures in Hong Kong vary with the index. With the exception of the intensifying Aleutian low, the trends of all indices are found to be consistent with the observed rising winter temperature in Hong Kong (and thus of southern China as discussed earlier [LEUNG et al, 2004b]) which has been attributed in part to global warming. The influences of the Aleutian low (ALPI) and the equatorial monsoon trough (EMT) are apparently slight as the difference in Hong Kong's winter temperature for large and small values of ALPI and of EMT are statistically not significant.

The lack of a significant trend in JET is in line with the result given in Section 3.1, namely no significant trend being found for the PCs associated with the first two EOFs of the 200 hPa zonal wind. On the other hand, the eastwards shift of the subtropical jet as suggested by EOF 4 (Fig. 3-3d) is consistent with the significant trend in EAT (i.e., eastward shift of the East Asian trough).

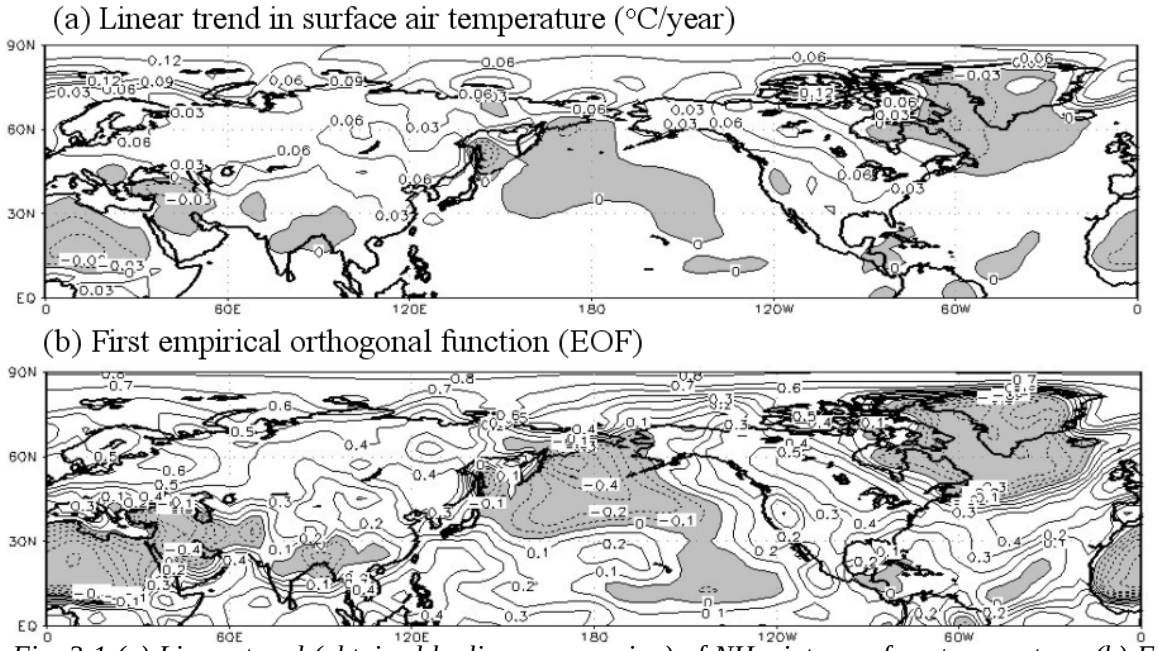

Fig. 3-1 (a) Linear trend (obtained by linear regression) of NH winter surface temperature. (b) First EOF of NH winter surface temperature which accounts for 16.6% variability. Negative values are shaded.

Table 3-2 Trend analysis of the components of the East Asian winter monsoon. Only trends significant at 5% level using MK test are given. Stdev is with reference to the period 1961-1990.

	Lower troposphere				Mid-troposphere					Aloft
	WMI	SMH	ALPI	EMT	SH_I	SH_R	SH_W	EAW	EAT	JET
Trend, (/decade)	1.67	-1.32	0.64	1.72	3.65	0.44	-6.06	0.04	1.28	-
Trend/Stdev	0.47	-0.53	0.22	0.34	0.31	0.33	-0.35	0.23	0.51	-
Stdev/Trend, (years)	21.5	18.9	45.2	29.8	32.2	30.5	28.4	43.6	19.7	-

*Table 3-3 The average of Hong Kong's winter temperature corresponding to the 10 highest values of an index minus that corresponding to the 10 lowest values of the index. The significance of the difference is tested using the Kolmogorov-Smirnov (KS) test [SIEGEL et al, 1988]. * denotes significance at the 5% level.*

Index		Difference (°C)	Change correspond to the trend of each index
Lower troposphere	WMI	1.48*	Weaker monsoon surge
	SMH	1.49*	Weaker Siberia-Mongolia High
	ALPI	-0.13	Deepening of the Aleutian low
	EMT	0.66	Weakening of the Equatorial monsoon trough
Mid-troposphere	SH_I	1.04*	Stronger subtropical high
	SH_R	1.47*	Subtropical high shift northwards
	SH_W	1.14*	Subtropical high shift westwards
	EAW	1.26*	Zonal flow dominate in Eurasia sector
	EAT	0.81*	East Asian trough shift eastwards

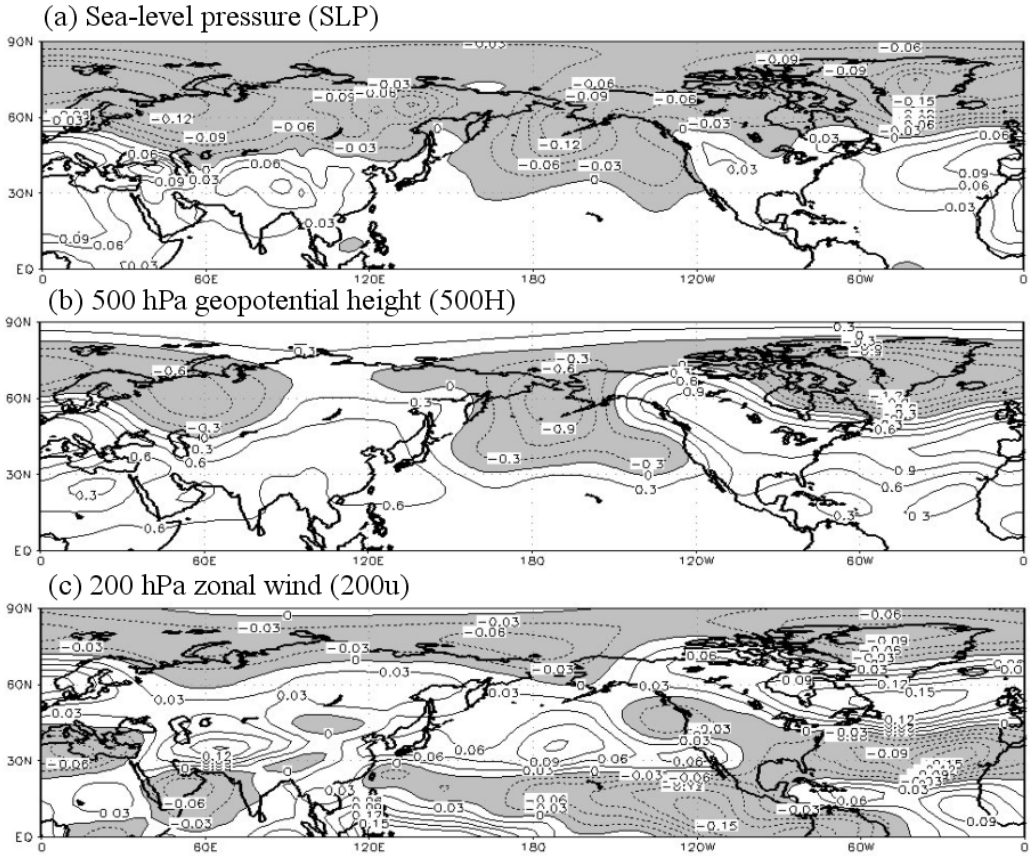

Fig. 3-2. As in Fig. 3-1a, but for NH winter (a) SLP, (b) 500 hPa geopotential height and (c) 200 hPa zonal wind. Negative values are shaded.

3.3 Changing covariability between different components

The covariability between different components of the East Asian winter atmospheric circulation in the mid-troposphere has been examined. Moving correlation analysis with a 29-year sliding window applied to time series reveals that the degree of correlations between the Eurasian Westerlies index (EAW) and the three different subtropical high indices (SH_I, SH_R and SH_W) are declining (Fig. 3-4). This decreasing covariability between the low latitude circulation (i.e., the subtropical high) and the mid-latitude circulation (i.e., the Eurasian westerlies) is another indication of the change in the East Asian winter atmospheric circulation [BRAGANZA et al, 2004]. While the correlation between the East Asian Trough index (EAT) and Subtropical High Intensity index (SH_I) is also declining and becoming insignificant, no significant correlation is found between the East Asian Trough index (EAT) and the Subtropical High Ridge Line index (SH_R) and between EAT and the Subtropical High Western Position index (SH_W) in any time slices (not shown). In contrast, the correlation between the East Asian trough (EAT) and the Eurasian westerlies (EAW) is increasing and the covariability among the subtropical high indices remains significant and robust throughout the period (not shown). Fig. 3-5 summarizes schematically the change in the interrelationship among the components of East Asian winter atmospheric circulation in the mid-troposphere.

To see if the above decline in covariability between the low latitude circulation and the mid-latitude circulation could possibly be related to global warming in terms of the rising trend of NH winter

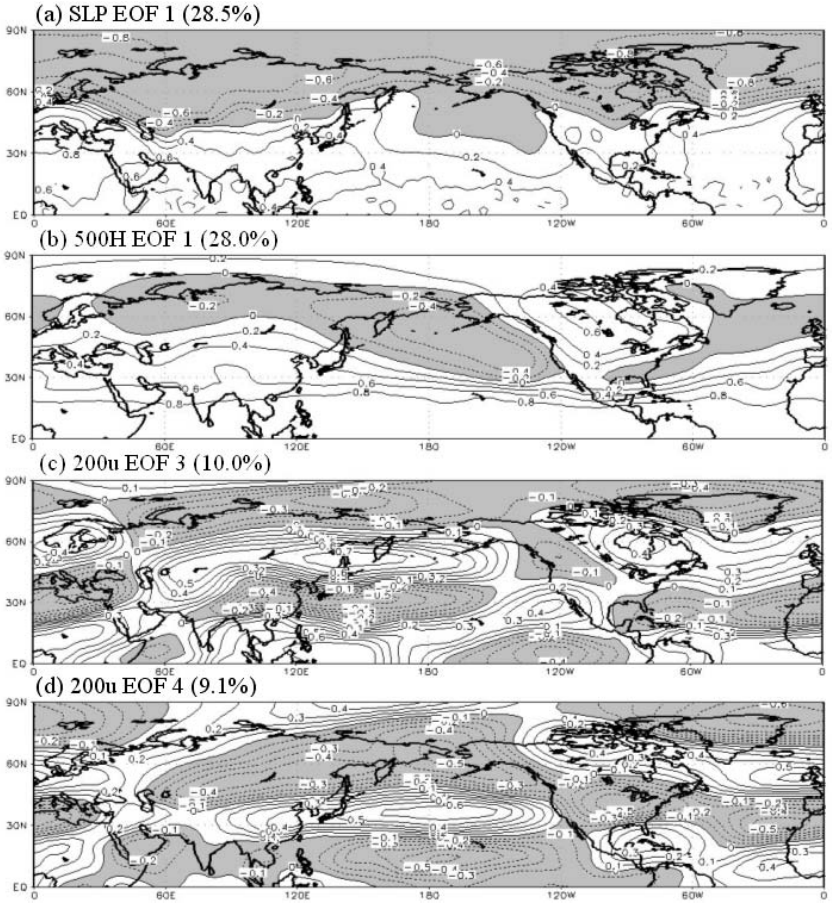

Fig. 3-3
The first EOF of NH winter SLP (a) and that of 500 hPa geopotential height (b), the third (c) and fourth (d) EOFs of winter 200 hPa zonal wind. Negative values are shaded. The bracketed value gives the total amount of field variance explained by each EOF. Note that no significant trend is found for the first two leading EOFs of 200 hPa zonal wind, and are therefore not shown.

temperature, the time series of EAW, SH_I, SH_R and SH_W are first grouped into 2 slices, each consisting of 29 years, according to the ranking of the detrended (using linear regression for simplicity and convenience) NH winter temperature. Each group with 29 years therefore corresponds to the relatively warmer (Group W) and colder (Group C) winters after the linear trend had been removed. The purpose of detrending is to ensure that one looks at the relationship between temperature and the index, not just the time variation of the index which had already been addressed earlier, in view of the increase in temperature with time under global warming. Table 3-4 compares the correlations among indices between the 2 groups. Apparently, with warmer NH winters, there is a decline in correlation between the Eurasian Westerlies index (EAW) and the subtropical high indices, most evident for SH_I and SH_W.

To consider the significance (in statistical sense) of the apparent decline in correlation between the Eurasian Westerlies index (EAW) and the subtropical high's intensity and western position index (SH_I and SH_W) with warmer NH winters, 29 years of the detrended EAT and SH_I are selected randomly (instead of according to the ranking of the detrended NH winter temperature) and the corresponding correlation coefficient is computed. This procedure is then repeated for 10,000 times so that we will have 10,000 correlation coefficients. Same consideration is also conducted between EAT and SH_W. Fig. 3-6 shows the distribution of the 10,000 realizations of correlation coefficients between EAT and SH_I and that between EAT and SH_W. It is noted that the percentage to have correlation between EAT and SH_I to be $\leqq$ +0.075 (with reference to the 0.07 for group W given in Table 3-4) and ≥+0.475 (with reference to the 0.47 for group C given in Table 3-4) is just ~5.4%

and ~3.1% respectively. Likewise, the percentage to have correlation between EAT and SH_W to be $\leqq$ -0.50 and $\geq$ -0.10 is ~10.5% and < 1%, respectively. In other words, the decline in correlation with warmer NH winters mentioned above could be rather significant.

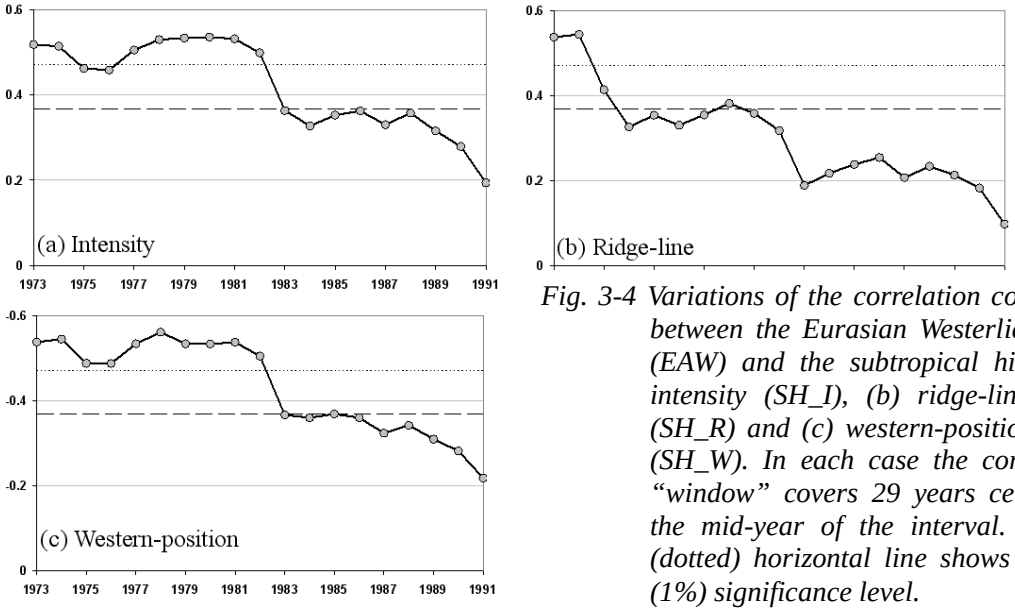

Fig. 3-4 Variations of the correlation coefficient between the Eurasian Westerlies index (EAW) and the subtropical high's (a) intensity (SH_I), (b) ridge-line index (SH_R) and (c) western-position index (SH_W). In each case the correlation "window" covers 29 years centred at the mid-year of the interval. Dashed (dotted) horizontal line shows the 5% (1%) significance level.

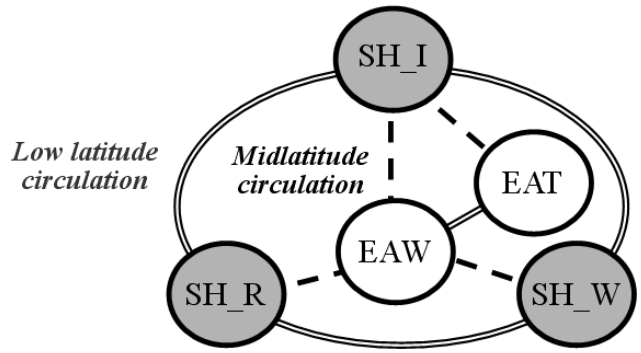

Fig. 3-5 Schematic diagram showing the interrelationships among the components of the East Asian winter atmospheric circulation in the mid-troposphere. Double line denotes significant correlation in recent decades. Dashed line represents a declining correlation from significant to insignificant.

*Table 3-4 Comparison of the correlations between Group C and Group W. Group W (C) corresponds to 29 relatively warmer (colder) years for the detrended NH winter temperature. * denotes correlation significant at 1% level.*

Indices	Correlation for group C	Correlation for group W
EAW vs SH_I	0.47*	0.07
EAW vs SH_R	0.29	0.26
EAW vs SH_W	-0.50*	-0.12

Besides global warming, changes in the components of the East Asian winter atmospheric circulation are compared with some dominant modes of oscillations of NH oceanic and atmospheric circulations, namely PDO and AO, using the CUSUM method. The CUSUM graph helps to locate abrupt changes in the trend in a time series. Abrupt changes in the subtropical high indices (SH_I, SH_R and SH_W) as well as the ENSO index are found to coincide with the well-recognized climatic shift in the PDO [MANTUA et al, 1997] in the mid-1970s (Fig. 3-7). At the same time, it is clear that the subtropical

high is more strongly influenced by PDO compared with the components in mid-latitudes (EAW and EAT).

Similar abrupt changes can be seen in the time series of the winter temperature of NH, winter temperature of Hong Kong, the Eurasian Westerlies and East Asian Trough indices (EAW and EAT) in the mid- to late 1980s, concurrent with the phase change in AO [OVERLAND et al, 1999]. As such, in line with the implication of the study by CORTI et al [1999], the observed changes of EAW, EAT and the three subtropical high indices SH_I, SH_R and SH_W could be a manifestation of some natural climate variability if AO and PDO are recognized as natural oscillations. However, CORTI et al [1999] has also pointed out that even if the observed change in a certain aspect of the climate is related to certain natural climate oscillations, the possibility of anthropogenic forcing of the former cannot be ruled out because the latter could have been affected. From Fig. 3-6(d), NH winter temperature exhibits an abrupt change around the mid-1980s, with a sharp increase in the rate of warming (though not as sharp as the change in AO, EAT, EAW or Hong Kong's winter temperature). As AO is strongly coupled with the surface temperature fluctuation over the Eurasian continent [THOMPSON et al, 1998] and thus the East Asian winter monsoon [GONG et al, 2001], it is therefore difficult to distinguish between natural variability and change due to anthropogenic forcing. For instance, while SHINDELL et al [1999] hypothesized that the change in AO is related to increase in greenhouse gases, COHEN et al [2005] recently argued that the global warming trend is largely independent of the AO.

4. Conclusion

Against the background of global warming, this study attempts to find out if there has been any change in the East Asian winter atmospheric circulation in the last several decades by examining the trends of the characteristics of its eight components and their correlations. Trends are noted in the characteristics of all the components studied except the strength of the subtropical jet aloft, indicating an apparent change in the atmospheric circulation pattern. With the exception of the intensifying Aleutian low, all trends found are consistent with the observed rising winter temperatures in southern China which has been attributed in part to global warming.

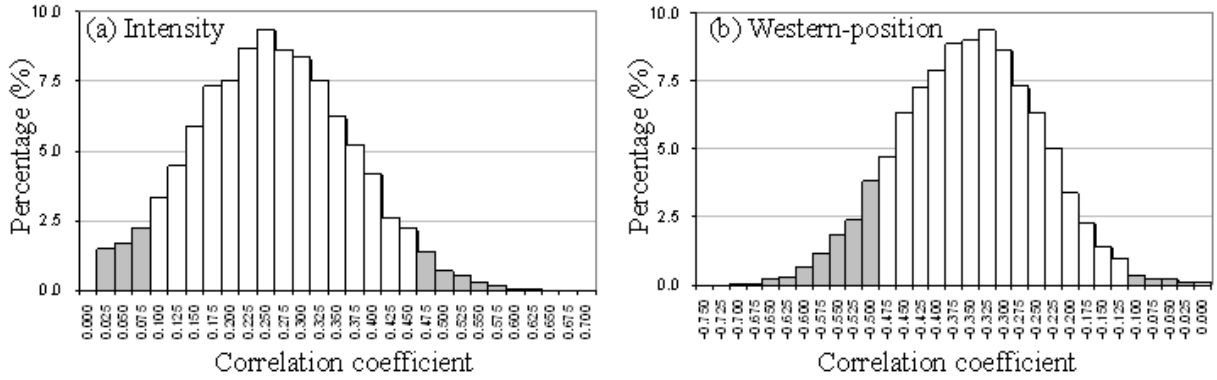

Fig. 3-6 Distribution of correlation coefficients between the Eurasian Westerlies index (EAW) and the subtropical high's (a) intensity (SH_I) and (b) western-position index (SH_W). With reference to the values of correlation given in Table 4 for EAT vs SH_I and EAT vs SH_W, correlation coefficients $\leq$ +0.075 and $\geq$ +0.475 for (a) and $\leq$ -0.50 and $\geq$ -0.10 for (b) are highlighted in grey.

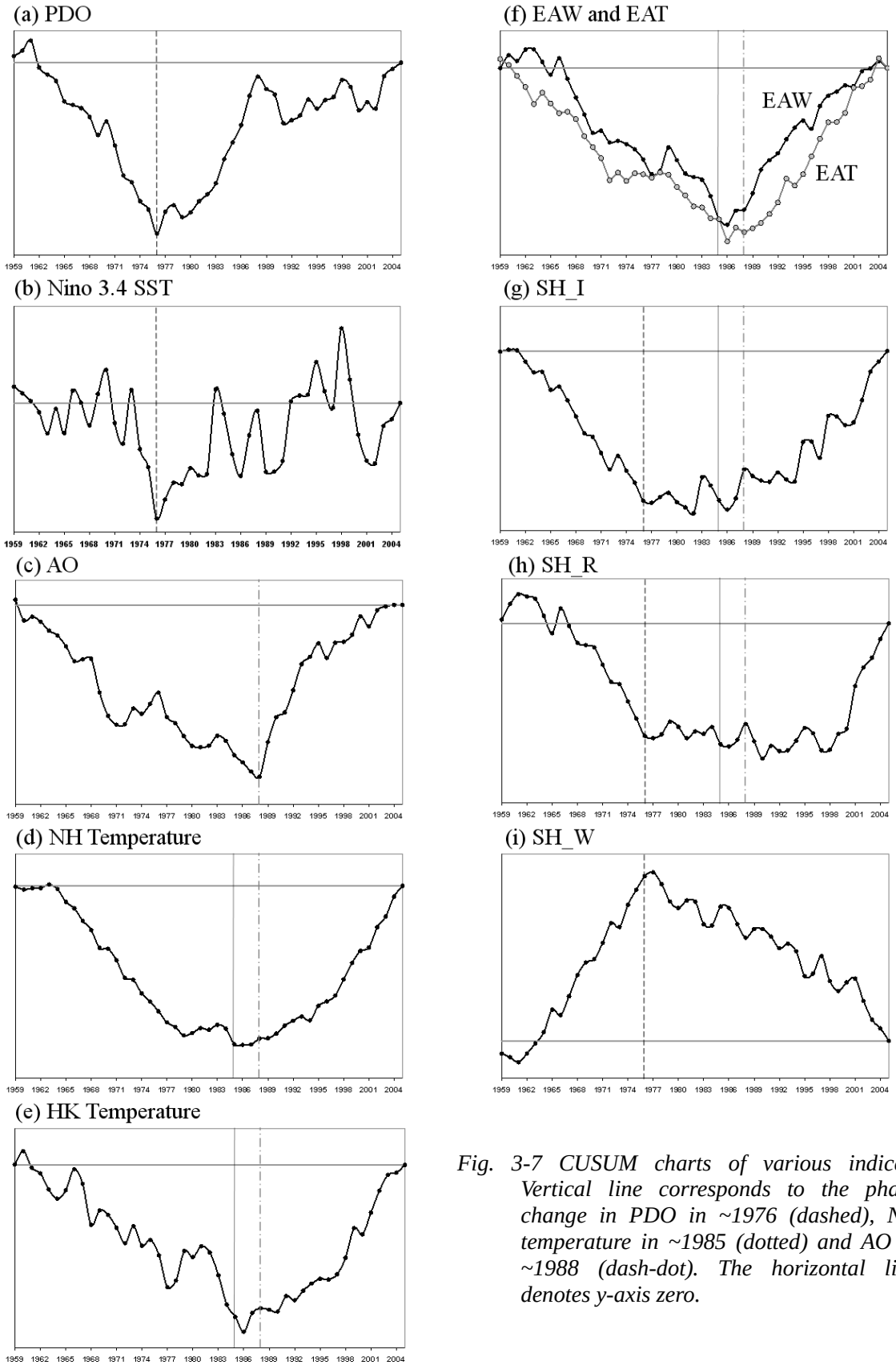

Fig. 3-7 CUSUM charts of various indices. Vertical line corresponds to the phase change in PDO in ~1976 (dashed), NH temperature in ~1985 (dotted) and AO in ~1988 (dash-dot). The horizontal line denotes y-axis zero.

Changes in some components of the East Asian winter atmospheric circulation have been suggested to be related to global warming based on the results of coupled GCMs simulations. These include for examples, the weakening of the Siberia-Mongolia high [BRANDEFLT, 2006], the deepening of Aleutian low [HU et al, 2000] and the weakening of the East Asian winter monsoon [HORI et al, 2006]. These changes are consistent with the findings of this paper.

The covariability between the low latitude circulation and the mid-latitude circulation is declining which is another indication of the climatic change in the East Asian winter atmospheric circulation. Whether or not such changes were due to global warming requires further investigation.

References

BEAMISH, R.J., C.E. Neville and A.J. Cass. 1997, Production of Fraser River sockeye salmon (Oncorhynchus nerka) in relation to decadal-scale changes in the climate and the ocean. *Can. J. Fish. Aquat. Sci*. **54**, 543-554.

BRANDEFLT, J, 2006, Atmospheric modes of variability in a changing climate, *J. Climate*, **19**, 5934-5943.

BRAGANZA, K., D. Karoly, A. Hirst, M. Mann, P. Stott, R. Stouffer, S. Tett, 2004, Simple indices of global climate variability and change: Part I-variability and correlation structure, *Climate Dynamics*, **20**, 491-502.

CHAN, J.C.L., and W. Zhou, 2005, PDO,ENSO and the early summer monsoon rainfall over south China, *Geophys. Res. Lttr*s., **32**, L08810, doi:10.1029/2004GL022015.

COHEN, J., and M. Barlow, 2005, The NAO, the AO, and Global warming: How closely related?, *J. Climate*, **18**, 4498-4513.

CORTI, S, F. Molteni, and T.N. Palmer, 1999, Signature of recent climate change in frequencies of natural atmospheric circulation regimes, *Nature*, **398**, 799-802.

EASTERLING, D.R., B. Horton, P.D. Jones, T.C. Peterson, T.R. Karl, D.E. Parker, M.J. Salinger, V. Razuvayev, N. Plummer, P. Jameson, C.K. Folland, 1997, Maximum and minimum temperature trends for the globe. *Science*, **277**, 364-367.

FU, Congbin, and Q. Wang, 1992, The definition and detection of abrupt climate change. *Scientia Atmospheric Sinica*, **16**, 482-493. (In Chinese with English Abstract).

GONG, D.Y, S.W. Wang and J.H. Zhu, 2001, East Asian winter monsoon and Arctic Oscillation. *Geophys. Res. Lttrs*., **28**, 2073-2076.

JHUN, J.G., and E..J. Lee, 2004, A new East Asian Winter Monsoon index and associated characteristics of the winter monsoon. *J. Climate*, **17**, 711-725.

HARE, S. R., 1996, *Low frequency climate variability and Salmon production*, Ph.D. Thesis, Univ. Washington, 306 pp.

HORI, M., and H. Ueda, 2006, Impact of global warming on the East Asian winter monsoon as revealed by nine coupled atmosphere-ocean GCMs, *Geophs. Res. Lttrs*., **33**, doi:10.1029/2005GL024961.

HU, Z.Z., L. Bengtsson, and K. Arpe, 2000, Impact of global warming on the Asian winter monsoon in a coupled GCM, *J. Geophys. Res*., **105**, 4607-4624.

IPCC, 1998, *The Regional Impacts of Climate Change: An Assessment of Vulnerability*, A Special Report of IPCC Working Group Ⅱ. Cambridge University Press, 517 pp

IPCC, 2007, Climate Change 2007, *The Physical Science Basis, Summary for Policymakers*. Contribution of the Working Group 1 to the Fourth Assessment Report of the Intergovernmental Panel on Climate Change. 21pp.

KALNAY, E., and Coauthors, 1996, The NCEP/NCAR 40-year reanalysis project. *Bull. Am. Meteorol. Soc*., **77**, 437-471.

KUZNETS, S., 1928, On moving correlation of time sequences. *J. Am. Statistical Ass*., **23**, 121-136.

LEUNG, Y.K., K.H. Yeung, E.W.L. Ginn and W.M. Leung, 2004a, Climate Change in Hong Kong. Hong Kong Observatory Technical Note No. **107**.

LEUNG, Y.K., E.W.L.Ginn, M.C.Wu, K.H. Yeung and W.L. Chang, 2004b, Temperature Projections for Hong Kong in the 21st Century. *Bull. HK. Met. Soc*., **14**, 21-48.

LEUNG, Y.K., and M. C. Wu, 2005, Regime Shift in Summer Rainfall in Southern China, Seventh Joint Meeting of Seasonal Prediction on East Asian Summer Monsoon, Nanjing, China, 11-13 May 2005, Reprint No. **586**, Hong Kong Observatory.

LIANG, J., and S. Wu 1999, Climate diagnosis of winter temperature trend in Guangdong. *J. Tropical Meteorol.* **15**, 221-229 (In Chinese).

MANTUA, N.J., S.R. Hare, Y.Zhang and J.M. Wallace, 1997, A Pacific interdecadal climate oscillation with impacts on salmon production. *Bull. Am. Meteorol. Soc*., **78**, 1069-1079.

MCCABE, G., and M. P. Clark, 2006, Shifting covariability of North American summer monsoon precipitation with antecedent winter precipitation, *Int. J. Climatol*., 26, 991-999.

OVERLAND, J.E., J.M. Adams and N.A.Bond, 1999, Decadal variability of the Aleutian low and its relationship to High-latitude circulation, *J. Climate*, **12**, 1542-1548.

SEN, P. K., 1968, Estimates of the regression coefficient based on Kendall's tau. *J. Am. Stat. Assoc*., **63**, 1379-1389.

SHINDELL, D.T., R.L.Miller, G.A.Schmidt, and L. Pandolfo, 1999, Simulation of recent northern winter climate trends by greenhouse gas forcing, *Nature*, **399**, 452-455.

SIEGEL, S., and N. J. Castellan, Jr., 1988, *Nonparametric Statistics for the Behavioral Sciences*, McGraw-Hill International, 399 pp.

SNEYERS, R. 1990, On the statistical analysis of series of observations. *WMO Technical Note* No. **143**.

THOMPSON, D.W.J., and J. M. Wallace, 1998, The Arctic Oscillation signature in the wintertime geopotential height and temperature fields. *Geophys. Res. Lttrs*., **25**, 1297-1300.

TRENBERTH, K. E., and D. A. Paolino Jr., 1980, The Northern Hemisphere sea-level pressure data set, Trends, errors and discontinuities. *Mon. Wea. Rev*., **108**, 855-872.

TRENBERTH, K. E., and Caron, 2000, The Southern Oscillation revisited: Sea level pressure, surface temperature, and precipitation, *J. Climate*, **13**, 4358-4365.

Von STORCH, Hans, and Francis W. Zwiers, 1999, *Statistical Analysis in Climate Research*, Cambridge University Press, 484 pp.

WANG, Z. Zhao, S. Wang, and W. Liu, 2003, Impact of climate change on agriculture, *Popular Topics on Global Climate Change Series*. (D. Qin Chief Editor; Y.H. Ding and Y.S. Mao co-editors), Meteorological Press, Beijing, 137 pp. (in Chinese only).

WILKS, Daniel S., 1995, *Statistical Methods in the Atmospheric Sciences, An Introduction*. Academic Press, 467 pp.

WU, M. C., and J. C. L. Chan, 1997, Upper-level features of winter monsoon surges over South China. *Mon. Wea. Rev*., **125**, 317-340.

WU, M.C., 2003, *Relationships between summer and winter monsoons over East Asia*. Ph.D. Thesis, City Univ. Hong Kong, 228 pp.

WU, M.C., Y.K.Leung and W.L.Chang, 2005: Relationship between winter temperature in Hong Kong and East Asian Winter Monsoon, Symposium on Asian Winter Monsoon Winter MONEX: A Quarter Century and Beyond (WMONEX 25+), Kuala Lumpur, Malaysia, 4-7 April 2006, Reprint No. **643**, Hong Kong Observatory.

YANG, S., and K. M. Lau and K. M. Kim, 2002, Variations of the East Asian jet stream and Asian-Pacific-American winter climate anomalies. *J. Climate*, **15**, 306-325.

YOUN, Y. H., 2005, The climate variabilities of air temperature around the Korea Peninsula. *Adv. Atmos. Sci*., **22**, 575-584.

ZHAO, H. (Eds), 1999, *Zhongguo Xiaji Hanlao Ji Huan Jing Chang*. Meteor. Press, 297 pp (in Chinese).

Trends in global solar radiation in Hong Kong

C.K. Ho, J.K.W. Chan and K.C. Tsui, Hong Kong Observatory, Hong Kong, China

Abstract

The long-term trends of global solar radiation, daytime cloud amount and bright sunshine duration from 1961 to 2005 in Hong Kong were analyzed. The intensity of solar radiation reaching the ground was found to have a quadratic dependence on time (significant at 1 % level), with the sharp decline in 1960s and 70s leveling off from early 1980s onwards. Seasonal differences in the relationship between solar radiation and cloud amount were revealed. While similar non-linear trends in solar radiation were detected in all four seasons, corresponding long-term changes in cloud amounts were only observed in spring and summer. It is inferred that the dominant mechanism leading to the long-term change in solar radiation is different in the individual seasons.

1. Introduction

Variations in solar radiation reaching the Earth's surface have important impacts on the climate system. Changes in the surface radiative balance could lead to alteration in the atmospheric circulation pattern, hydrological and carbon cycle (Stanhill, 2005). The main aims of this study are to analyse the trends in annual and seasonal global solar radiation in Hong Kong and to identify possible causes of any trends observed. These are achieved by a statistical analysis of the relationship between solar irradiance and other meteorological variables.

2. Review on observed trends in solar radiation

Since the establishment of a global network measuring the Earth's radiation balance in the late 1950s, significant long-term changes in solar irradiance have been observed. These were characterized first by a widespread reduction of global solar radiation up to the 1980s, often known as 'global dimming'. Liepert (2002) estimated that the average global solar radiation worldwide decreased by 4 % from the 1960s to 1980s, while the decrease estimated by Stanhill and Moreshet (1992) was 5.3 % from 1958 to 1985. Such decline, however, was followed by an apparent reversal in solar irradiance or 'brightening' primarily in stations in the northern hemisphere from the 1990s onwards (Wild et al., 2005).

There are some evidence suggesting that the use of the word 'global' in describing 'dimming' or 'brightening' is not fully justified. Satellite data from 1983 to 2001 suggested that while there was a slight decrease in solar irradiance over land, the trend over the oceans was positive and significant (at 1 % level) (Pinker et al., 2005). In addition, Alpert et al. (2005) estimated that from 1964 to 1989, that 'dimming' trend in highly populated areas with population over 0.1 million was about 2.5 times the trend in sparsely populated areas. These observations show that changes in solar irradiance might actually be regional in nature, and therefore could be associated with meteorological processes in regional or even local scales.

Previous research, such as Liepert and Kukla (1997) and Stanhill and Ianetz (1997), have linked the observed dimming to changes in cloud cover and atmospheric transmittivity. These factors are in turn associated with the amount of moisture and the concentration of aerosols in the atmosphere (Liepert et al., 2004). The way how cloud cover affects solar radiation is not straightforward. It was suggested that the extent to which solar radiation is attenuated by clouds is a function of both cloud amounts

(Abakumova et al., 1996; Liepert, 2002) and cloud types (Angell, 1990; Liepert, 1997; Turner and Mujahid, 1984). The impacts of increased concentration of aerosols due to human emission on radiative fluxes are even more complex. Some of the major effects include (IPCC, 2001; Lohmann and Feichter, 2005):

(a) absorbing and scattering incoming solar radiation (direct effect);

(b) increasing the cloud albedo (first indirect effect);

(c) increasing the thickness, height, amount and life-time of clouds (second indirect effect);

(d) affecting relative humidity and vertical stability, thus affecting the environment of cloud formation (semi-direct effect).

In respect of dimming observed in China, Ren et al. (2005) estimated that the annual sunshine duration averaged over more than 400 stations in China decreased by 37.6 hours per decade. Such decrease mostly occurred in southeastern China. Qian et al. (2006) found that the average solar radiation at 537 stations in China decreased by 3.1 W m-2 or 1.9 % per decade from 1955 to 2000, but the total cloud cover also decreased by 0.33 % per decade in the same period. Haze associated with the increase in air pollution was identified by Qian et al. (2006) as the main cause of these seemingly conflicting trends.

3. Data and Methodology

The meteorological data analysed in this study included daily global solar radiation measured by the thermo-electric pyranometers at King's Park Meteorological Station (22.31°N, 114.17°E) and hourly cloud amount estimated by trained observers at the Hong Kong Observatory headquarters (22.30°N, 114.17°E) from 1961 to 2005. Fig. 4-1 shows a map of Hong Kong and the locations of the Hong Kong Observatory headquarters and the King's Park Meteorological Station. The daily daytime (0600h to 1800h local time inclusive) mean cloud amounts were calculated. Only about 0.8 % of the days studied contained one or more observations without cloud amount information during these hours. Such observations were mostly made when the sky was obscured by dense fog. This was assumed to be having very slight, if any, effects on the analysis.

Human observations of cloud amount are somewhat subjective. Comparing cloud cover data estimated by sunshine duration recorders with those made by weather observers, Hoyt (1977) found that human observers tend to over-estimate the cloud cover. To provide a more reliable estimate of cloud cover, data of bright sunshine duration measured by sunshine recorders at King's Park Meteorological Station were analysed. In addition, the numbers of 'clear' and 'overcast' days in each year were counted because clear and overcast skies could be more objectively determined (Qian *et al.*, 2006). In this study, a day was classified as 'clear' if the mean daytime cloud amount was less than or equal to 1 okta, while an 'overcast' day had the mean daytime cloud amount equal to or more than 7 oktas.

In order to identify the seasonal variation in aerosol loading over Hong Kong and its surroundings, monthly mean data of aerosol optical depth (AOD) at 0.55 μm over grids of $1° \times 1°$ in the region were obtained. These data were available from March 2000 to July 2006, and were derived from measurements made by MODIS (Moderate Resolution Imaging Spectroradiometer) onboard NASA's

EOS-Terra satellite (Chu *et al.*, 2002). Since these records are short, the percentage of time of reduced visibility at the Hong Kong Observatory headquarters from 1968 to 2005 was also used to give a rough and indirect measure of atmospheric transmittivity near the surface. Here, the time of reduced visibility is defined as the time during which the visibility is below 8 km, the relative humidity is below 95 %, and no fog, mist or precipitation is observed (Chang and Koo, 1986).

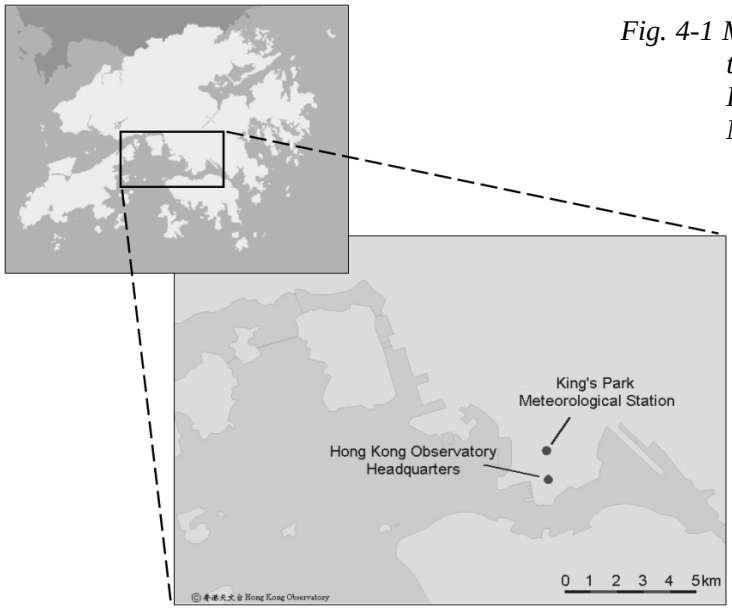

Fig. 4-1 Map of Hong Kong and the locations of the Hong Kong Observatory Headquarters and the King's Park Meteorological Station in Kowloon.

The trends of the above variables were investigated by fitting a linear regression model $Y = \beta_0 + \beta_1 x + \varepsilon$ using ordinary least squares (OLS). Y is the meteorological variable concerned, x is time in years with origin the first year of the time series, and ε represents the residuals, which are assumed to be Normal uncorrelated random variables. Higher order terms (x^2, x^3, ... with parameters β_2, β_3, ...) were fitted successively if non-linearity was observed from the residual diagnostic plots. The statistical significance of a trend parameter estimate is assessed by a two-tailed t-test on the ratio of the estimate and its standard error, with null hypothesis $H_0 : \beta = 0$ and alternative hypothesis $H_1 : \beta \neq 0$. The proportion of variation explained by each regression model is measured by the coefficient of determination R^2. The same form of model was fitted when examining the association among solar radiation, sunshine duration and cloud amount. Although Poisson regression is considered to be a more appropriate method when the response is in the form of counts (Dobson, 2001), simple linear regression method using OLS is still justified here when analysing the time trends of the number of 'clear' days and 'overcast' days. This is because in most cases (except for the seasonal number of 'clear' days), the counts are large enough so that the errors could be approximated by a Normal distribution.

4. Results

4.1 Annual trends

The trend parameter estimate $\hat{\beta}_1$ of the first order model fitted to the mean daily global solar radiation time series is –0.10 ± 0.01 (standard error) MJ m^{-2} $year^{-1}$ and is statistically significantly 1

% level ($p < 0.01$). Although 64 % of the variance is explained by this linear model, this is clearly inadequate to describe the long-term trend. After a sharp decline at a rate much larger than the global average in the 1960s and 70s, solar irradiance became generally steady from early 1980s onwards [Fig. 4-2(a)], but it is still not obvious that 'brightening' has occurred in the past decade. This non-linear behaviour explains why this trend parameter estimate is lower than that obtained (–0.16 MJ m^{-2} $year^{-1}$) in a previous analysis for the same location from 1958 to 1992 by Stanhill and Kalma (1995). The second order model with $\hat{\beta}_1 = -0.32 \pm 0.03$ MJ m^{-2} $year^{-1}$ and $\hat{\beta}_2 = 0.0047 \pm 0.0007$ MJ m^{-2} $year^{-2}$ (p-values both < 0.01) is more appropriate with the coefficient of determination increased to 83 %.

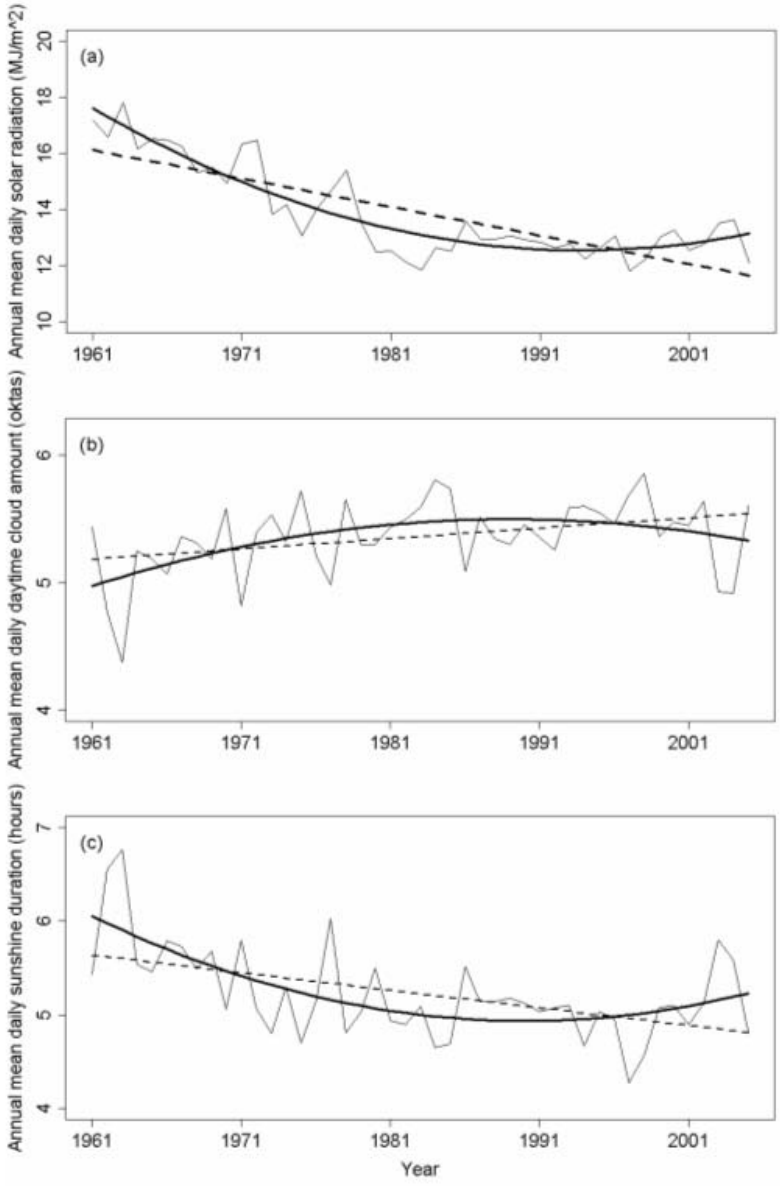

Fig. 4-2
Time series of annual mean daily (a) global solar radiation, (b) daytime cloud amount and (c) sunshine duration from 1961 to 2005. The dashed lines show the predicted values of the linear models fitted, while the thick solid lines show that of the second order models fitted.

The linear model fitted to the daytime cloud amount suggests that it increases at a rate of 0.008 ± 0.003 okta $year^{-1}$ [Fig. 4-2(b)]. This is different from zero at the 5 % level ($p = 0.01$), but the

coefficient of determination is only 13 %, indicating that the inter-annual variation is much larger than the long-term trend. Similar increasing trend in cloud amount is also observed in the study of Leung *et al.* (2004) (an increase of 0.18% per year) which took both daytime and nighttime cloud amounts into account. The second order model with $\hat{\beta}_1 = 0.04 \pm 0.01$ okta year^{-1} ($p < 0.01$) and $\hat{\beta}_2 = -0.0007 \pm 0.0003$ okta year^{-2} ($p = 0.01$) again provided a better fit on daytime cloud amount ($R^2 = 25$ %), showing that its increase has been leveling off after mid-1980s. It appears that there is a negative association in the time series between the daytime cloud amount and solar radiation. However as we will see later, a different statistical pattern evolves for different seasons.

The change in sunshine duration [Fig. 4-2(c)] with time is also best described by a second order model with $\hat{\beta}_1 = -0.08 \pm 0.02$ hour year^{-1} and $\hat{\beta}_2 = 0.0013 \pm 0.0003$ hour year^{-2} (p-values both < 0.01), which explains 42 % of the variation.

4.2 Seasonal trends

Highly significant decreasing trends (at 1 % level) in solar radiation are observed in all four seasons (Table 4-1). As shown in Figs. 4-3(a)(i), (a)(ii) and (a)(iv), 'dimming' in winter (DJF), spring (MAM) and autumn (SON) did not persist into the late 1980s, therefore the time trends are better described by quadratic models rather than linear models. Solar radiation in the summer (JJA), however, appears to decline linearly throughout the time series [Fig. 4-3(a)(iii)]. The situation for daytime cloud amount is more complex. No discernible significant trends are observed in the winter and autumn series [Figs. 4-3(b)(i) and (b)(iv)], both of which have larger inter-annual variability as indicated by the low coefficients of determination (Table 4-2). A non-linear trend is observed in the spring series [Fig. 4-3(b)(ii)], where the increase in cloud amounts leveled off after mid-1980s. A highly statistically significant (at 1 % level) but a modest increase (0.1 okta per decade) in daytime cloud amount is found in summer [Fig. 4-3(b)(iii)]. The time trends of sunshine duration are generally similar, but in the opposite sense to the trends of cloud amount series in each season [compare Figs. 4-3(b) and (c)].

4.3 Correlation between solar radiation and cloud amount

Changes in sunshine duration are well explained by the changes in daytime cloud amount (Fig. 4-4). The linear model explains 81 % of the variation with parameter estimates $\hat{\beta}_0 = 13.6 \pm 0.3$ hours and $\hat{\beta}_1 = -1.5 \pm 0.1$ hour okta^{-1} ($p < 0.01$). The strong association between sunshine duration and daytime cloud amount indicates that there is little difference between the uses of these two variables in studying the impact of cloud amount on solar radiation.

The scatter plots in Figs. 4-5 and 4-6 show the expected negative association between solar radiation and daytime cloud amounts annually and in different seasons respectively. When linear models, in which solar radiation is set as the response variable, are fitted to the daytime cloud amount data (Table 4-4), the slopes are more negative for spring and summer. This is not surprising considering the higher level of solar radiation in these two seasons due to a higher solar angle. The coefficient of determination is the highest in spring, suggesting the strongest relationship between solar radiation and cloud amount in this season.

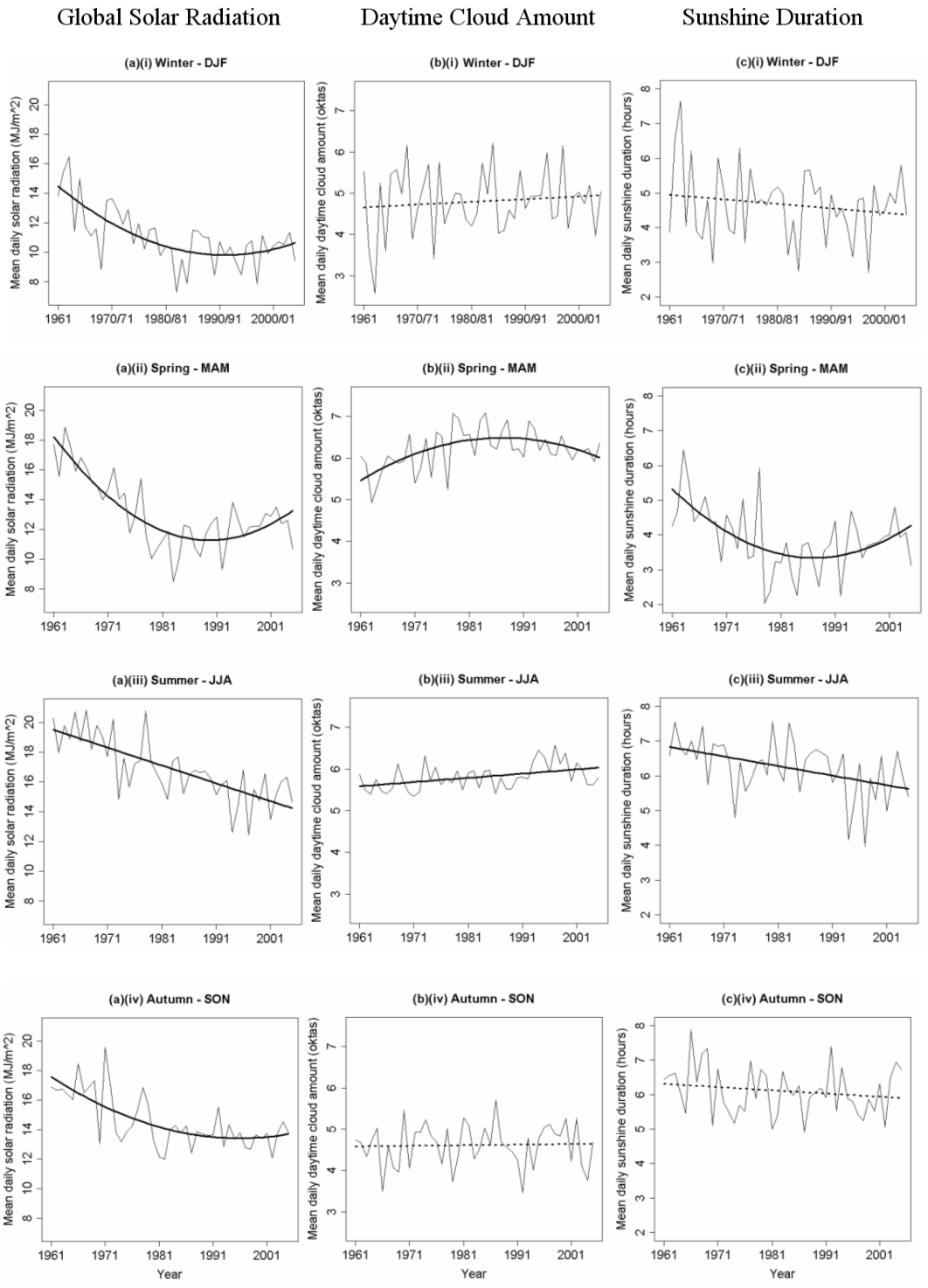

Fig. 4-3 Time series of seasonal mean daily (a) global solar radiation, (b) daytime cloud amount and (c) sunshine duration from 1961 to 2005. The thick solid lines show the best polynomial models fitted with parameters significantly different from zero at 5 % level, while the dotted lines represent non-statistically significant linear trends (at 5 % level). The values for the first points in the winter series (i) were calculated using only the data of Jan. and Feb. 1961.

Period	$\hat{\beta}_0$	$\hat{\beta}_1$ (linear)		$\hat{\beta}_2$ (quadratic)		R^2
		estimate	p	estimate	p	
Annual	17.9 (0.3)	–0.32 (0.03)	< 0.01	0.0047 (0.0007)	< 0.01	0.83
Winter	14.8 (0.7)	–0.31 (0.07)	< 0.01	0.005 (0.001)	< 0.01	0.50
Spring	18.7 (0.6)	–0.50 (0.06)	< 0.01	0.008 (0.001)	< 0.01	0.70
Summer	19.6 (0.4)	–0.12 (0.02)	< 0.01			0.56
Autumn	17.8 (0.6)	–0.24 (0.06)	< 0.01	0.003 (0.001)	0.01	0.50

Table 4-1 Parameter estimates with their standard errors in parentheses, p-values and coefficients of determination of models fitted to mean daily solar radiation time series for different seasons.

Period	$\hat{\beta}_0$	$\hat{\beta}_1$ (linear)		$\hat{\beta}_2$ (quadratic)		R^2
		estimate	p	estimate	p	
Annual	4.9 (0.1)	0.04 (0.01)	< 0.01	–0.0007 (0.0003)	0.01	0.25
Winter	4.7 (0.2)	0.007 (0.009)	0.47			0.01
Spring	5.4 (0.2)	0.08 (0.02)	< 0.01	–0.0015 (0.0004)	< 0.01	0.33
Summer	5.57 (0.09)	0.010 (0.003)	< 0.01			0.18
Autumn	4.6 (0.2)	0.001 (0.006)	0.81			0.001

Table 4-2 Same as Table 4-1, but for the mean daily daytime cloud amount time series.

Period	$\hat{\beta}_0$	$\hat{\beta}_1$ (linear)		$\hat{\beta}_2$ (quadratic)		R^2
		estimate	p	estimate	p	
Annual	6.1 (0.2)	–0.08 (0.02)	< 0.01	0.0013 (0.0003)	< 0.01	0.42
Winter	5.0 (0.3)	–0.01 (0.01)	0.28			0.03
Spring	5.5 (0.4)	–0.16 (0.04)	< 0.01	0.0029 (0.0008)	< 0.01	0.34
Summer	6.9 (0.2)	–0.028 (0.008)	< 0.01			0.20
Autumn	6.3 (0.2)	–0.009 (0.008)	0.26			0.03

Table 4-3 Same as Table 4-1, but for the mean daily sunshine duration time series.

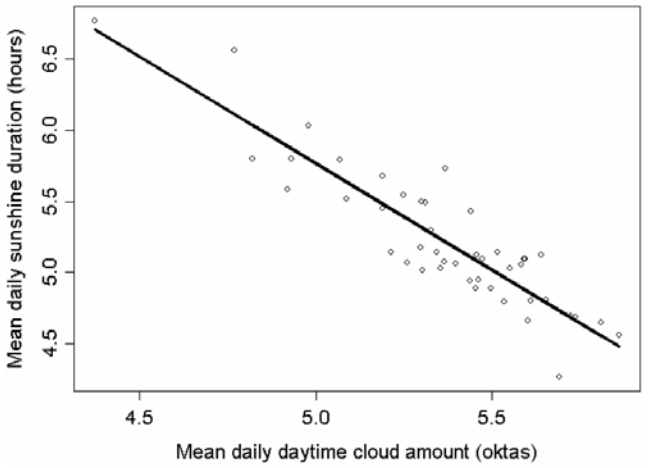

Fig. 4-4
Scatter plot of annual mean daily sunshine duration against that of daytime cloud amount (1961 to 2005). The linear regression line is overlaid.

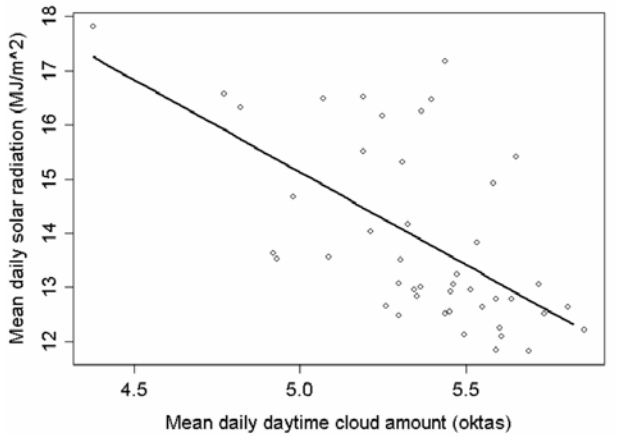

Fig. 4-5 Scatter plot of annual mean daily solar radiation against that of daytime cloud amount (1961 to 2005). The linear regression line is overlaid.

Period	$\hat{\beta}_0$	$\hat{\beta}_1$ (cloud)	R^2
Annual	32.2 (3.7)	–3.4 (0.7)	0.37
Winter	19.1 (1.3)	–1.7 (0.3)	0.46
Spring	37.2 (2.7)	–3.9 (0.4)	0.65
Summer	43.8 (4.4)	–4.6 (0.8)	0.47
Autumn	23.0 (2.1)	–1.8 (0.4)	0.28

Table 4-4. Parameter estimates with their standard errors in parentheses and coefficients of determination of linear regression models with solar radiation being the response, and daytime cloud amount being the explanatory variable in each season. The p-values of the slope parameter estimates are all < 0.01.

4.4 Trends in the frequency of clear and overcast days

The mean annual number of 'overcast' days (day with mean daytime cloud amount ≥ 7 oktas) was 116, compared to only 24 for 'clear' days (day with mean daytime cloud amount ≤ 1 okta). There was no significant trend in the annual number of 'clear' days at any reasonable level of significance. The trend parameter for the linear model fitted $\hat{\beta}_1$ is –0.14 ± 0.10 day year^{-1} (p = 0.16), but only 5

% of the variance is explained by this model. Similar to the annual mean daytime cloud amount [Fig. 4-2(b)], the number of 'overcast' days has quadratic dependence on time (Fig. 4-7). The parameters estimated are $\hat{\beta}_1 = 2.8 \pm 0.8$ days year^{-1} and $\hat{\beta}_2 = -0.05 \pm 0.02$ day year^{-2} (p-values both < 0.01). The coefficient of determination of this quadratic model is 33 %.

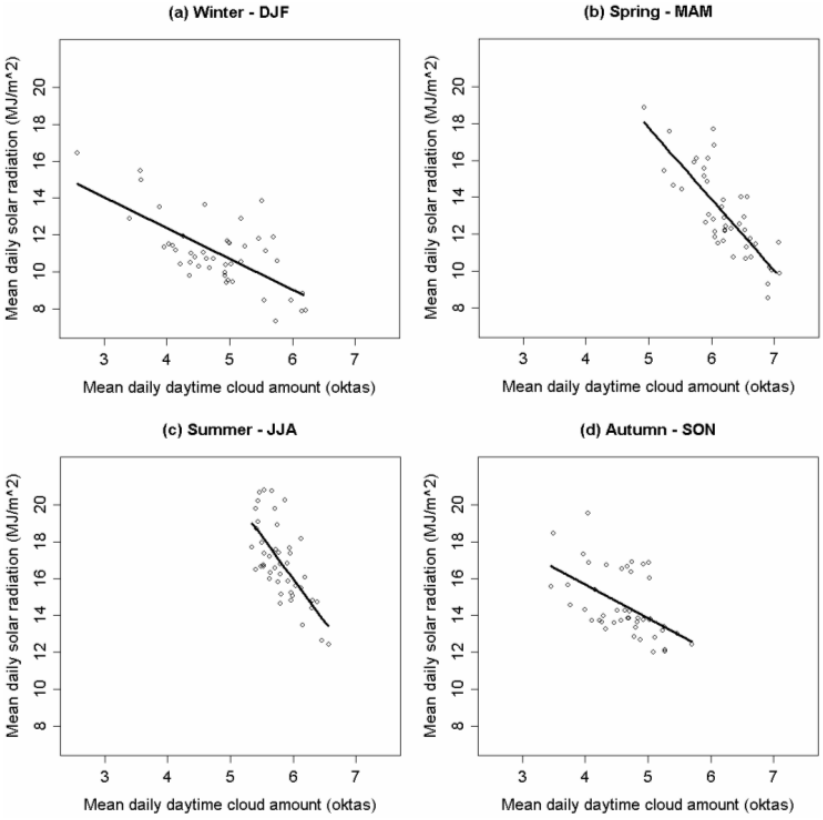

Fig. 4-6
Scatter plots of seasonal mean daily solar radiation against that of daytime cloud amount in each season (1961 to 2005). Linear regression lines are overlaid.

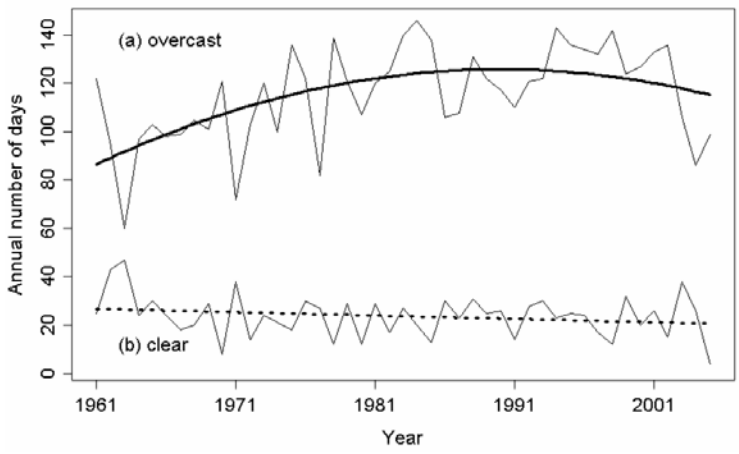

Fig. 4-7
Time series of annual number of (a) 'overcast' and (b) 'clear' days from 1961 to 2005. The solid line shows the predicted values of the second order trend line fitted to time series (a), while the dotted line shows the linear trend line (non-significant at 5 % level) fitted to time series (b).

The seasonal trends for the number of 'overcast' days are summarized in Table 4-5. They again generally agree well with the seasonal trends in cloud amount [compare Figs. 4-3(b) and 4-8], except that the number of 'overcast' days in winter has weak non-linear dependence on time, but the

quadratic trend term is not significant at 5 % level. The number of 'clear' days in each season is small; in particular only 8 'clear' days were recorded in 45 summers. As such, seasonal analyses for the number of 'clear' days were not attempted.

Season	$\hat{\beta}_0$	$\hat{\beta}_1$ (linear)		$\hat{\beta}_2$ (quadratic)		R^2
		estimate	p	Estimate	p	
Winter	19.2 (4.7)	1.0 (0.5)	0.04	–0.018 (0.010)	0.07	0.10
Spring	24.4 (4.4)	1.8 (0.4)	< 0.01	–0.034 (0.009)	< 0.01	0.32
Summer	21.1 (2.1)	0.26 (0.08)	< 0.01			0.19
Autumn	15.7 (2.0)	0.04 (0.08)	0.57			0.007

Table 4-5 Same as Table 4-1, but for the number of 'overcast' days for different seasons.

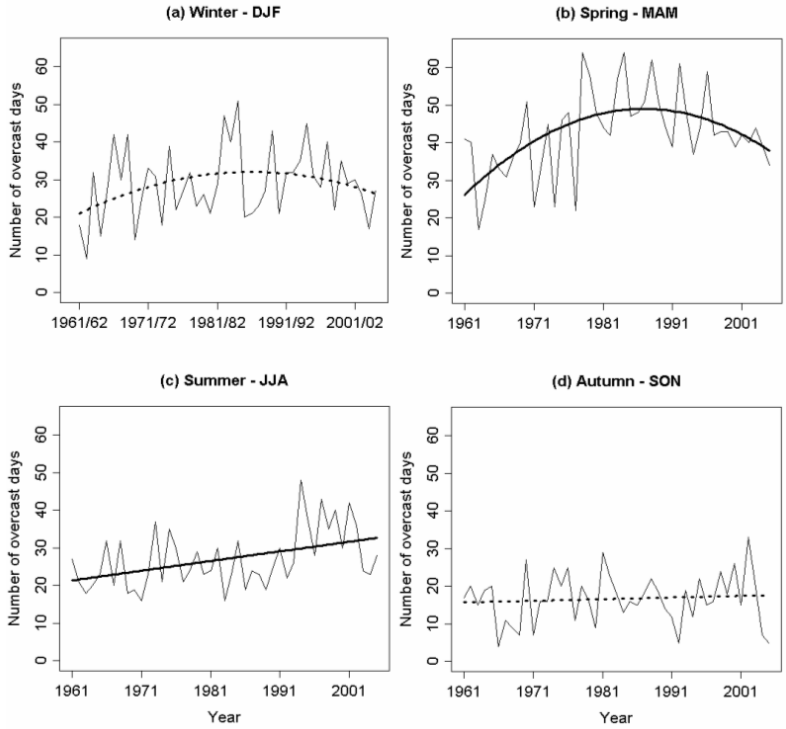

Fig. 4-8
Time series of the number of 'overcast' days in different seasons from 1961 to 2005. The solid lines show the trends significant at 5 % level, while the dotted lines show non-significant trends at 5 % level.

4.5 MODIS AOD data

Seasonal variation of aerosol optical depth over Hong Kong is presented in Fig. 4-9. The highest values of AOD are found in the spring months, and the lowest values are found in the winter months. Similar variations are also observed at the land grid to the north of Hong Kong. For the sea grid to the south of Hong Kong, the AOD values were in general lower than those over land, in particular in

the summer months when maritime airstream dominated.

4.6 Trends in visibility

The duration of reduced visibility at the Hong Kong Observatory headquarters has risen rapidly and at an increasing rate since the mid-1980s (Fig. 4-10). Such trend is best described by a cubic polynomial model with $\hat{\beta}_1 = 0.4 \pm 0.2$ % year^{-1} (p = 0.08), $\hat{\beta}_2 = -0.03 \pm 0.01$ % year^{-2} (p = 0.02) and $\hat{\beta}_3 = 0.008 \pm 0.002$ % year^{-3} (p < 0.01). The coefficient of determination is 88 %. There are no noticeable differences among the time trends for individual seasons (not shown). It is worth noting from Fig. 4-11 that January to April has the longest duration of reduced visibility and hence possibly the lowest atmospheric transmittivity near the surface, while June and July has the shortest duration with reduced visibility.

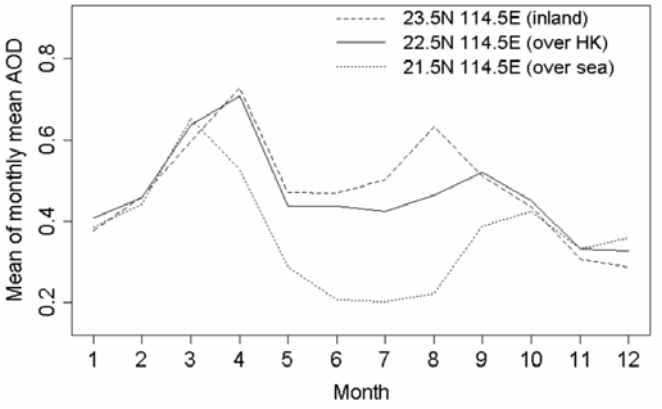

Fig. 4-9
Variation of the mean value of monthly mean aerosol optical depth (AOD) derived by MODIS measurements from March 2000 to July 2006 in the 1° 1° grid centred over 22.5°N, 114.5°E (covering Hong Kong) in solid line, 23.5°N, 114.5°E (covering parts of inland Guangdong) in dashed line, and 21.5°N, 114.5°E (covering the seas south of Hong Kong) in dotted line.

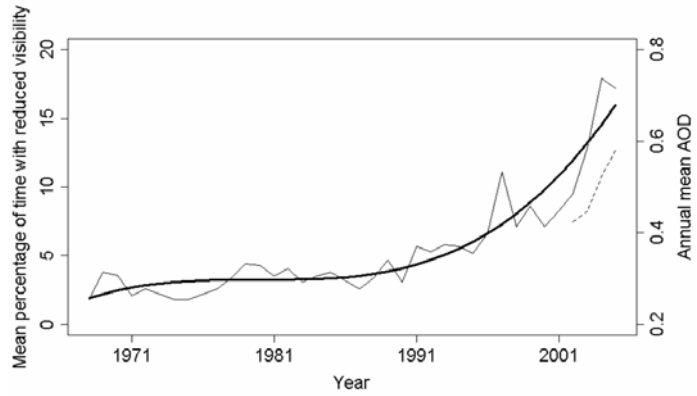

Fig. 4-10
Time series of mean percentage of time with reduced visibility at the Hong Kong Observatory headquarters from 1968 to 2005. The predicted values of a third order polynomial regression model is overlaid. [The dashed line shows the change of annual mean AOD in the grid covering Hong Kong from 2002 to 2005. The means for 2000, 2001 and 2006 were not calculated, as the data were incomplete.]*

*Note: * The time of reduced visibility is defined as the time during which the visibility is below 8 km, the relative humidity is below 95% and no fog, mist or precipitation is observed.*

5. Discussion

The long-term change in global solar radiation in Hong Kong is similar to that observed at a number of Asian and European sites, where from late 1980s onwards, the decrease in solar radiation levelled off, or in some cases, 'brightening' occurred (Wild *et al.*, 2005). The annual trend of solar radiation observed in Hong Kong appears to be well explained by the corresponding change in daytime cloud

cover, i.e. an increase up to the mid-1980s followed by a decrease. However, our seasonal analyses indicate a far more complex situation. Even though solar radiation decreased significantly during the 1960s and 1970s in all four seasons, significant increases in daytime cloud amounts were only observed in spring and summer. There were no discernible trends in cloud amounts in winter and autumn over the past 45 years. The changes in the number of 'overcast' days (day with mean daytime cloud amount ≥ 7 oktas) for each season, which are considered to be more reliable measures of cloud cover change, show similar results. This suggests that such differences are unlikely to be caused by biases or errors by individual human observers over the years. It is more likely that the dominant mechanism leading to changes in solar radiation is different in the individual seasons.

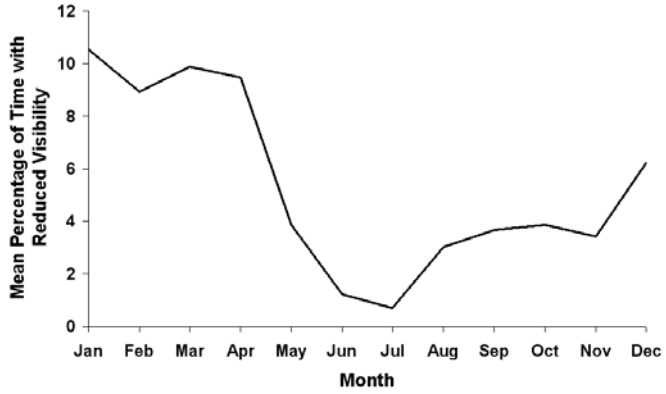

Fig. 4-11
Variation of the Mean Percentage of Time with Reduced Visibility at the Hong Kong Observatory headquarters from 1968 to 2005.*

*Note: * The time of reduced visibility is defined as the time during which the visibility is below 8 km, the relative humidity is below 95% and no fog, mist or precipitation is observed.*

Cloud cover has the most obvious and dominant effect on the solar radiation received at ground level. The strong correlation between the trends of solar radiation and daytime cloud amounts in spring and summer is evident. The mean amounts of daytime cloud cover in these two seasons (spring: 6.2 oktas; summer: 5.8 oktas for the period 1961 – 2005) are higher than those in autumn (4.6 oktas) and winter (4.8 oktas). Such effect dominates over other effects, such as the direct aerosol effect to be discussed below.

Atmospheric transmittivity is another important factor in determining the degree of attenuation of incoming solar radiation. In this investigation, two measures, satellite-derived AOD and horizontal visibility observed by trained observers on the ground, have been used. Aerosol optical depth has the advantage that it takes into account the whole column of air rather than a thin layer of atmosphere near the ground where visibility is estimated. However, AOD data period is short as the data only became available recently. A conclusive trend analysis using AOD is still not possible though it appears in Fig. 4-10 that AOD follows the trend of reduced visibility in the recent few years where data are available.

Rainfall pattern could be one of the reasons for the seasonal differences in the relationships between solar radiation and daytime cloud amount. The wash-out process is very complex. It depends on a number of factors such as the types, duration, intensity and rate of the precipitation, atmospheric stability as well as the nature and sizes of the aerosols in the atmosphere. The present study will not go deep into the wash-out process, but in general longer rain duration will be more effective in scavenging aerosols in the atmosphere. The average rain durations in Hong Kong (data from 1961 to 1990) in different seasons are 154 hours (winter), 279 hours (spring), 262 hours (summer) and 154 hours (autumn) (Hong Kong Observatory 2006). In the autumn and winter seasons in Hong Kong, which have shorter rain duration, it is considered that aerosols could remain in the atmosphere for a longer time, so that incoming solar radiation could be more effectively scattered. As a result, the

direct aerosol effect will have more weight in these two seasons, and the association between solar radiation and cloud amount is weaker. With longer rain duration in spring and summer, the direct aerosol effect is less prominent, and changes in solar radiation are related more closely to changes in cloud amount. This is somewhat similar to the situation in the intertropical convergence zone, where the smaller decline in solar radiation observed compared to other regions is believed to be linked to higher rainfall in the equatorial region (Alpert *et al.*, 2005).

Apart from the changes to the hydrological cycle in a global warming situation, a number of factors could contribute to long-term changes in cloud amount. For example, increasing jet traffic may lead to an increase in the frequency of cirrus clouds, while variations in the synoptic pattern and sea surface temperatures affect convective activity, and hence cloudiness (Angell *et al.*, 1984; Liepert, 1997). It is therefore difficult to determine the extent to which cloud-aerosol interactions (indirect aerosol effects) affect the amount of solar radiation received in Hong Kong. Adding to this complexity is the urbanization of the measurement site. There have been substantial developments around King's Park Meteorological Station in recent years and such urbanization effect has clear impacts on the measurement of other meteorological parameters such as winds and evaporation at the site (Chan, 2007). It is likely that urbanization could have effect on the measurement of global solar radiation at King's Park Meteorological Station. Nevertheless, given the strong association between solar radiation and cloud amounts in spring and summer, it is plausible to suggest that if the intensity of solar radiation reaching the ground is dependent on aerosol concentration, the indirect aerosol effects, such as the changes in cloud thickness and albedo, are likely to dominate over the direct aerosol effects in these two seasons.

Alpert *et al.* (2005) and Wild *et al.* (2005) speculated that the implementation of clean-air regulations, the decline of the eastern European economy in the late 1980s and the recovery of aerosol loadings from the Pinatubo explosion in 1991 lead to the observed reversal from dimming in various sites in the 1990s. Such explanations could not fully explain the observed trends in Hong Kong. Luo *et al.* (2001) found that the aerosol optical depth (AOD) at 0.75 μm averaged over 4 stations in southern China increased by about 40 % from 1961 to 1990. Our visibility data (Fig. 4-10) suggest a sharp decrease in atmospheric transmittivity near the surface from the early 1990s onwards. The short record of satellite-derived AOD also showed signs of increase in the past few years. Combined with the fact that human emission of aerosol precursors in southern China was still increasing in the 1990s (Qian *et al.*, 2006), it is quite likely that the aerosol loading in the region has not decreased.

Study showed that there was a high correlation between visibility and PM2.5 concentration (one of the indicators of aerosol loading) at surface level in Hong Kong (Leung *et al.*, 2007). However, we should keep in mind that routine visibility observations only consider the surface layer of the atmosphere, so any effects of aerosols higher up in the atmosphere could not be represented by the visibility reading alone. Another point is that there was no significant change in 'reduced' visibility in Hong Kong during the 1970s, when the 'dimming' trend was already apparent. But one should also note that the possible change in visibility for ranges over 8 km has not been taken into account in the study. Increase in aerosol loading for such changes in visibility at the higher end (> 8 km) may already have significant impact to the solar radiation reaching the surface. Therefore, without any homogeneous AOD data for our region in the 1990s when the annual mean solar radiation became steady, it is not possible yet to explain this recent trend with confidence.

Impacts of the changes in the world's climate to the local environment are evident (Lam, 2006). The present study attempts to link up the trends in global solar radiation with other meteorological

parameters. It is understandable that the relationships between different parameters are complex and hard to be explained simply by one-to-one corresponding relations. Notwithstanding this, further studies in revealing such complex relationships will allow meteorologists to better understand the mechanisms and may possibly help us to prepare for the impacts brought by climate changes.

6. Conclusions

The annual mean solar radiation in Hong Kong is found to have quadratic dependence on time, with the decline occurring in the 1960s and 70s leveling off from early 1980s onwards. This is similar to the trends observed in other parts of the world.

The most important finding in this study is the seasonal differences in the trends of solar radiation and daytime cloud amounts. Though decreasing trends similar to the annual trend are observed in solar radiation in all four seasons, the trends for daytime cloud amount are not quite the same in different seasons. There are no discernible trends in daytime cloud amount in autumn and winter. However, a non-linear trend is observed in spring with the increase leveling off after mid-1980s whereas a linear increasing trend is found in summer.

It is likely that the dominant effect of aerosols in affecting the amount of solar radiation reaching the ground is different in the individual seasons. In spring and summer, the solar radiation has a stronger dependence on daytime cloud amount whereas the weaker association between solar radiation and daytime cloud amount in winter and autumn suggests that changes in solar radiation are more likely to be caused by the direct aerosol effect.

The non-availability of adequate data is the major limitation in this study. Firstly, the degree of attenuation of solar radiation might be affected by changes in the occurrence of different cloud types in addition to the cloud amount. Secondly, changes in the atmospheric transmittivity could not be accurately estimated because long homogeneous records of AOD and the direct and diffuse components of solar radiation were not available. These data will certainly be needed in future investigations in order to gain a better understanding of the causes leading to variations of solar radiation reaching the ground.

Acknowledgements

The MODIS AOD data used in this study were acquired as part of the NASA's Earth Science Enterprise. The algorithms were developed by the MODIS Science Teams. The data were processed by the MODIS Adaptive Processing System (MODAPS) and Goddard Distributed Active Archive Center (DAAC), and are archived and distributed by the Goddard DAAC. In addition, the authors would like to thank Mr. C.Y. Lam, Drs. B.Y. Lee, C.M. Cheng and T.C. Lee of the Hong Kong Observatory for their comments on the manuscript.

References

Abakumova, G.M., E.M. Feigelson, V. Russak and V.V. Stadnik (1996) Evaluation of long-term changes in radiation, cloudiness, and surface temperature on the territory of the former Soviet Union. *J. Climate*, **9**, 1319-1327.

Alpert, P., P. Kishcha, Y.J. Kaufman and R. Schwarzbard (2005) Global dimming or local dimming?: Effect of urbanization on sunlight availability. *Geophys. Res. Lett.*, **32**, L17082.

Angell, J.K. (1990) Variation in United States cloudiness and sunshine duration between 1950 and the drought year of 1988. *J. Climate*, **3**, 296-308.

Angell, J.K., J. Korshover and G.F. Cotton (1984) Variation in United States cloudiness and sunshine, 1950-82. *J. Clim. Appl. Meteor.*, **23**, 752-761.

Chan, J.K.W. (2007) Pan Evaporation in Hong Kong. *Weather*, **62**, 147-153.

Chang, W.L. and E. Koo (1986) A study of visibility trends in Hong Kong. *Atmos. Environ.*, **20**, 1847-1858.

Chu, D.A., Y.J. Kaufman, C. Ichoku, L.A. Remer, D. Tanré and B.N. Holben (2002) Validation of MODIS aerosol optical depth retrieval over land. *Geophys. Res. Lett.*, **29**, 8008.

Dobson, A.J. (2001) *An Introduction to Generalized Linear Models*. Chapman & Hall/CRC, London.

Hong Kong Observatory (2006) Summary of Meteorological Observations in Hong Kong 2005

Hoyt, D.V. (1977) Percent of possible sunshine and the total cloud cover. *Mon. Wea. Rev.*, **105**, 648-652.

IPCC (2001) *Climate change 2001: The scientific basis: Contribution of Working Group I to the Third Assessment Report of the Intergovernmental Panel on Climate Change*. J.T. Houghton *et al.* (eds) IPCC, Geneva.

Lam, C.Y. (2006) On Climate Changes Brought About by Urban Living. *HKMetS Bulletin*, **16**, 15-20.

Leung, Y.K., K.H. Yeung, E.W.L. Ginn and W.M. Leung (2004) Climate change in Hong Kong. *Hong Kong Observatory Technical Note No. 107*.

Leung, Y.K., M.C. Wu, K.K. Yeung (2007) A preliminary study on the relationship between visibility and atmospheric suspended particulate concentration in Hong Kong. *21st Guangdong-HongKong-Macau Seminar on Meteorological Science and Technology* (in Chinese)

Liepert, B.G. (1997) Recent changes in solar radiation under cloudy conditions in Germany. *Int. J. Climatol.*, **17**, 1581-1593.

Liepert, B.G. (2002) Observed reductions of surface solar radiation at sites in the United States and worldwide from 1961 to 1990. *Geophys. Res. Lett.*, **29**, 61.

Liepert, B.G. and G.J. Kukla (1997) Decline in global solar radiation with increased horizontal visibility in Germany between 1964 and 1990. *J. Climate*, **10**, 2391-2401.

Liepert, B.G., J. Feichter, U. Lohmann and E. Roeckner (2004) Can aerosols spin down the water cycle in a warmer and moister world? *Geophys. Res. Lett.*, **31**, L06207.

Lohmann, U. and J. Feichter (2005) Global indirect aerosol effects: a review. *Atmos. Chem. Phys.*, **5**, 715-737.

Luo, Y., D. Lu, X. Zhou, W. Li and Q. He. Characteristics of the spatial distribution and yearly variation of aerosol optical depth over China in the last 30 years. *J. Geophys. Res.*, **106**, 14501-14513.

Pinker, R.T., B. Zhang and E.G. Dutton (2005) Do satellites detect trends in surface solar radiation? *Science*, **308**, 850-854.

Qian, Y., D.P. Kaiser, R. Leung and M. Xu (2006) More frequent cloud-free sky and less surface solar radiation in China from 1955 to 2000. *Geophys. Res. Lett.*, **33**, L01812.

Ren, G. Y., J. Guo, M. Xu, Z. Chu, L, Zhang, X. Zhou, Q. Li and X. Liu (2005) Climate changes of China's mainland over the past half century. *Acta Meteorologica Sinica*, **63**, 942-956 (in Chinese).

Stanhill, G. (2005) Global dimming: A new aspect of climate change. *Weather*, **60**, 11-14.

Stanhill, G. and A. Ianetz (1997) Long-term trends in, and the spatial variation of, global irradiance in Israel. *Tellus*, **49B**, 112-122.

Stanhill, G. and J.D. Kalma (1995) Solar dimming and urban heating in Hong Kong. *Int. J. Climatol.*, **15**, 933-941.

Stanhill, G. and S. Moreshet (1992) Global radiation climate change: the world network. *Clim. Change*, **21**, 57-75.

Turner, W.D. and A. Mujahid (1984) The estimation of hourly global solar radiation using a cloud cover model developed at Blytheville, Arkansas. *J. Clim. Appl. Meteor.*, **23**, 781- 786.

Wild, M., H. Gilgen, A. Roesch, A. Ohmura, C.N. Long, E.G. Dutton, B. Forgan, A. Kallis, V. Russak and A. Tsvetkov (2005) From dimming to brightening: Decadal changes in solar radiation at Earth's surface. *Science*, **308**, 847-850.

Presentation of Zhu Kezhen Prize (竺可禎獎)

Dr. Martin L.M. Wong from Department of Physics and Materials Science, City University of Hong Kong, won the award for his research paper titled "Tropical Cyclone Motion in response to Land Surface Friction". The paper was published in Journal of the Atmospheric Sciences in 2006. The jury for the Zhu Kezhen Prize this year consisted of Dr. K.S. Lam from Hong Kong Polytechnic University, Dr. Alexis K.H. Lau from Hong Kong University of Science and Technology and Dr. H.Y. Lam from Hong Kong Observatory. The jury opined that although the studies of Dr. Wong were based on idealized tests, the deduction and scientific meaning were all clear and persuasive. The work of Dr. Wong was of high quality and usefulness and would form valuable reference of the subject concerned.

The prize presentation ceremony took place on 28 September 2007 in the Annual General Meeting of the Society. Since Dr. Wong and his supervisor Prof. Johnny Chan were not in Hong Kong on the

day, Prof. M.A. Van Hove, Head of Department of Physics and Materials Science, City University of Hong Kong, received the prize for Dr. Wong and Dr Zhou Wen presented the winning paper.

Prof. M.A. Van Hove (left), Head of Department of Physics and Materials Science, City University of Hong Kong, received Zhu Kezhen Prize for Dr. Martin L.M. Wong from Society Vice Chairman Dr. K.S. Lam (right).

Dr. K.S. Lam (left) presenting souvenir to Dr. Zhou Wen (right) from Department of Physics and Materials Science, City University of Hong Kong, to thank her for presenting Dr. Martin L.M. Wong's winning paper.

'Climate Change' Painting and Web Page Design Competition organized by Hong Kong Meteorological Society in collaboration with the Hong Kong Society for Education in Art and Hong Kong Education City

A competition was organized in collaboration with the Hong Kong Society for Education in Art and Hong Kong Education City in 2007, for both primary and secondary school students to represent their concerns for climate change by painting and web page respectively. Again it received very enthusiastic support from schools. The prize-giving ceremony was conducted on 15 September 2007. The following colour pages show the winning entries of the competitions.

香港氣象學會主辦　香港美術教育協會及香港教育城協辦
「氣候轉變」繪畫比賽(小學組)及網頁設計比賽(中學組)

香港氣象學會、香港美術教育協會及香港教育城在 2007 年舉辦了「氣候轉變」繪畫比賽(小學組)及網頁設計比賽(中學組)，讓同學們利用圖畫或網頁來表達對氣候轉變的關注。比賽如往年一般反應熱烈，頒獎典禮已於 2007 年 9 月 15 日舉行。下頁是得獎作品。

「氣候轉變」繪畫比賽(小學組)冠亞季軍作品
'Climate Change' – Painting competition for primary school students

Champion
冠軍
潘卓基
浸信會呂明才小學

First Runner-up
亞軍 馬彬 馬頭涌官立小學〔紅磡灣〕

Second Runner-up
季軍 唐穎琳 瑪利諾修院學校〔小學部〕

優異獎作品 Merit Prize

蔡子堯 慈幼學校

陳雪瑩 馬頭涌官立小學〔紅磡灣〕

黃冠之 聖公會聖雅各小學〔下午校〕

李思慧
佛教榮茵學校〔上午校〕

譚卓文 東華三院鄧肇堅小學

張肇桓 循道學校

曾詠兒 伊斯蘭學校

朱芷晴 拔臣小學

林淑君 聖公會聖雅各小學〔下午校〕

陳夕欣 路德會梁鉅鏐學校

袁樂知
香港真光中學〔小學部〕

許翹 浸信會呂明才小學

「氣候轉變」網頁設計比賽(中學組)得獎作品

'Changing Weather' – Web page design competition for secondary school students

Champion
冠軍 陳均漢
中華基督教會蒙民偉書院

First Runner-up
亞軍 林杰勇
中華基督教會全完中學

Second Runner-up
季軍 陳佩容
瑪利諾神父教會學校

鍾慧賢 瑪利諾神父教會學校

劉嘉誠
中華基督教會全完中學

優異獎作品
Merit Prize

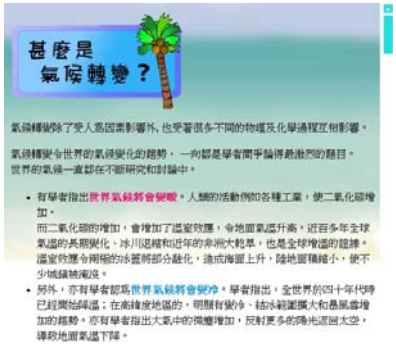

陳嘉賢 麗澤中學

林慧懿 旅港開平商會中學

甄三育 香港三育中學

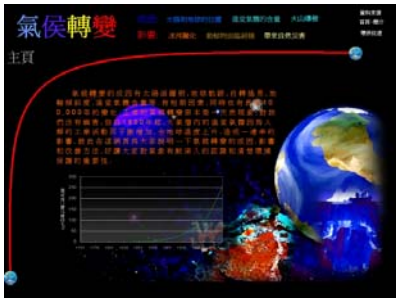

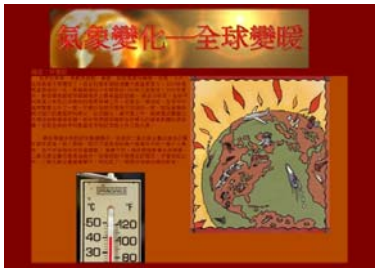

COLOUR PLATES

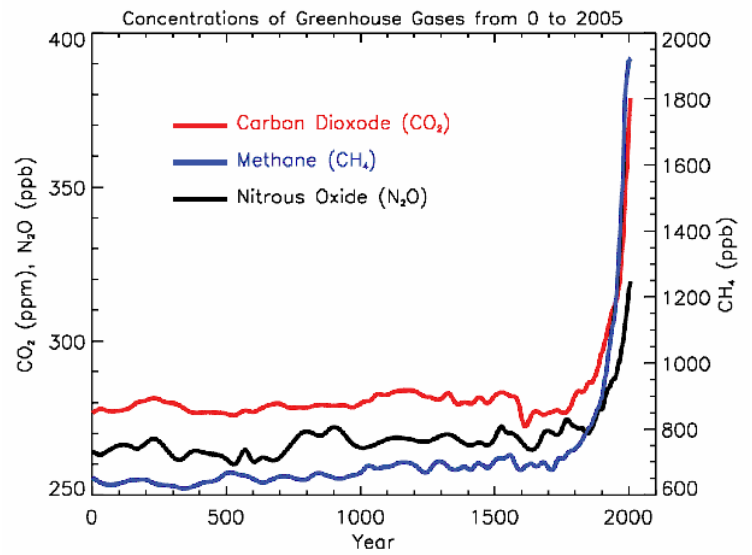

Fig. C1-1 Variations of atmospheric concentrations of carbon dioxide, methane and nitrous oxide during the last 2000 years, in units of parts per million (ppm) or parts per billion (ppb). Source: IPCC AR4 Report.

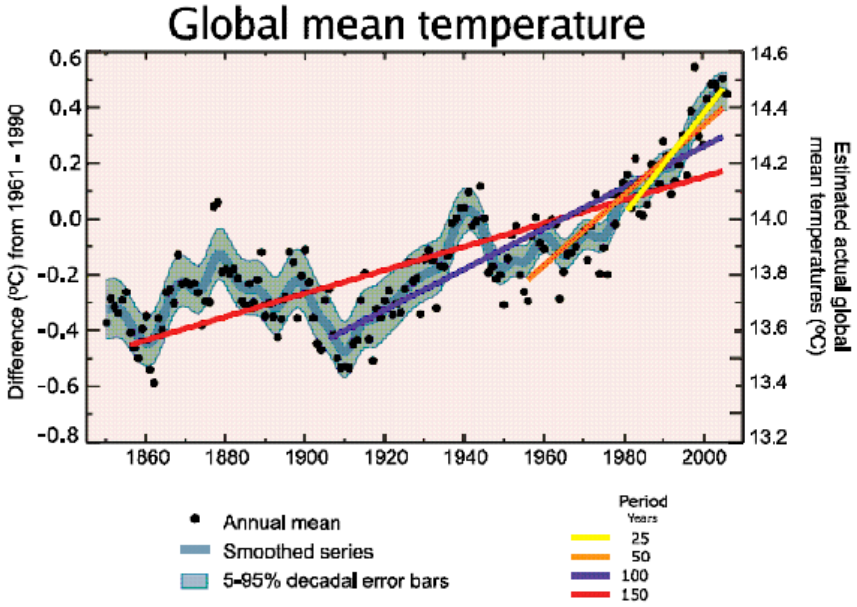

Fig. C1-2 Variations of annual global mean surface temperatures (black dots) as observed from 1850 to present. Left axis shows departures from 1961-1990 average. Right axis shows actual temperatures. Blue curve indicates smoothed variations with time scales longer than a decade. Pale blue band centered on that curve indicates the extent of the 5-95% decadal error bars. Yellow, orange, magenta and red segments represent slopes of linear trends for the last 25, 50, 100 and 150 years, respectively. Source: IPCC AR4 Report.

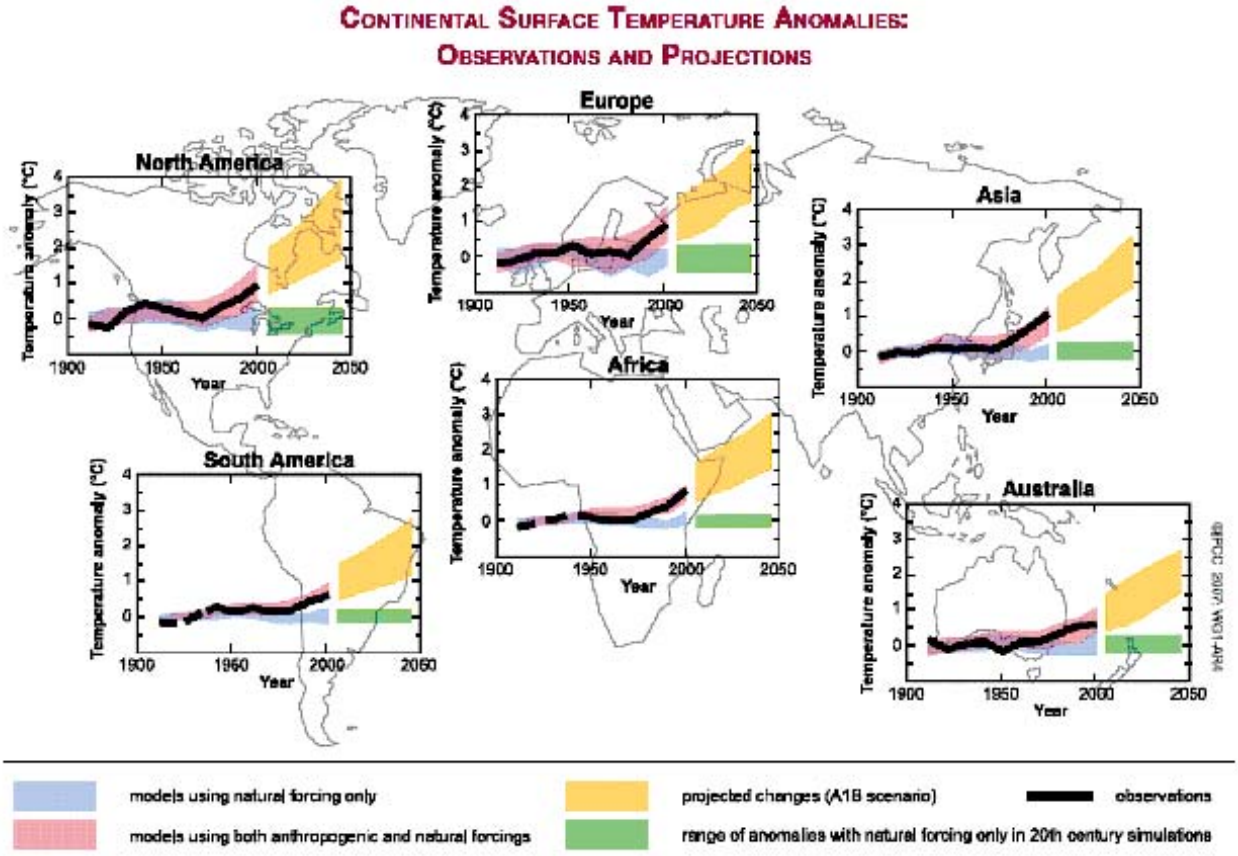

Fig. C1-3 Variations of decadal mean surface temperatures over different continents, as deduced from observations and model simulations for 1906-2005, and from model projections for 2001-2050. All values represent departures from 1901-1950 average. Black lines indicate observations. Blue bands show the 5th-95th percentile range of responses in different models to natural forcings only. Red bands show the corresponding range of model responses to anthropogenic and natural forcings. Yellow bands depict the 5th-95th percentile range of model projections based on the A1B emission scenario. Green bars provide a measure of natural variability, as inferred from model simulations for the 20th century with natural forcings only. Source: IPCC AR4 Report.

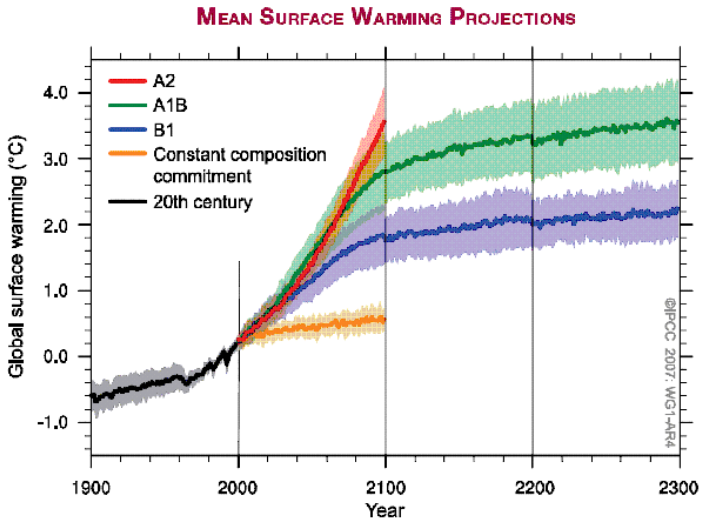

Fig. C1-4 Variations of annual global mean surface temperatures, as simulated by various models using natural and anthropogenic forcings for the 20th century (black curve), and as projected by some of these models on the basis of 21st century scenarios B1 (blue curve), A1B (green curve) and A2 (red curve). Projections based on the B1 and A1B scenarios, with forcings fixed at the 2100 level, are extended to the 22nd and 23rd centuries. Projections for the 21st century, with forcings fixed at the 2000 level, are shown using the orange curve. All temperature values represent departures from the 1980-1999 average. Curves show averages over all available model simulations or projections. Shaded bands centered on these curves indicate the ranges for ± one standard deviation of the results from individual models. Source: IPCC AR4 Report.

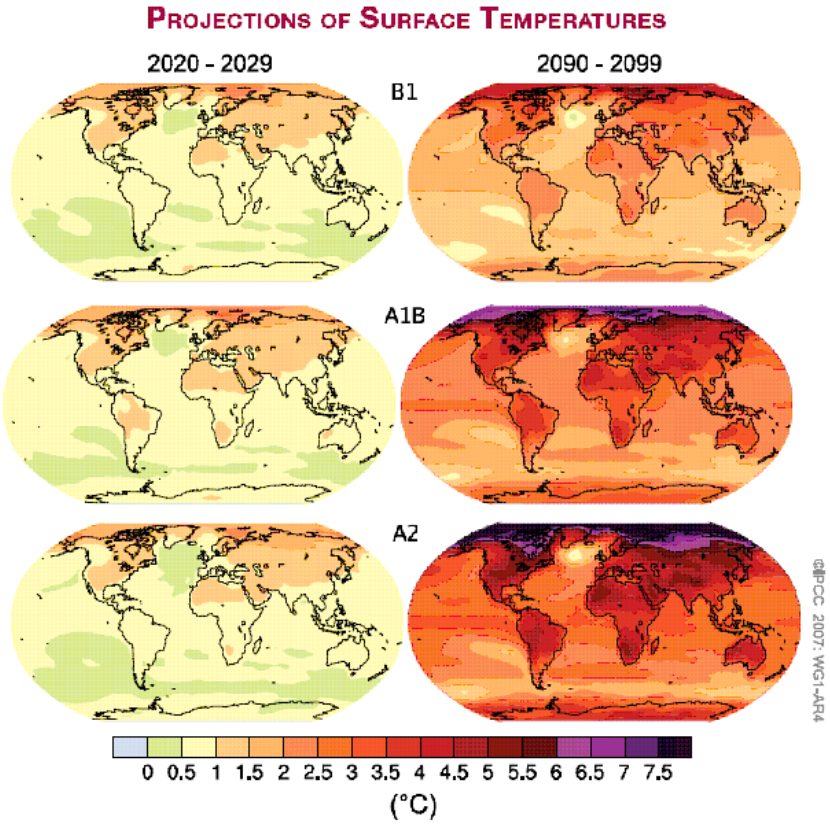

Fig. C1-5 Distributions of the projected surface temperature changes in 2020-2029 (left panels) and in 2090-2099 (right panels), as obtained by averaging the results from individual models based on emission scenarios B1 (top), A1B (middle) and A2 (bottom). All values represent departure from the 1980-1999 average. Source: IPCC AR4 Report.

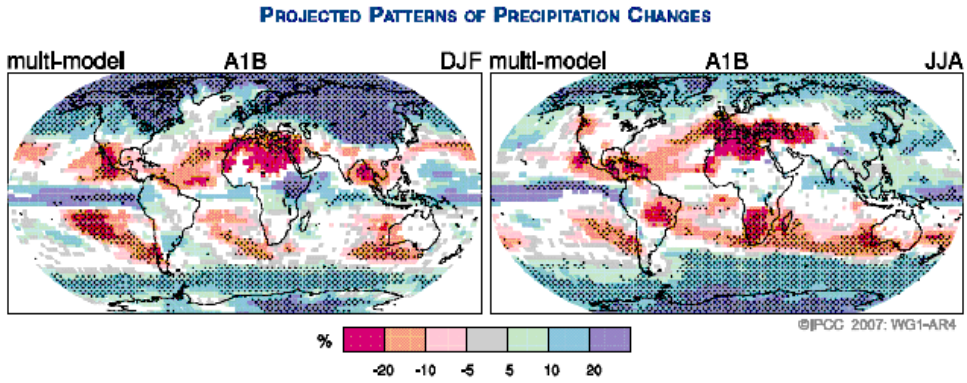

Fig. C1-6. Distributions of the projected precipitation changes (in percent) in 2090-2099, as obtained by averaging the results from individual models for the December-January-February (left panel) and June-July-August (right panel) seasons in the A1B scenario. All values represent departure from the 1980-1999 average. Regions where more than 90% of the models project changes with the same polarity are stippled. Regions where less than 66% of the models project the same polarity are left blank. Source: IPCC AR4 Report.

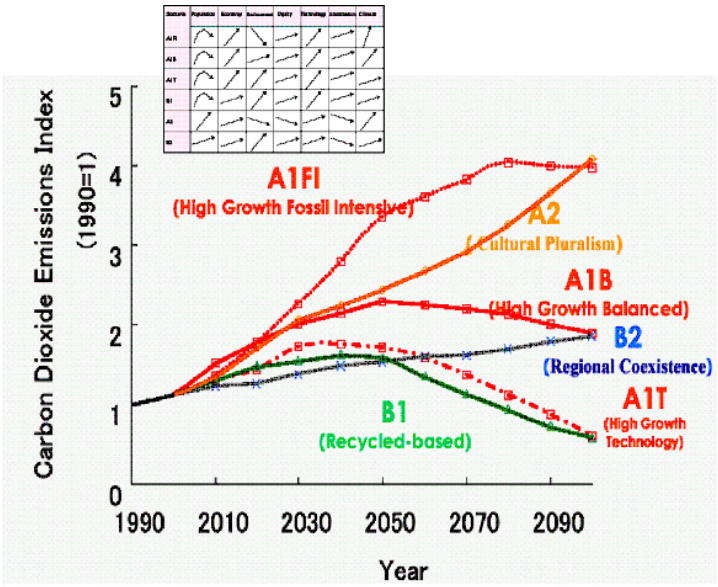

Fig. C2-1. Projections of carbon dioxide emission under the six SRES emission scenarios. The inset reflects the various assumptions made on the future population, economy, technology, energy and land use patterns of the world (source from IPCC).

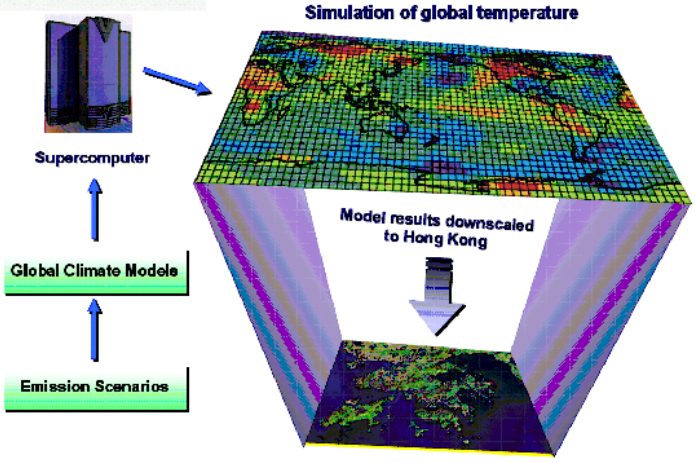

Fig. C2-2. Schematic diagram showing the methodology for temperature projections.

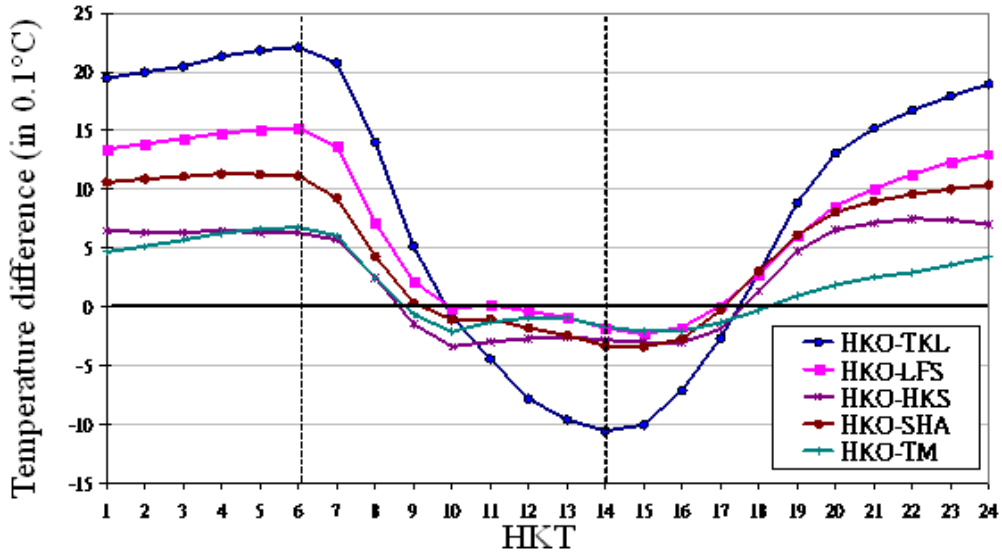

Fig. C2-3. Mean temperature difference between HKO and the stations Ta Kwu Ling (TKL), Lau Fau Shan (LFS), Hong Kong South (HKS), Shatin (SHA) and Tuen Mun (TM) respectively for each hour (1989-2006).

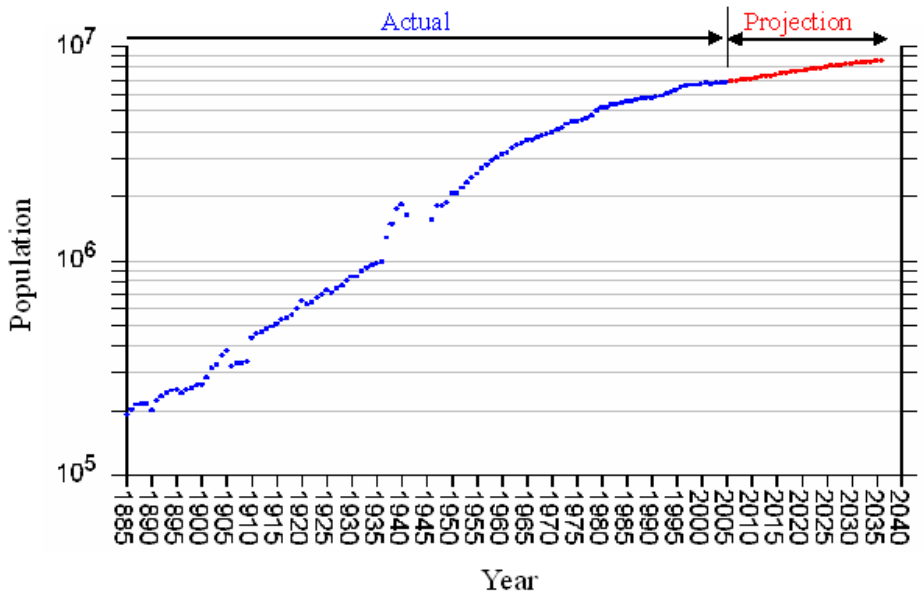

Fig. C2-5 Time series of the population (in logarithm scale) in Hong Kong (1885-2036). Blue curve represents past actual data and red curve the projected data.

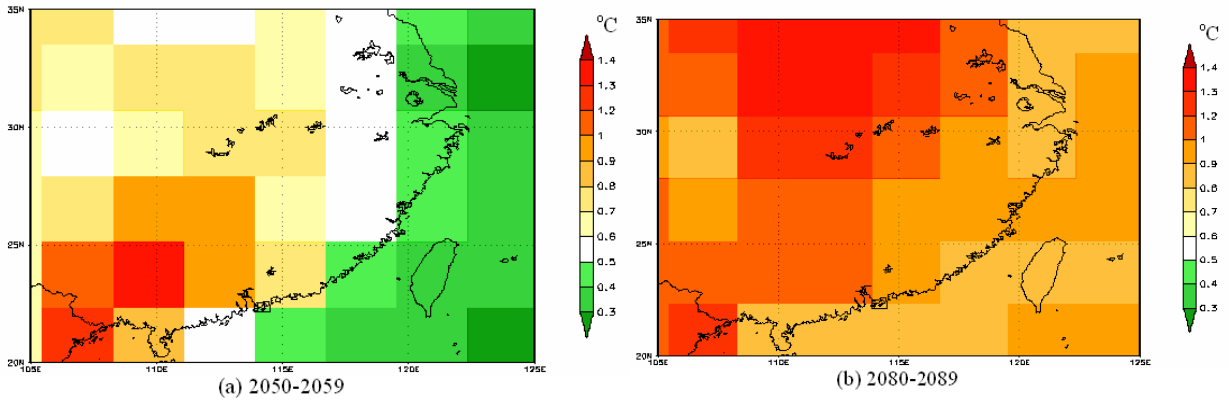

Fig. C2-6. Temperature change projected at (a) 2050-2059 and (b) 2080-2089 (relative to 2000-2009) using model BCM2 for the SRES scenario B1.

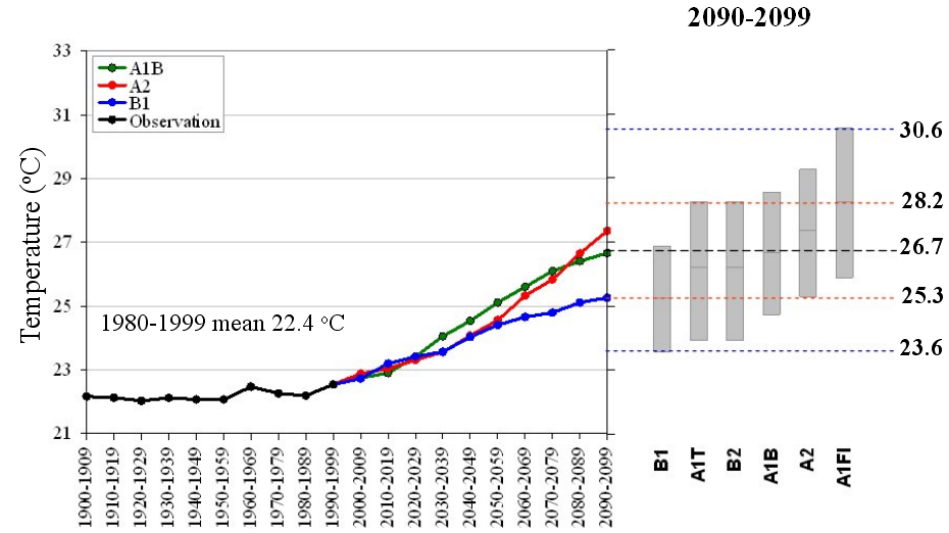

Fig. C2-11 Theoretical temperature projections in Hong Kong in which the urbanization effect has been removed.

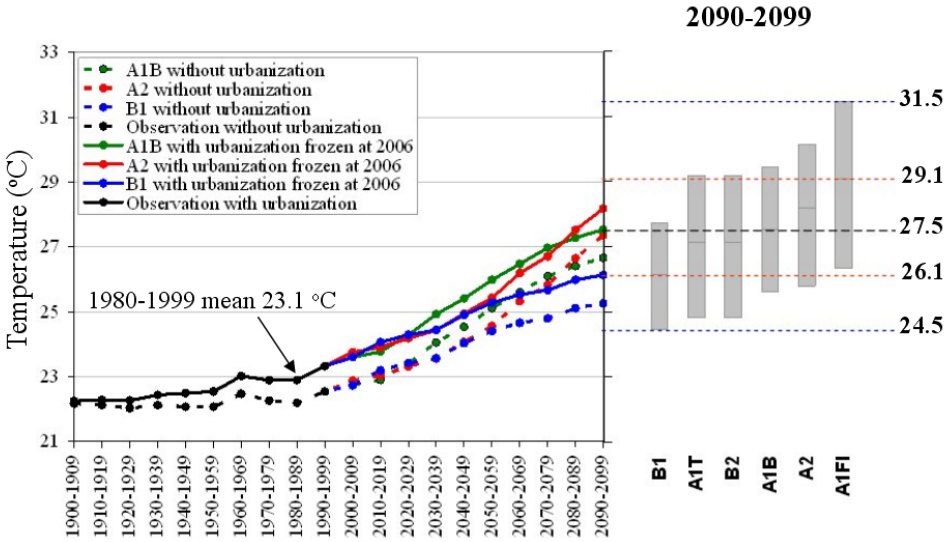

Fig. C2-12 Temperature projections in Hong Kong assuming that the urbanization effect is frozen at the 2006 level (solid lines). The theoretical projections without urbanization (dashed lines, same as Fig. C2-11) are shown for comparison.

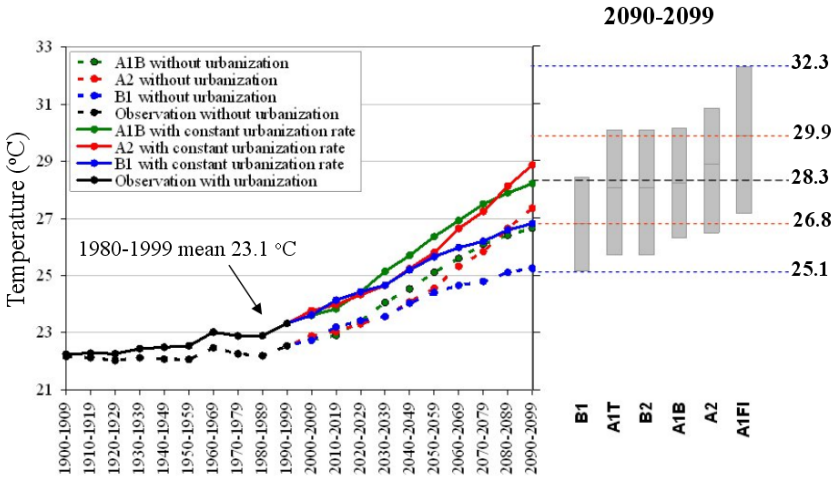

Fig. C2-13
Temperature projections in Hong Kong assuming a constant urbanization rate (solid lines). The theoretical projections without urbanization (dashed lines, same as Fig. C2-11) are shown for comparison.

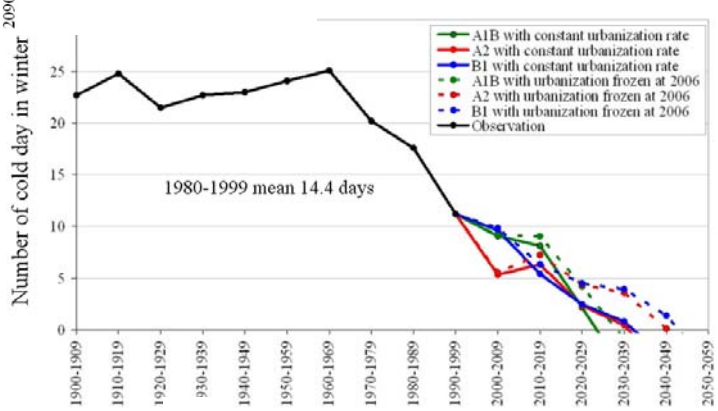

Fig. C2-14
Projected number of cold days in winter for constant urbanization rate (solid lines) and urbanization frozen at the 2006 level (dashed lines).

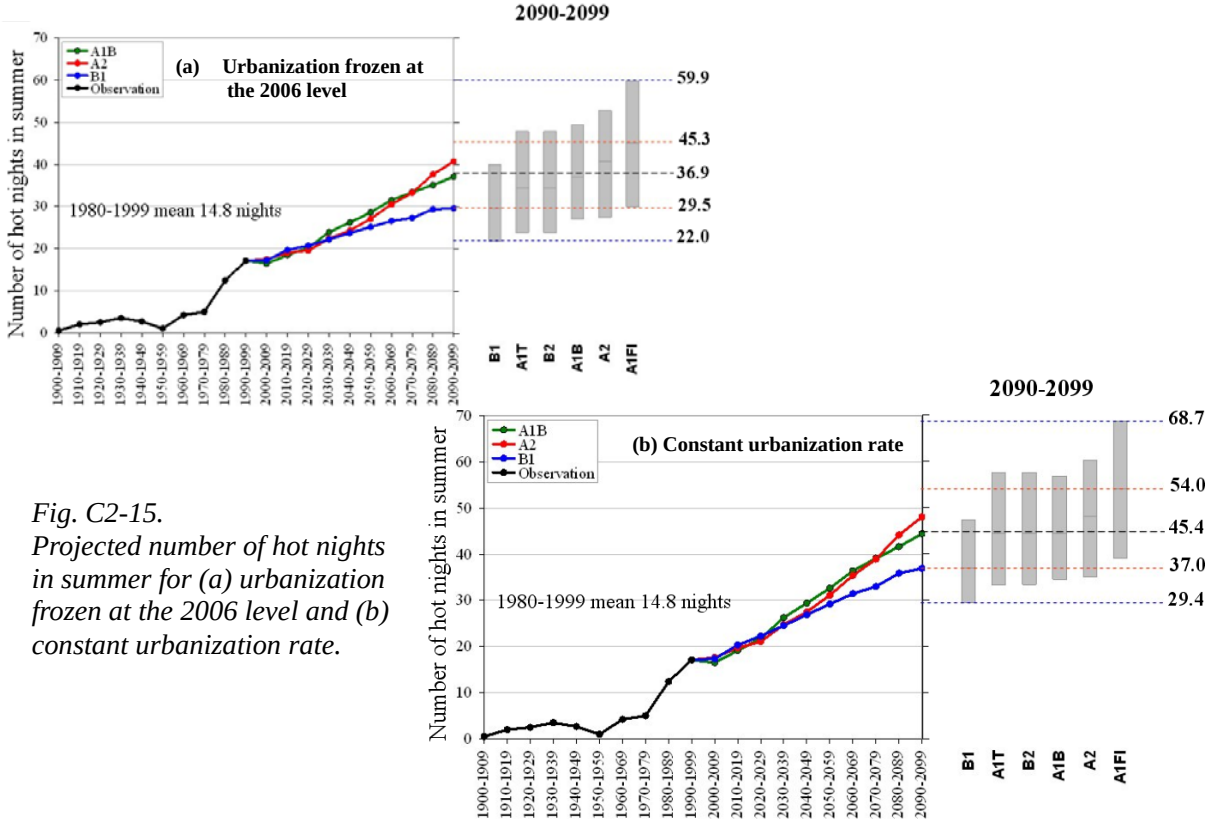

Fig. C2-15.
Projected number of hot nights in summer for (a) urbanization frozen at the 2006 level and (b) constant urbanization rate.

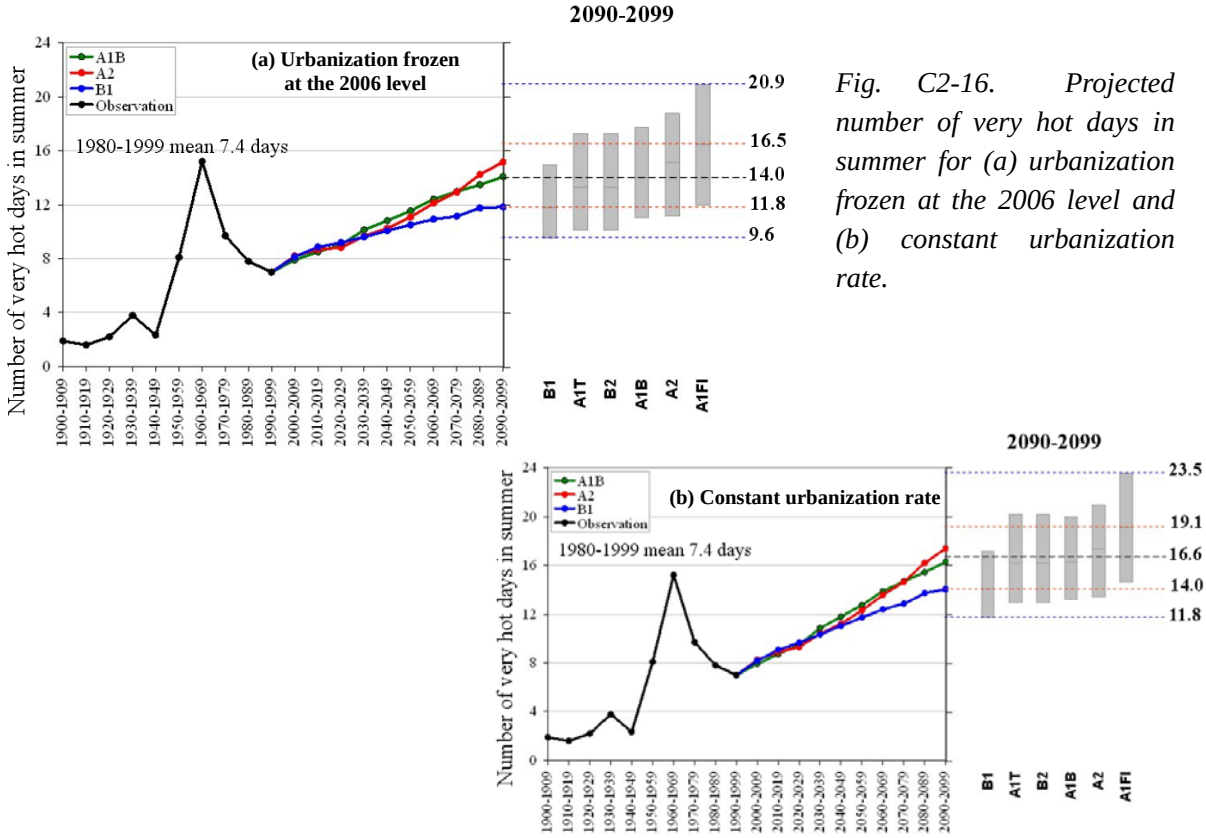

Fig. C2-16. Projected number of very hot days in summer for (a) urbanization frozen at the 2006 level and (b) constant urbanization rate.

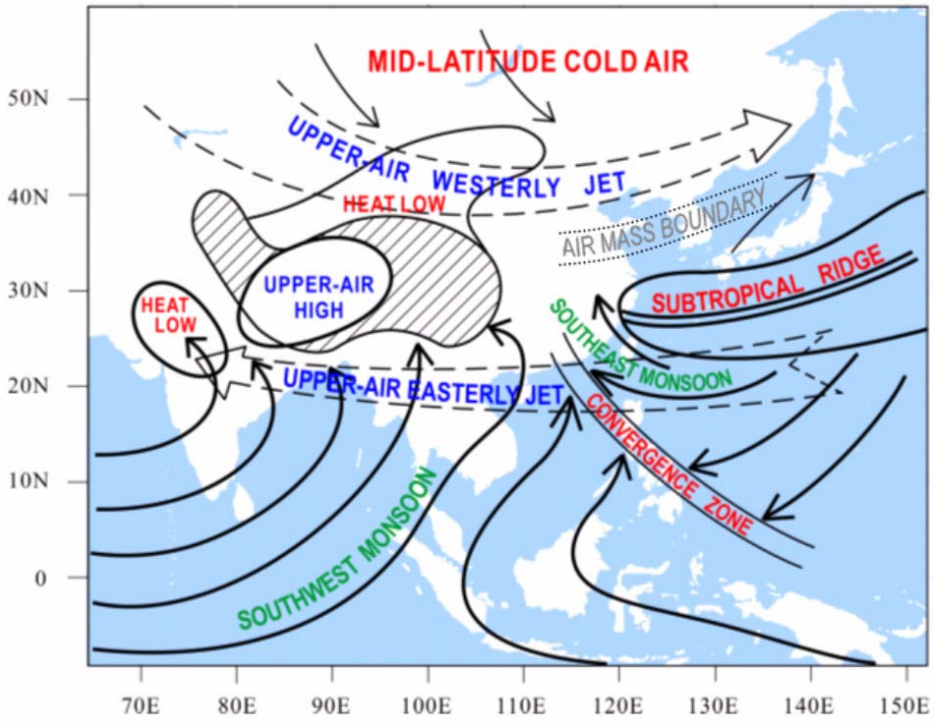

Fig. C6-1
A schematic diagram showing the main components of the airflow in the lower and upper levels in the summer monsoon in July. (Adapted from Tao 1978, with modification).

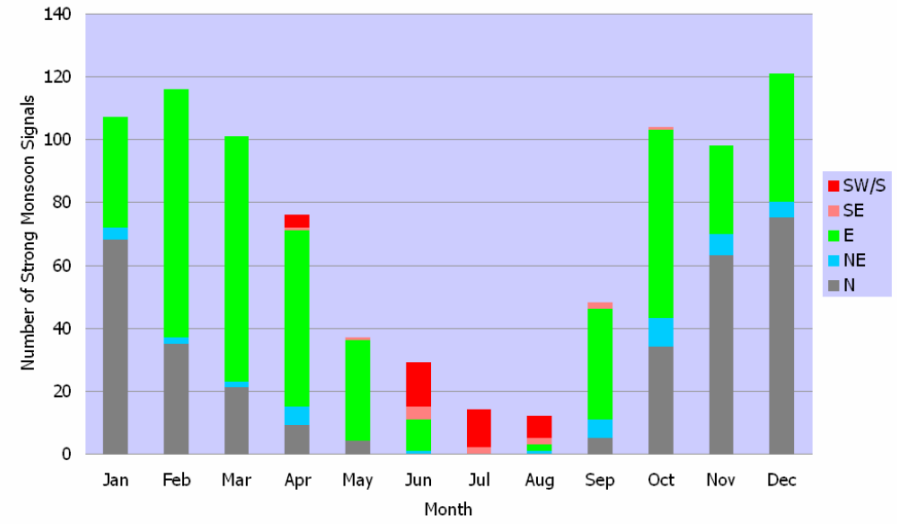

Fig. C6-4
The frequency distribution of strong monsoon signals for the Northeast Monsoon, Southwest Monsoon and Southeast Monsoon based on the dataset from 1951 to 2006.

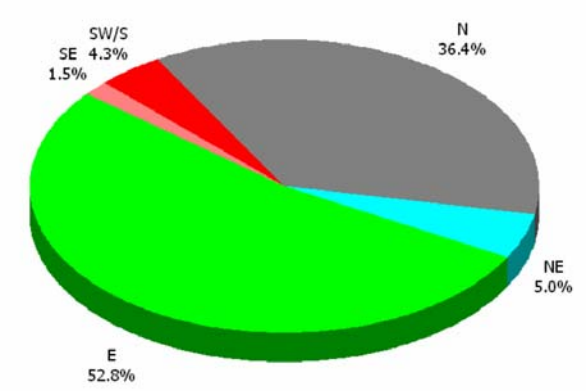

Fig. C6-5
Percentage of strong monsoon signals issued for different wind directions based on the dataset from 1951 to 2006 with a total number of 863 cases.

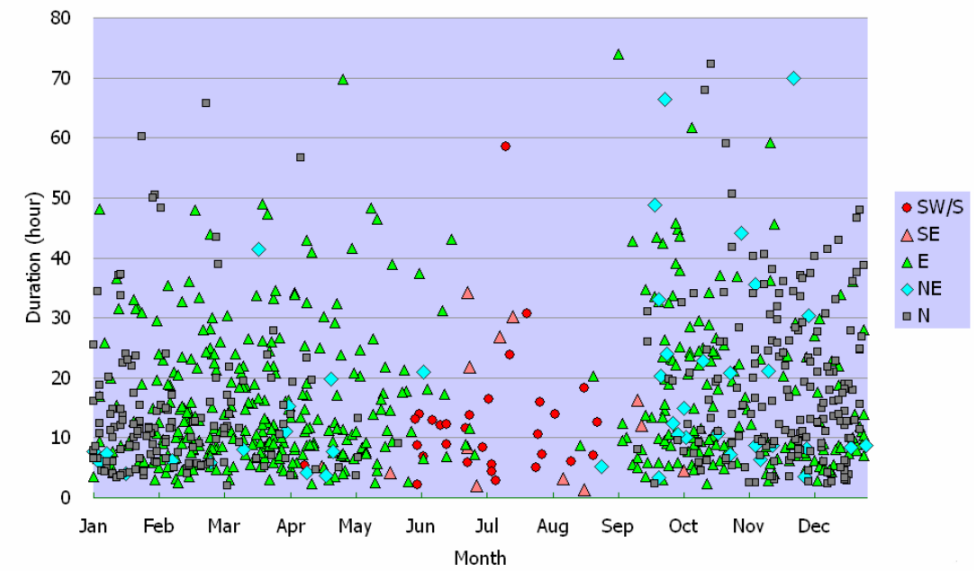

Fig. C6-6 Duration of strong monsoon signals for winter and summer monsoons based on the dataset from 1951 to 2006.

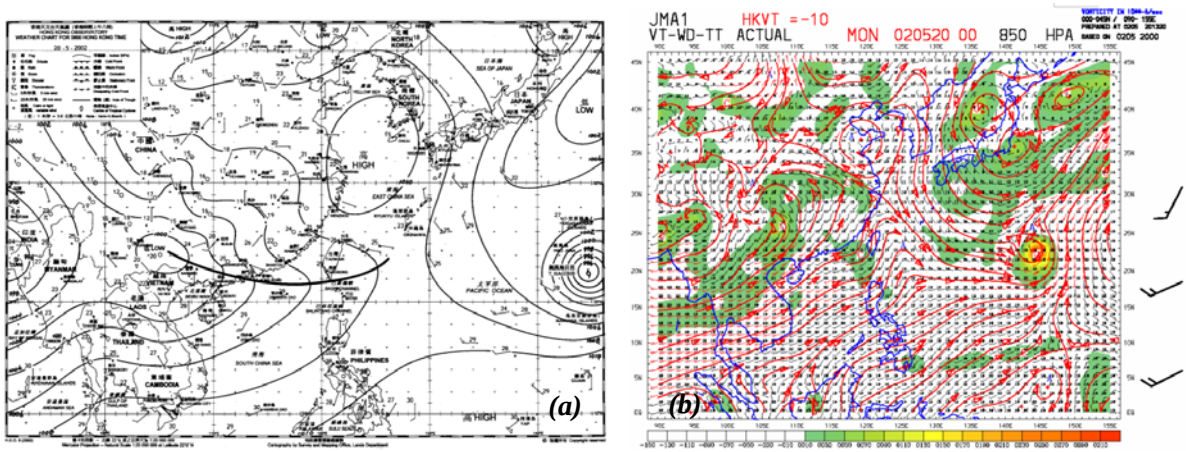

Fig. C6-7 (a) Subjective analysis of mean sea-level pressure chart; and (b) JMA model analysis of 850-hPa wind, temperature (in numeric) and relative vorticity (in color shading) at 00 UTC on 20 May 2002. (The three wind barbs on the right-hand side of the model analysis field are 850-hPa winds at selected grid points (top: 25°N, 115°E; middle: 22.5°N, 115°E; bottom: 20°N, 115°E) in the vicinity of Hong Kong.)

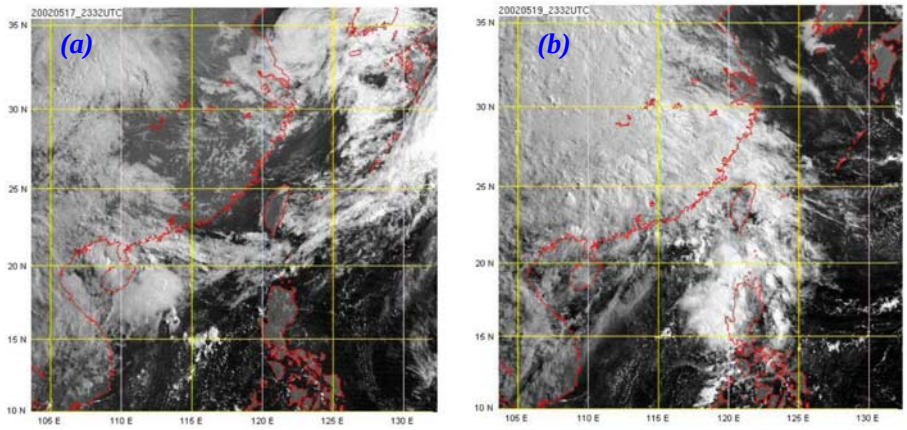

Fig. C6-8 Visible satellite imagery for (a) 00 UTC on 18 May 2002, two days before the onset of strong southeasterly winds in Hong Kong; and (b) 00 UTC on 20 May 2002, the day of onset.

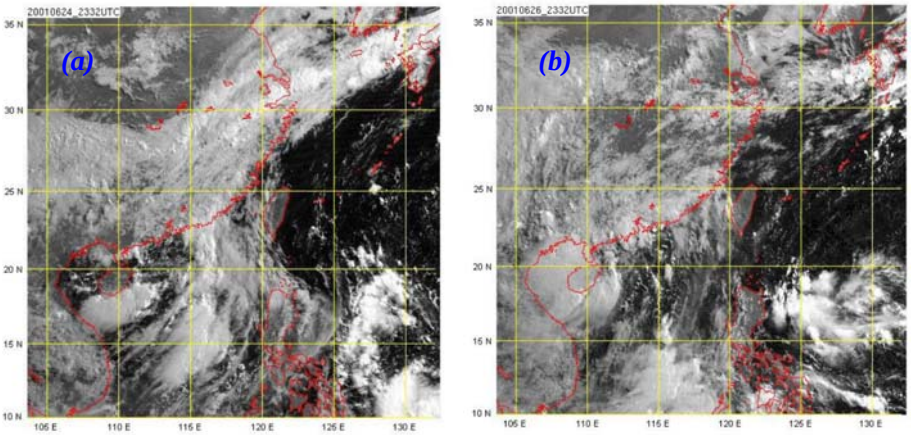

Fig. C6-9 Visible satellite imagery for (a) 00 UTC on 25 June 2001, the day before the onset of strong southeasterly winds in Hong Kong; and (b) 00 UTC on 27 June 2001, the day after.

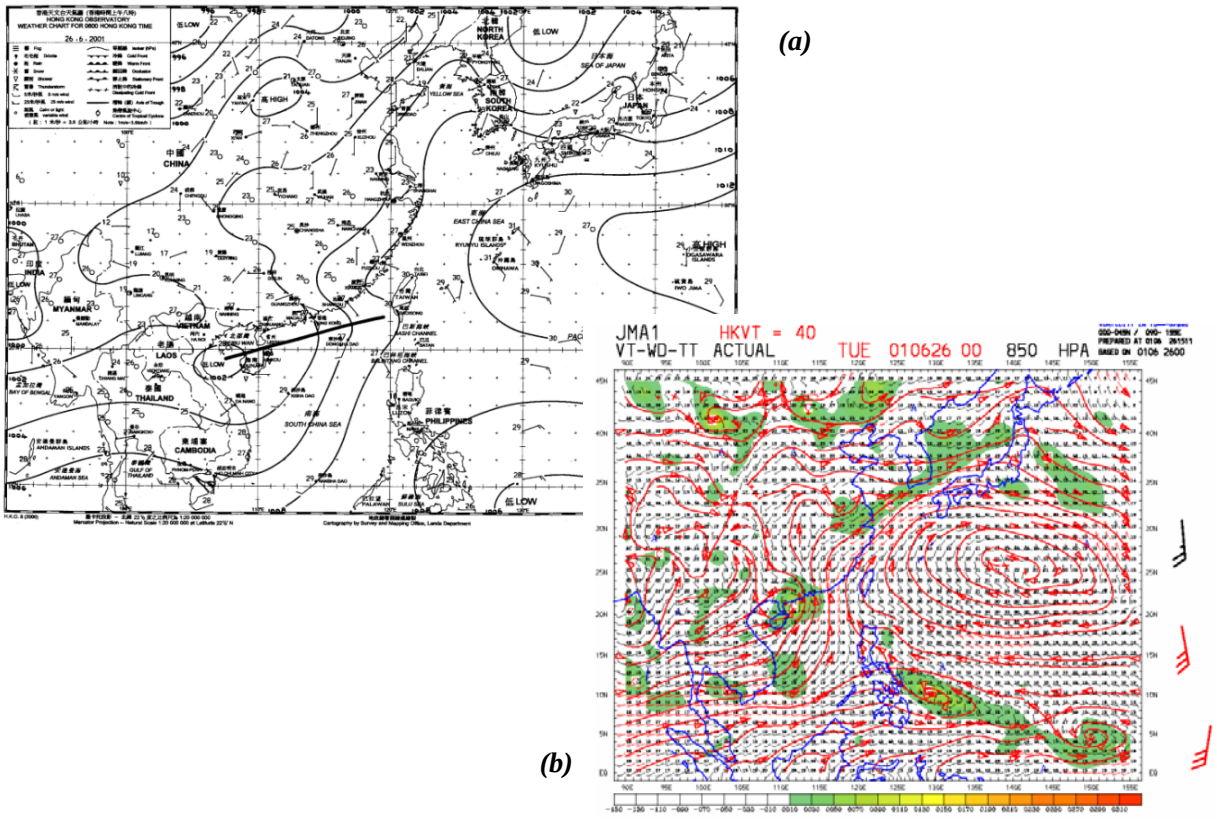

Fig. C6-10 Similar to Fig. C6-7 except for 00 UTC on 26 June 2001.

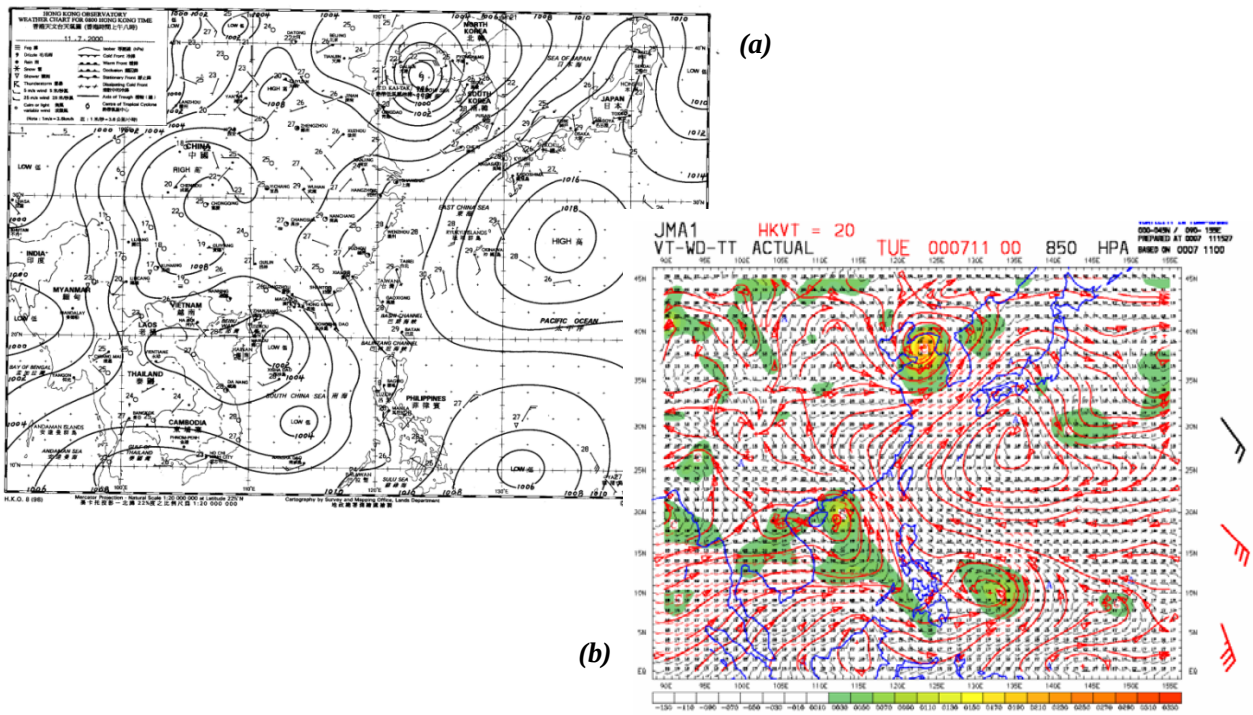

Fig. C6-11 Similar to Fig. C6-7 except for 00 UTC on 11 July 2000.

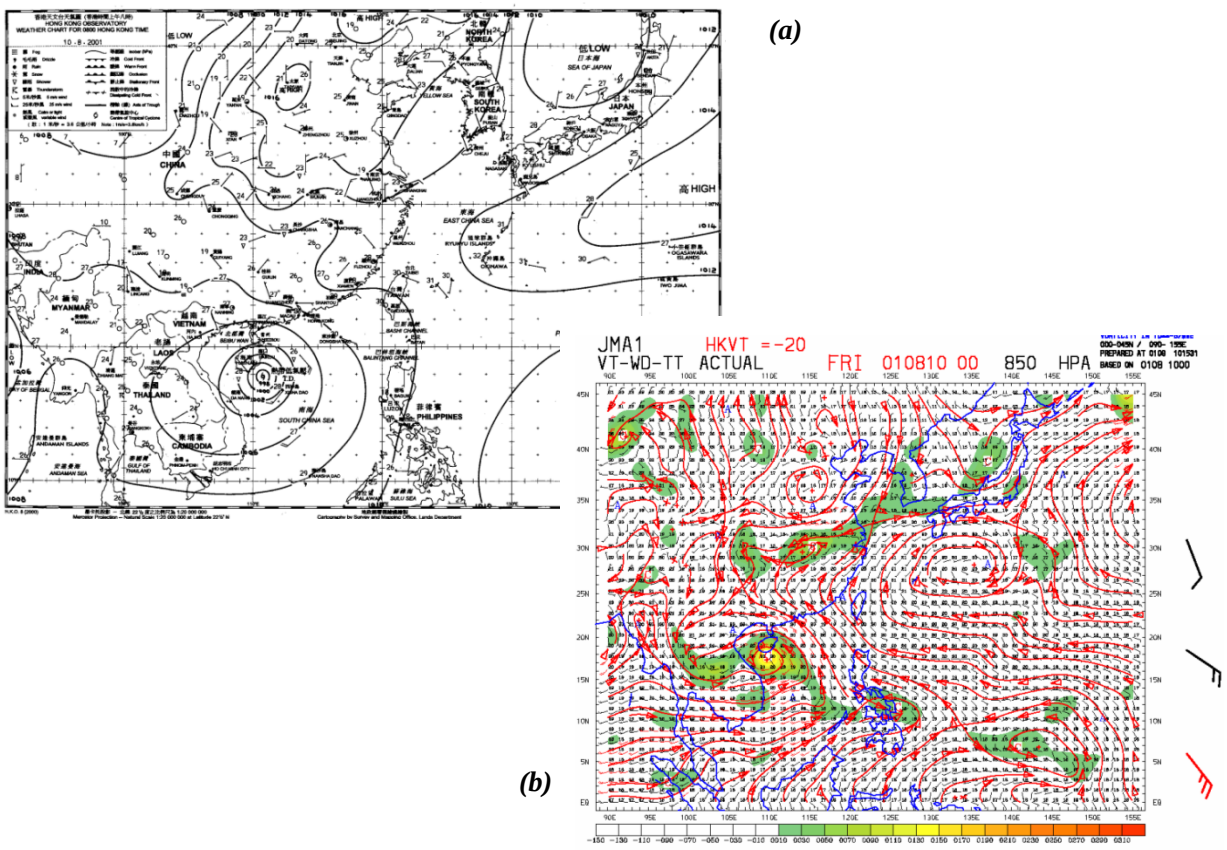

Fig. C6-12 Similar to Fig. C6-7 except for 00 UTC on 10 August 2001.

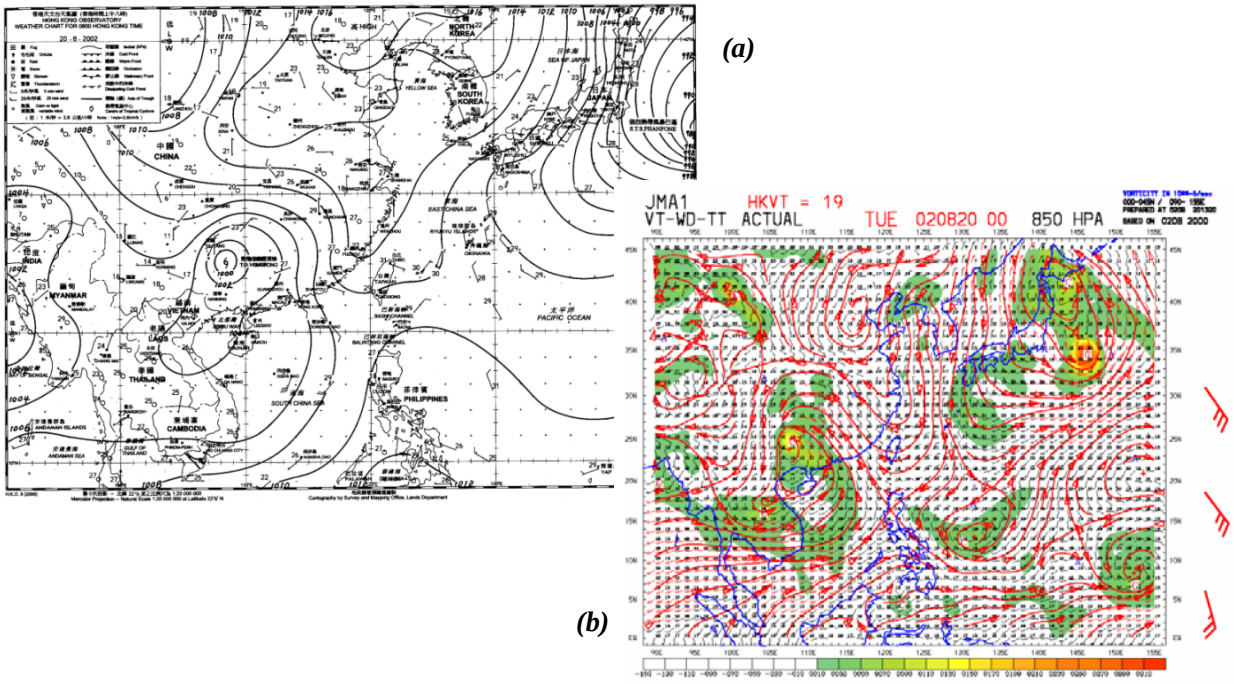

Fig. C6-13 Similar to Fig. C6-7 except for 00 UTC on 20 August 2002.

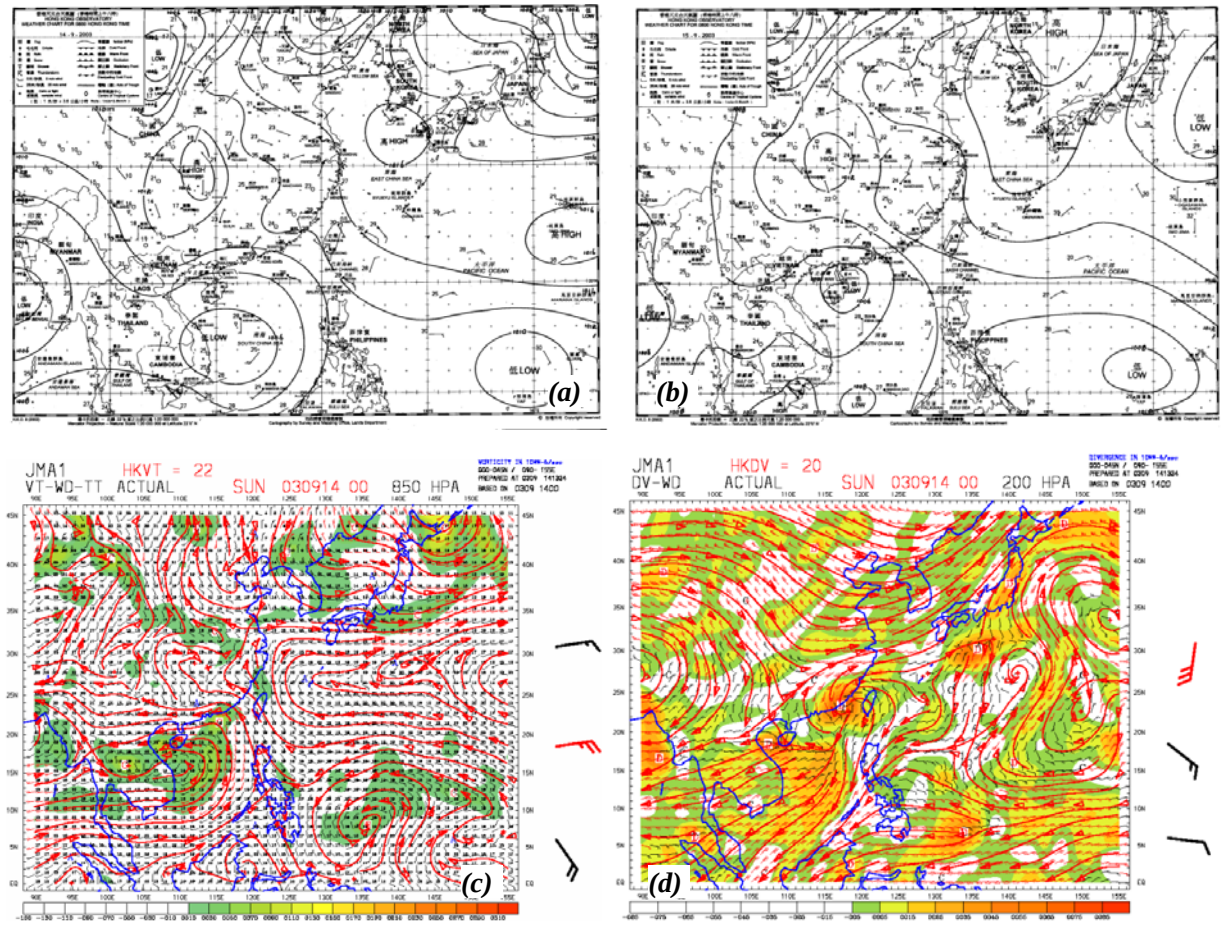

Fig. C6-14 Subjective analysis of mean sea-level pressure chart at 00 UTC on (a) 14 September 2003 and (b) 15 September 2003; (c) JMA model analysis of 850-hPa wind, temperature (in numeric) and relative vorticity (in color shading) and (d) 200-hPa wind and divergence (in color shading) at 00 UTC on 14 September 2003.

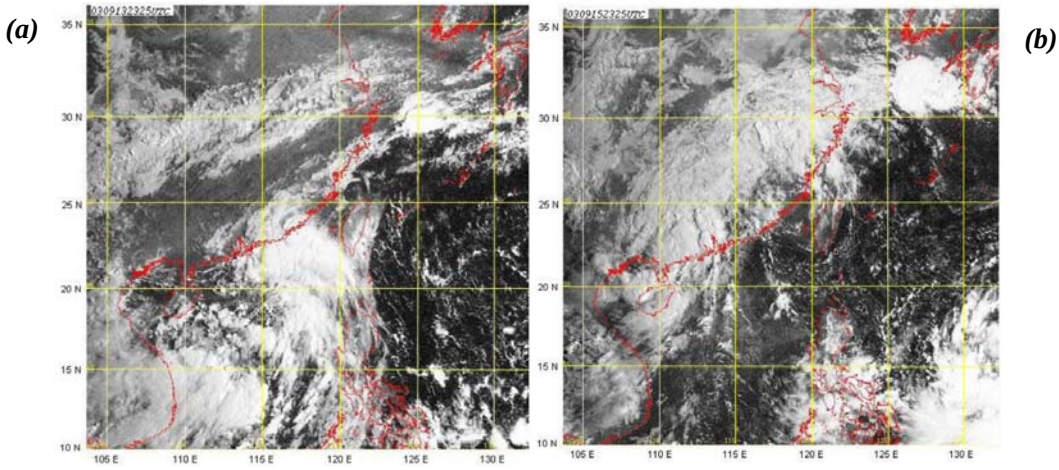

Fig. C6-15 Visible satellite imagery for (a) 00 UTC on 14 September 2003 showing the convections associated with the monsoon depression; (b) 00 UTC on 16 September 2003, the day on which the southeasterlies prevailing over Hong Kong gradually weakened in the afternoon after the monsoon depression made landfall over southwestern China.

Hong Kong Meteorological Society Helps Promote the Awareness of Climate Change in Hong Kong

The Nobel Peace Prize 2007 goes to the Intergovernmental Panel on Climate Change (IPCC) under the World Meteorological Organization and United Nations Environment Programme and the ex-Vice President of the United States Mr Albert Arnold Gore (Al Gore) "for their efforts to build up and disseminate greater knowledge about man-made climate change, and to lay the foundations for the measures that are needed to counteract such change". By awarding the Nobel Peace Prize to IPCC and Al Gore, the Norwegian Nobel Committee wished human could help "protect the world's future climate, and thereby to reduce the threat to the security of mankind".

As a matter of fact, the Hong Kong Meteorological Society (HKMetSoc) has been promoting the awareness of climate change in local community in the past few years. HKMetSoc has been organizing a number of Popular Lecture Series emphasizing on climate and climate changes with the following themes:

2005: 認識大氣候 Know the Climate

2006: 城市，氣候，人 Meteorology-City-Life

2007: 氣候變化與你 Climate Change and You

2007: 諾貝爾和平獎與氣候變化 Nobel Peace Prize & Climate Change

Meanwhile, the Society has also organized a number of activities along the same line for the participation of local primary and secondary schools:

2005: 風之足印 'Footprints of Winds' painting and 3D arts competition

2006: 風雲變色 'Changing Weather' painting and photo taking competitions

2006: 氣候轉變 'Climate Change' painting and webpage design competitions

The Chairman of the HKMetSoc, Mr Chiu-yin Lam, is also involved in the drafting the IPCC 4th Assessment Report (Working Group I). The Society is delighted to have been contributing in this most significant subject with which everybody in the world, including our next generations, inevitably have to face. As to promote the public's interest in meteorological science and awareness in the impacts brought by weather/climate is one of the main objectives of the Society, the Society will strive to continue to arrange more activities in this respect, hoping to improve the living quality of the general public and maintain the sustainability of our society under the impact of climate change.

For more information regarding the HKMetSoc and its activities, please visit our website at http://www.meteorology.org.hk

Forecast of Ultraviolet Index in Hong Kong

L.S. Lee and M.Y. Leung, Hong Kong Observatory, Hong Kong, China

Abstract

The Hong Kong Observatory (HKO) developed a methodology for forecasting the Ultraviolet Index (UVI) in Hong Kong. The methodology consisted of the computation of UVI in clear sky conditions using an empirical equation and the application of a set of factors to adjust the UVI for cloudy days or days with weather. The maximum UVI forecast service was launched in 2006. During a one-year operational experience, about 75% of the UVI forecasts were within 2 units of the actual UVI. This paper aims to document the development of the UVI forecast methodology and the forecast verification results.

1. Introduction

Excessive exposure to ultraviolet (UV) radiation may bring about health effects on human body, including sunburn, wrinkling and increased risk of skin cancers and cataracts. The UVI is a measure of the intensity of UV radiation relevant to the effect on human body (World Health Organization, 2002). The UVI observed in Hong Kong typically ranges from 0 to 15. To raise the public awareness on the potential harm of UV radiation, the HKO started a UVI advisory service in 1999 to provide information on measured UV radiation to the public (Leung, 2003). In 2006, the HKO completed the development of UVI forecasting technique and started the forecasting service in May of the same year, thus enabling members of the public to plan protective measures against possible harm from UV radiation. This paper documents the development of forecast technique and the verification of forecast performance.

It is well known that the variation of surface UV radiation depends on a number of factors including ozone concentration, cloud cover, elevation of the sun, rainfall, particulates and water droplets suspended in the air (World Health Organization, 2002). Ozone and clouds absorb some of the UV radiation that would otherwise reach the earth's surface. Sun rays are attenuated by absorption and scattering from gases and particles in the atmosphere. Therefore, the lower the sun in the sky, the lower will be the UV radiation level. Rain, suspended particulates and water droplets generally reduce the UV radiation by reflection, scattering and absorption.

To forecast UVI in clear sky conditions, i.e. the clear sky UVI, there are two approaches. The first approach is the development of an empirical formula relating surface UV radiation to elevation of the sun, ozone concentration and the time of year. Canada is among the countries adopting this method (Burrows, 1994). The second approach involves the development of a Radiative Transfer Model (RTM) which calculates the change of solar radiation energy through the emission, absorption and scattering processes as the sun beam traverses the atmosphere and interacts with gases and particles, such as ozone and aerosols. The United States of America is one of the countries using such method (Long, 1996).

Irrespective of whether the empirical formula or the RTM is used, the UV value calculated by these methods is the maximum amount of UV radiation expected under clear sky conditions. In the presence of clouds and weather, i.e. under non-clear sky condition, the attenuation of UV has to be taken into account. One of the recommendations coming from the project undertaken by the European Commission, namely COST Action 713, is the use of modification factors for different

cloud amounts/elevations and weather conditions (Vanicek, 2000).

The present study drew on the experience of the Canadian approach and the COST project. An empirical equation for clear sky UVI was developed based on observed UV radiation. A set of cloud and weather modification factors, broadly based on those used in the COST project but found to be suitable for the circumstances of Hong Kong, was determined.

In developing the forecast technique, focus has been placed on forecasting the daily maximum UVI, as this parameter is more meaningful than the daily mean UVI when it comes to taking protective measures against UV.

2. Data

Past observational data from 1999 to 2003 was studied to find out the correlation between UVI and the relevant astronomical, geophysical and meteorological conditions. The data included:

(i) 5-minute mean UVI data measured by the UV pyranometer at the King's Park meteorological station (about 1 kilometre north of the Observatory Headquarters and 65 metres above mean sea level);

(ii) hourly cloud cover (in oktas) observed by weather observers at the Observatory headquarters;

(iii) hourly total rainfall data (in millimetres) recorded at the Observatory headquarters;

(iv) hourly report of presence of mist, fog or haze at the Observatory headquarters. This roughly represents the amount of particulates and water droplets suspended in the air;

(v) daily ozone concentration (in Dobson Units (DU)) for Hong Kong measured by the satellite-borne Total Ozone Mapping Spectrometer (TOMS); and

(vi) 1-minute solar elevation (in degrees) calculated using astronomical formulas.

3. Methodology

3.1 Clear sky UV

The Canadian approach was adopted to calculate the clear sky UVI. It assumed that the clear sky UV radiation could be represented by this equation:

$$\text{clear sky UVI} = 0.04\, C \cos\theta \exp(a+b\mu\Omega+c\mu+d(\mu\Omega)^2+e\mu^2)$$

where C is the earth-sun distance correction factor defined as (World Meteorological Organization, 1985):
$1.00011+0.034221\cos(y)+0.00128\sin(y)+0.000719\cos(2y)+0.000077\sin(2y)$
in which $y = 2\pi[(\text{Julian Date} - 1) / 365]$. The factor C reflects the modulation of solar energy arriving at the top of the earth's atmosphere due to varying distance from the sun;

θ is the zenith angle. The term $\cos\theta$ describes the reduction in solar radiation arriving at a

slant due to absorption and scattering, as compared with that coming vertically downwards;

μ is defined as $1/\cos\theta$; and

Ω is the column ozone concentration in DU / 1000.

Since Canada is at a higher and very different latitude , parameters a to e in the equation above could not be directly adopted in Hong Kong. A new set of parameters applicable to Hong Kong was required. This was achieved by performing regression analysis using a set of training data selected from clear sky days during October 1999 to June 2003.

Regression analysis showed that the correlation between clear sky UVI and individual factors in the above equation was high, with a correlation coefficient R of 0.98. Parameters a to e of the clear sky UV equation were found to be 6.4, -1.5, -0.30, -0.99 and -0.077 respectively. The empirical equation was found to perform well when applied to an independent set of test data from July 2003 to June 2004. Fig. 5-1 shows that the UVI computed by the empirical equation was close to the measured UVI, except for those values close to or above 10 when the computed values tended to be underestimates. The limitation of the empirical equation for cases of UVI above 10 will be discussed further in Section 3.5.

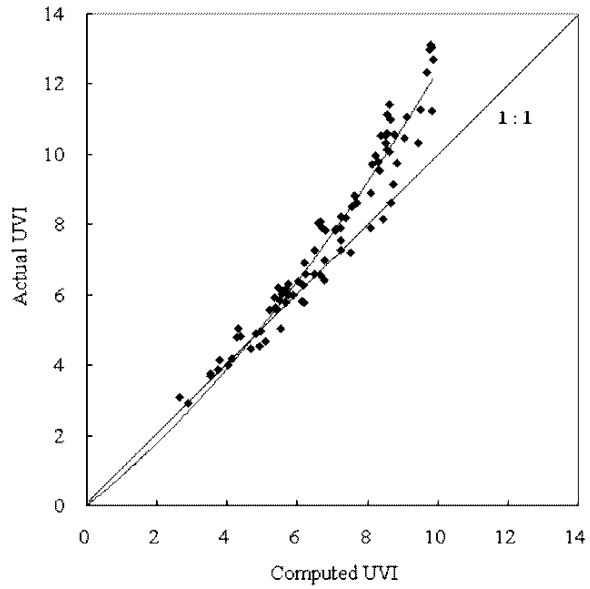

Fig. 5-1 Actual UVI versus computed UVI for clear sky days during July 2003 to June 2004. The curve which best fits the data points is close to the diagonal (which represents a ratio of 1:1 between actual and computed UVI) except when the measured UVI is close to or above 10.

3.2 UV under clouds and/or weather

After obtaining an empirical equation for clear sky situation, the next step was to analyze how the UVI was attenuated when there were clouds and/or weather, i.e. to calculate the non-clear sky UVI. The project COST Action 713 undertaken by the European Commission in 2000 recommended a set of factors (Table 5-1) to modify the clear sky UVI under different weather conditions and cloud amounts/altitudes.

As can be seen from the above table, the cloud factors are stratified according to whether the clouds are low, medium or high. However, starting from April 2000, cloud observations at the Observatory headquarters were reported in total cloud amount regardless of the altitude. As such, it was not

possible to use all the factors recommended by the COST project directly. A new set of factors depending only on total cloud amount had to be developed, so that the performance in respect of the cloud modification factors could be verified using the available observations. Operationally, it would also be easier and less time-consuming for the weather forecaster to predict the total cloud amount than to predict the cloud amounts at different altitudes.

	0 to 2 oktas	3 to 4 oktas	5 to 6 oktas	7 to 8 oktas
Low Clouds	1	0.8	0.5	0.2
Medium Clouds	1	1	0.8	0.5
High Clouds	1	1	1	0.9

Weather	Fog	Rain
Factor	0.4	0.2

Table 5-1 Cloud and weather modification factors recommended by the COST Action 713 project of the European Commission

The new set of factors, as shown in Table 5-2, was derived by taking the average of factors for low, medium and high clouds as suggested by the COST project. The performance in respect of the new set of cloud factors was verified by applying them to days with clouds but no weather during the period October 1999 to June 2004. Fig. 5-2 shows how the computed UVI correlated with the measured UVI, with a correlation coefficient R of 0.76.

Total cloud amount	0 to 2 oktas	3 to 4 oktas	5 to 6 oktas	7 to 8 oktas
Factor	(1+1+1) ÷ 3 = 1	(0.8+1+1) ÷ 3 = 0.93	(0.5+0.8+1) ÷ 3 = 0.77	(0.2+0.5+0.9) ÷ 3 = 0.53

Table 5-2 Computation of simplified cloud modification factors depending only on total cloud amount

Haze and mist/fog are suspension of particulates and water droplets in the air. They lead to attenuation of the UV radiation through reflection, scattering and absorption. The COST project recommended modification factor for fog only. The modification factors for mist and haze were identified in this study by carrying out a sensitivity analysis which involved varying the factors from 0.5 (starting from the value just higher than the factor for fog) to 0.9 for those days with no clouds but with one type of weather, either mist or haze. The optimal factors for both mist and haze were found to be 0.8.

It was also found that if the single factor of 0.2 for rain as suggested by the COST project for all the rain cases was adopted, the UVI would be much underestimated when the rainfall rate was less than 1 mm per hour. To achieve an optimal forecast performance, it was found by testing with past data that the rain factor should be applied only when significant rain was forecast. In other words, the rain factor should not be used if light rain was forecast.

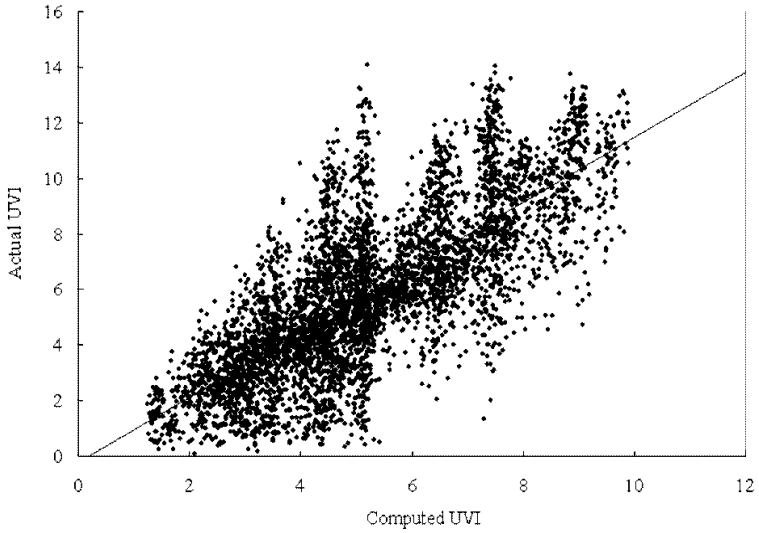

Fig. 5-2
Actual UVI versus computed UVI based on cloud observations at the Observatory headquarters for days with clouds but no weather during the period October 1999 to June 2004. The correlation coefficient R is 0.76.

3.3 Forecasting the astronomical, geophysical and meteorological factors affecting the UVI

With respect to the methodology of UVI calculation discussed in Sections 3.1 and 3.2, a prerequisite for forecasting the UVI for the next day is to forecast the relevant geophysical (ozone concentration), astronomical (the sun's elevation) and meteorological (cloud cover and weather) factors of the next day. Forecast of the sun's elevation is straightforward through the use of the relevant astronomical formulas. Forecast of cloud amount, fog, mist, haze and rain is available from the day-to-day weather forecast. Since ozone concentration is not forecast routinely by the Observatory, extrapolation was used in this study as the day-to-day ozone variation near latitudes such as that of Hong Kong is usually only a few percents (Hudson, 2003; Long, 1996). The total column ozone concentration over Hong Kong of the next day could thus be approximated by the following equation:

$$\Omega_{\text{tomorrow}} = a + b\,\Omega_{\text{yesterday}} + c\,\Omega_{\text{the day before yesterday}}$$

where Ω is the total column ozone concentration

Ozone concentrations measured by the satellite-borne TOMS from August 1999 to June 2004 were used to perform a regression analysis. The parameters a, b and c in the above equation were found to be 18.52 DU, 0.73 and 0.20 respectively. Operationally, ozone column data for the past couple of days is readily available from the TOMS database on the Internet for input into the empirical equation. Fig. 5-3 shows how the computed ozone concentration correlated with the measured ozone concentration, with a correlation coefficient R of 0.91.

3.4 Forecasting the maximum UVI for the next day

The forecast 15-minute UVI values between 11 a.m. and 1 p.m. the next day were calculated using the clear sky empirical equation, followed by application of the set of cloud and weather modification factors determined in Section 3.2 above. The maximum of these eight 15-minute UVI values was then regarded as the maximum UVI for the day. This assumed that the UVI usually

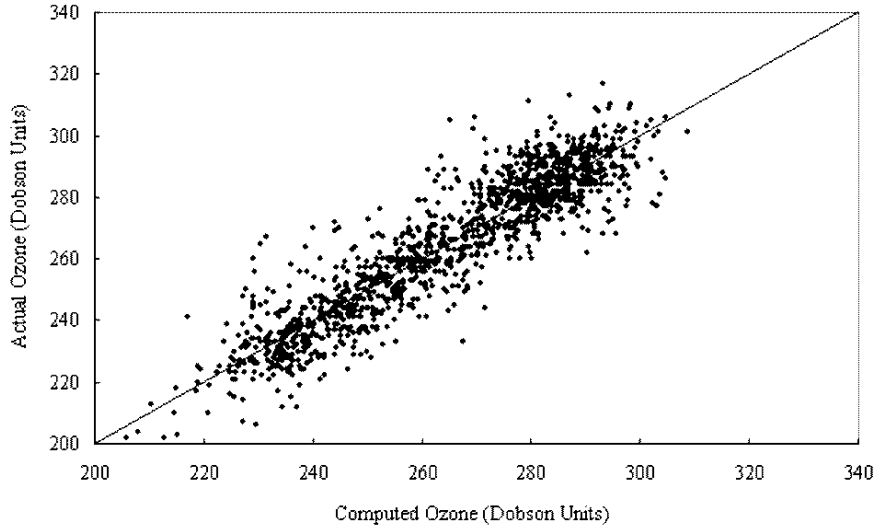

Fig. 5-3
Actual ozone concentration versus computed ozone concentration based on extrapolation. The correlation coefficient R is 0.91.

attained its maximum between 11 a.m. and 1 p.m., on the basis of past record of occurrences of maximum UVI. Although the maximum may take place outside this period on a non-clear sky day, there is a degree of difficulty in determining the peak hour operationally as this involves the problem of accurately forecasting all the weather elements affecting UVI for every hour, from sunrise to sunset.

3.5 Limitation of forecasting UV in the extreme category

According to international practice (World Health Organization, 2002), different UVI values can be grouped under five UV exposure categories: low (UVI=0-2), moderate (UVI=3-5), high (UVI=6-7), very high (UVI=8-10) and extreme (UVI 11). It was found that the methodology discussed above was handicapped in forecasting the 'extreme' category. This is because extreme exposure is a rare event relative to the occurrence of other exposure categories and as such, is not fully represented in the statistical processes involved in the regression analysis. Another reason is that, in the methodology discussed above, any presence of clouds would only attenuate the UVI, not enhance it. This would result in a statistical bias as UV radiation can actually be enhanced by reflection from the sides of broken clouds. In this study, it was found that of all cases of 'extreme' UV category during October 1999 to June 2004, only 3.4% were days with 0 or 1 okta of cloud, and the rest were days with 2 to 7 oktas of clouds.

To alleviate the above problem, persistence was used as a supplementary tool. Specifically, if the measured UV for the day is in the 'extreme' category and the synoptic weather situation for the following day is forecast to be similar, then the UV for the following day is likely to be also in the 'extreme' category in view of the significant role of the prevailing weather in affecting the surface UV intensity. Operationally, if the day's measured UV is in the 'extreme' category and the forecast UV for the next day is in the category of 'very high', the forecast UV will be automatically adjusted upward to 'extreme'.

4. UV forecast performance verified using a set of independent test data

Data from April 2004 to April 2005 was used as an independent set of test data to verify the

performance of the methodology discussed in Section 3. Daily maximum UVI values for this period were computed and the accuracy was assessed against actual observations. The histogram in Fig. 5-4 presents the results, showing the distribution of forecast errors. It was found that about 71% of the UVI forecasts were within 2 units of the actual UVI.

Category-wise, about 86% of UV forecasts were accurate to within 1 UV category, as shown by the contingency table in Table 5-3.

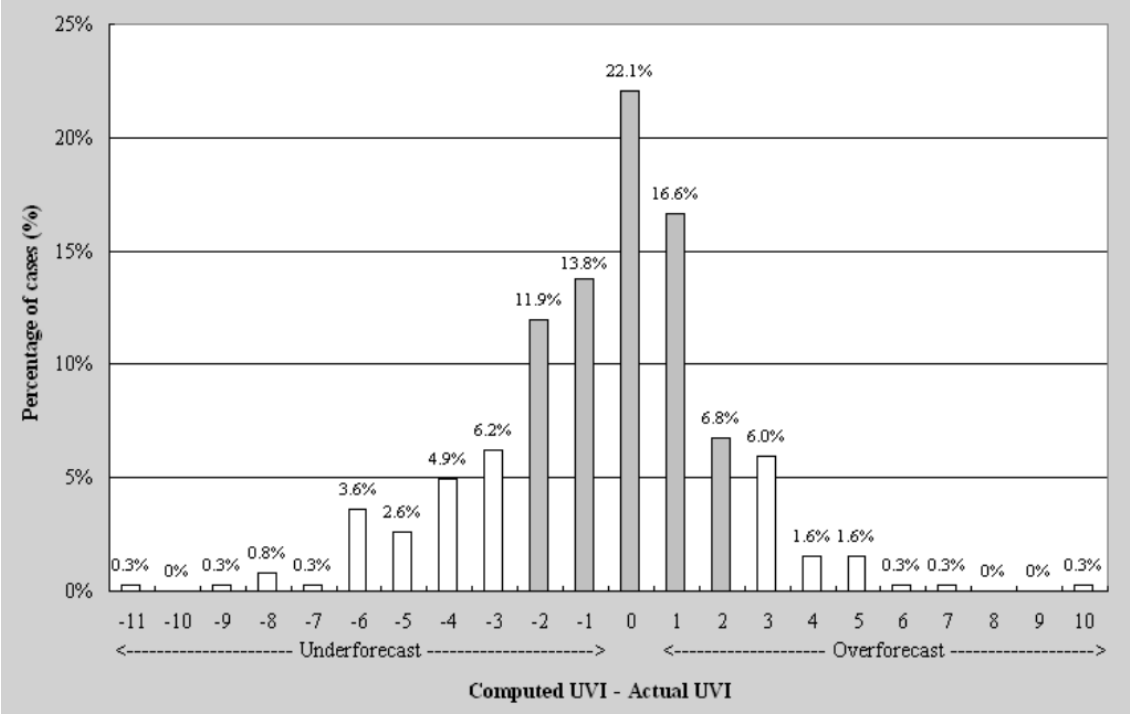

Fig. 5-4 Distribution of errors in computing the daily maximum UVI based on an independent set of test data from April 2004 to April 2005. Statistics for those within 2 units of the actual UVI are shown in grey (71% of total).

Computed UV \ Actual UV	Low (0-2)	Moderate (3-5)	High (6-7)	Very High (8-10)	Extreme (>=11)
Extreme (>=11)	0.0%	0.3%	0.3%	3.4%	8.3%
Very High (8-10)	0.3%	2.3%	3.4%	7.0%	3.6%
High (6-7)	1.3%	6.0%	8.8%	8.6%	1.8%
Moderate (3-5)	4.7%	18.2%	7.3%	2.1%	1.0%
Low (0-2)	1.6%	4.9%	2.3%	2.3%	0.3%

Table 5-3
Contingency table of computed versus actual daily maximum UV for the set of independent test data from April 2004 to April 2005. Statistics for those computed values within 1 UV category are shown in grey (86% of total).

5. Start of the UV forecast service and its performance so far

With satisfactory results obtained with the UV forecast methodology, the HKO initiated issuance of UVI forecast on 25 January 2006 internally. The UVI was routinely computed by the methodology, and before its issuance the weather forecaster was allowed to adjust it on the basis of the latest assessment of the weather situation. The information for such assessment included a time series forecast of the meteorological factors (obtained from numerical weather prediction products) affecting the UVI at King's Park between 11 a.m. and 1 p.m., the time period on which the maximum UVI forecast was based.

The UVI forecast service was launched formally on 11 May 2006 in anticipation of the arrival of summer season. Advisory statements reminding the public to take protective measures against UV are routinely included in the UVI forecast bulletin whenever UV levels in the extreme exposure category are expected.

The performance of UVI forecast issued operationally by the Observatory from January 2006 to January 2007 was verified. The histogram in Fig. 5-5 showing the distribution of forecast errors indicates that 75% of the UVI forecasts issued by weather forecasters were within 2 units of the actual UVI. Without the intervention of the forecasters (i.e. forecasts issued purely based on the methodology), the corresponding figure would have been 69%. The improvement of about 6% demonstrated the value of the weather forecaster in the provision of the service.

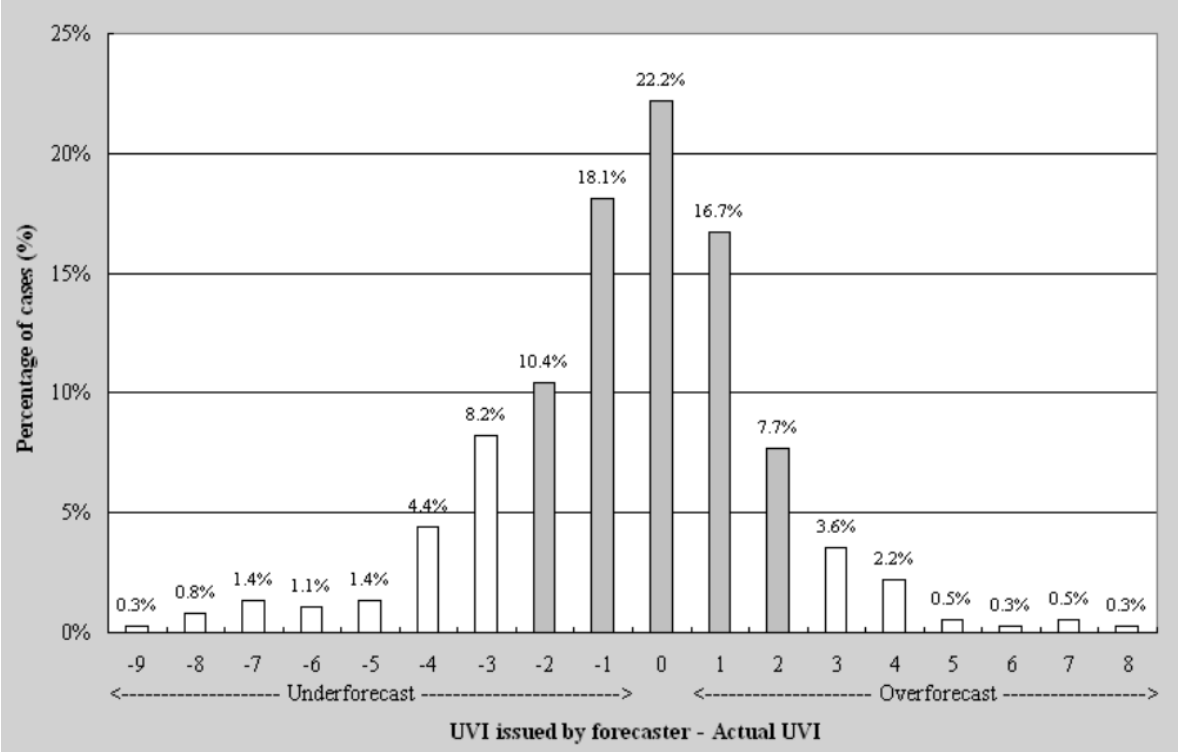

Fig. 5-5 Distribution of errors in forecasting daily maximum UVI from January 2006 to January 2007. Those within ±2 units of the actual UVI are shown in grey (75% of total).

Category-wise, 87% of UV forecasts were found to be accurate to within 1 UV category, as shown by the contingency table in Table 5-4.

The verification analysis also revealed that it was technically more difficult to forecast 'very high' or 'extreme' UV levels than the rest. A histogram showing the distribution of UVI forecast error according to the different actual UV exposure categories is given in Fig. 5-6. It can readily be seen that errors were higher in the 'very high' and 'extreme' categories. This seems to be a problem inherent in forecasting the maximum value of UV. When cloudy weather is forecast for the next day, a transient break in the clouds, which is very difficult to forecast, could lead to a sudden jump in the UV intensity and thus ruin an UVI forecast. Such error is especially more common in summer time when the noontime UV can reach the 'very high' or 'extreme' category even for only a short duration when the clouds break. In addition, the performance of the supplementary method in forecasting 'extreme' UV category as discussed in Section 3.5 depends on whether the weather is actually persistent.

UV forecast issued by forecaster	Low (0-2)	Moderate (3-5)	High (6-7)	Very High (8-10)	Extreme (>=11)
Extreme (>=11)	0.0%	0.5%	1.1%	2.2%	8.5%
Very High (8-10)	0.3%	1.9%	3.0%	6.8%	4.9%
High (6-7)	0.0%	4.9%	12.6%	4.4%	1.6%
Moderate (3-5)	5.5%	21.4%	8.8%	4.7%	1.1%
Low (0-2)	2.2%	2.2%	0.0%	1.4%	0.0%
	Actual UV				

Table 5-4
Contingency table of forecast versus actual daily maximum UV from January 2006 to January 2007. Statistics for those forecasts accurate to within $\pm$ 1 UV category are shown in grey (87% of total).

6. Conclusion

Development of a methodology for forecasting the UVI was described and its performance studied. The development work included the determination of an empirical equation, which correlated surface UV radiation with the sun's elevation, ozone concentration and the time of year. The application of the empirical equation to forecasting the clear sky UVI was found to give results of high accuracy. A set of cloud and weather modification factors was also determined for application to cloudy days or days with weather, and the results were found to be satisfactory. During the Observatory's one-year operational experience in issuing the UVI forecast from January 2006 to January 2007, 75% of the UVI forecasts were found to be within 2 units of the actual UVI. Category-wise, 87% of UV forecasts were found to be accurate to within 1 UV exposure category. It was also

found that the overall performance of UVI forecast depended very much on how good the cloud and weather forecasts were.

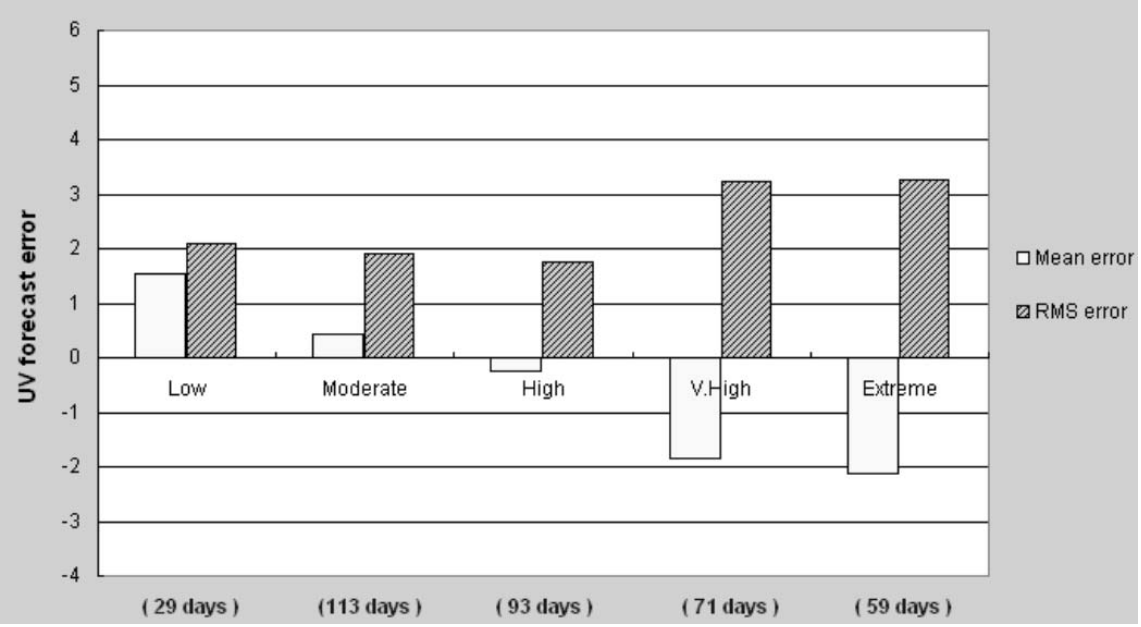

Fig. 5-6 UVI forecast error (maximum UVI issued by forecaster minus actual maximum UVI) grouped according to different actual UV exposure categories, for the period January 2006 to January 2007. Positive and negative errors stand for over-forecast and under-forecast respectively.

7. Future work

The UVI forecast was a new service introduced by the HKO in 2006. The service will continue to be improved after gaining more operational experience. Some improvement areas worth pursuing in the future were identified:

(i) As an effort to further improve the performance, especially in forecasting UV in the 'extreme' category, the method of using an empirical equation to calculate clear sky UVI can be fine-tuned by deriving different sets of equations for different seasons.

(ii) An ensemble of hourly cloud forecasts generated by numerical weather prediction models can be used so that the UVI for each hour throughout daytime can be calculated, with a view to giving a more objective forecast for the forecaster's reference.

(iii) The effect of aerosols on the intensity of UV radiation through absorption, reflection and scattering can be studied by using the Aerosol Optical Depth (AOD) product from satellite imageries, though the infrequent passes (1 to 2 times) each day over the region covering Hong Kong may limit the full potential of this useful tool.

(iv) The single-number representation of the modification factor for rain suggested by the COST project does not take account of the rainfall rate. Differences in UV attenuation brought

about by light, medium and heavy rain can be studied in the future.

(v) The present method employs extrapolation to forecast the total column ozone concentration for the next day. An empirical equation correlating the variation of ozone concentration with changes in temperature and geopotential height fields at upper atmospheric levels can be developed by performing regression analysis on past observational data. Similar study was carried out by Long (1996) and the result was found to be satisfactory.

Acknowledgement

The authors would like to thank Mr. K.M. Tse, undergraduate student of the Chinese University of Hong Kong in 2004, for his contribution in developing the empirical equation for forecasting clear sky UV. Also thanks to Mr. H.T. Poon for his guidance in the development of UV forecast methodology and Dr. B.Y. Lee, Dr. C.M. Cheng and Mr. W.M. Ma for their comments on this report.

References

Burrows, W.R., M. Vallee, D.I. Wardle, J.B. Kerr, L.J. Wilson and D.W. Tarasick, 1994: The Canadian operational procedure for forecasting total ozone and UV radiation. *Met Apps* **1**, pp 247-265.

Hudson, R.D., A.D. Frolov, M.F. Andrade, and M.B. Follette, 2003: The Total Ozone Field Separated into Meteorological Regimes. Part I: Defining the Regimes. *J. Atm. Sci.*, **Vol. 60, Issue 14**, pp 1669–1677.

Leung, Y.K., Y.Y. Cheung and E.W.L. Ginn, 2003: Solar Ultraviolet Index in Hong Kong 1999-2003. Hong Kong Observatory Technical Note (Local) **No. 80**.

Long, C.S., A.J. Miller, H.T. Lee, J.D. Wild, R.C. Przywarty and D. Hufford, 1996: Ultraviolet Index forecasts issued by the National Weather Service. *Bull. Amer. Met. Soc.*, **Vol. 77, No. 4**, pp 729-748.

Vanicek K., T. Frei, Z. Litynska, A. Schmalwieser, 2000: UV-Index for the Public, COST-713 Action 'UVB Forecasting', Brussels.

World Health Organization, 2002: Global Solar UV Index – A Practical Guide.

World Meteorological Organization, 1985: Guide to Meteorological Instruments and Methods of Observation. WMO Report **No. 8**, pp 949-950.

The Characteristics of the Southeast Monsoon in Hong Kong

C.C. Lam, Hong Kong Observatory, Hong Kong, China

1. Introduction

The monsoon is a reversal of wind with the season by definition. It is due to the seasonal changes in differential heating of continents and oceans. The direction and speed of large-scale prevailing wind are generally used to determine the type of monsoon. The East Asian monsoon, in particular, exhibits a distinct summer and winter component. The principal synoptic components of the East Asian summer monsoon system include the monsoon trough or the intertropical convergence zone (ITCZ) in the South China Sea and the western North Pacific, the cross-equatorial flow to the east of 100° E, the cold anticyclone in Australia, the subtropical high in the western North Pacific, the upper-level tropical easterly jet, the convection along the monsoon trough, the Mei-yu (the equivalent of Baiu in Japanese) frontal zones, and the mid-latitude disturbances (Tao and Chen, 1987).

Various studies by Chinese meteorologists (Tao, 1978; Chen *et al*., 1981; Tang *et al.*, 1981; Pan, 1984) indicated that the summer monsoon in China composes of Southeast Monsoon and Southwest Monsoon. Under the influence of Southeast Monsoon, a southeasterly airstream from the western North Pacific affects the region, while under the Southwest Monsoon, a southwesterly airstream from the Bay of Bengal or from the cross equatorial flow from the Southern Hemisphere prevails over the region. Whether the monsoon is southeasterly or southwesterly depends on the relative location and strength of the subtropical ridge over the western North Pacific, the monsoon trough or the ITCZ, the equatorial anticyclone and the variation of Somalia low-level jet. Of the two, the Southwest Monsoon is relatively dominant in the Asian summer monsoon. In Hong Kong, the monsoonal winds would usually be from the north or the east in winter and from the southwest in summer.

To warn the public of strong winds, the Hong Kong Observatory (HKO) had a Strong Wind Signal in the local storm warning code up to 1956. From 1956 onwards, the Strong Wind Signal has been replaced by the Tropical Cyclone Warning Signal No.3 warning of strong winds due to tropical cyclones and a separate Strong Monsoon Signal warning of strong monsoon winds. The two signals remain in use today.

Most previous studies on the summer monsoon in East Asia have emphasized the onset, break, advance and retreat of the Southwest Monsoon and its associated heavy rain belts, as well as teleconnection with sea surface temperature. There are relatively few documentations of the Southeast Monsoon although Zhu (Zhu, 1934) started discussion about the Southeast Monsoon in China as early as 1934. This paper aims at documenting the characteristics of strong Southeast Monsoon in Hong Kong. In this study, cases of strong winds associated with the Southeast Monsoon in Hong Kong from 1956 to 2006 are analysed. The associated synoptic patterns are also discussed.

2. Synoptic Patterns associated with Strong Southeast Monsoon in Hong Kong

Before the onset of the Asian summer monsoon, gradual heating over the land mass of South Asia

takes place and surface heat lows develop in the vicinity of the Tibetan Plateau. The subtropical ridge over the western North Pacific is typically located to the south of 16°N. During the onset in

early May, the upper-level westerly jet on the Tibetan Plateau weakens and retreats to the north of the Plateau. The Tibetan high in the upper level moves onto the Plateau, and the Southwest Monsoon advances northward. A trough of low pressure extending from Northeast Africa to Southeast Asia develops. The trough of low pressure that develops over the coast of southern China in late spring possesses frontal characteristics with significant temperature contrast across the trough axis and is often referred as the pre-Mei-yu front. Heavy convective rainfall develops along the pre-Mei-yu front which extends from the southern coast of China into the western North Pacific south of Japan (Johnson *et al*., 1993). The subtropical ridge over the western North Pacific advances northward to around 18°N. The heat low on land becomes established, the cross-equatorial flow at 105°E intensifies and the upper-level tropical easterlies with speeds greater than 20 m/s appear at 200 hPa over the northern part of the South China Sea. The southwesterly winds over the South China Sea may have different origins, with the western branch emanating from the Bay of Bengal, and the central and eastern branches originating from the cross-equatorial winds between 100°E and 110°E (Tao and Chen, 1987). The Southwest Monsoon with a low-level jet prevails throughout the South China Sea and the rainfall over southern China increases rapidly. The onset of the Asian summer monsoon is characterized by the establishment of strong convection and the change of the prevailing wind over the Bay of Bengal, the Indochina peninsula and the South China Sea (He *et al*., 1987; Matsumoto, 1992; Lau and Yang, 1997: Wu and Zhang 1998 and Hsu *et al*., 1999).

The East Asian Monsoon has complex space and time structures that are distinct from the South Asian (Indian) monsoon. It covers the Tropics and mid-latitudes and its rainfall season consists of staged progression of zonally oriented rain belts that contain mixed tropical and baroclinic properties (Chen and Chang, 1980). The Southeast Monsoon coincides with the break in the Southwest Monsoon. Past studies on the breaks in the monsoon emphasized the propagation of low-frequency modes and mid-latitude interactions.

During the breaks in a Southwest Monsoon, there is a phase transition from low pressure to high pressure over the northern part of the South China Sea. The subtropical ridge over the western North Pacific extends westwards covering eastern China, bringing southeasterly winds over its southwestern flank to southeastern China. An air mass boundary lies to the north of the subtropical ridge, delineating the mid-latitude cold air and the warmer airmass with higher equivalent potential temperature from the southeasterly flow over the southwestern flank of the subtropical ridge. The southwesterlies from Indochina or cross-equatorial flow meet with the southeasterlies associated with the subtropical ridge and a low-level convergence zone develops. The convergence zone usually orientates itself in NW-SE direction, extending from the Philippines to the coastal areas of southeastern China. The enhancement of southwesterlies increases the horizontal cyclonic shear over the northern part of the South Chin Sea when they encounter the southeasterlies. During the high pressure phase in July, a Southeast Monsoon generally prevails over southeastern China. A schematic diagram summarizing the main components of the airflow in the lower and upper levels during the summer monsoon is shown in Fig. C6-1 (COLOUR PLATES).

Following the seasonal change of synoptic patterns as described in the above, the synoptic patterns associated with strong southeast monsoon in Hong Kong can be broadly stratified into the following four main types (Fig. 6-2):

(i) Type MH - A trough of low pressure (pre-Mei-yu front) over the northern part of the South China Sea and a ridge of high pressure over southeastern China

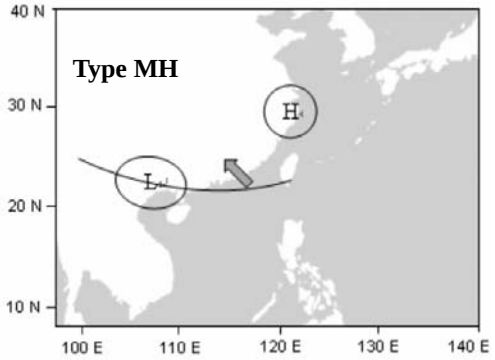

Fig. 6-2(a) Schematic diagram showing the synoptic pattern Type MH associated with strong Southeast Monsoon in Hong Kong.

The onset of summer monsoon normally occurs in May when heavy convective rainfall develops along a trough of low pressure or the pre-Mei-yu front that extends from the coast of southern China into the western North Pacific. This trough of low pressure lingers over the south China coastal region with an E-W orientation, and becomes more active when an area of low pressure develops over southwestern China. The strengthening of the trough will manifest itself as an increase of convective activities extending from Hainan area to the Philippines. When a high pressure cell over northern China advances southeastwards to eastern China, the pressure gradient and low-level horizontal shear over southeastern China will increase, especially when the trough to its south strengthens with the passage of upper-level low-latitude waves. With the strengthening of the southwesterlies to the south of the trough, the trough may jump northwards towards the south China coast, further increasing the low-level cyclonic shear over southeastern China and enhancing the southeasterlies over the region. The southeasterlies associated with this type of synoptic pattern in the early season are usually shallow. In addition, relatively strong baroclincity may exist in the pre-Mei-yu front where significant temperature difference across the trough can be found.

Hong Kong may experience strong southeasterly winds as early as late April or May, but the surge of Southeast Monsoon of this type is relatively short-lived and localised. Strong winds in Hong Kong typically last for several hours only. It may be related to the fact that the high pressure cell over eastern China usually moves eastwards rather quickly in spring time. A schematic diagram showing the synoptic pattern that will bring about strong southeasterly winds to Hong Kong in late April or May is given in Fig. 6-2(a).

(ii) Type TR - A trough of low pressure (monsoon trough) over the northern part of the South China Sea and the subtropical ridge over the western North Pacific extending westwards and strengthening

In June, the subtropical ridge extends westwards to affect the South China Sea and Indochina. There is a phase change of low pressure to high pressure over the northeastern part of the South China Sea. The westward extension of the subtropical ridge can be visualized as the westward advancement of a reduced cloudiness region on the satellite imagery. Southerly flow prevails in the low levels with a monsoon trough extending from Pakistan and Burma to the South China Sea and the Philippines. The westward extension of the subtropical ridge increases the pressure gradient over the northern part of the South China Sea. This type of pattern associated with strong southeast monsoon is characterized by the convergence between the cyclonic southwesterlies originated from the Bay of Bengal crossing Indochina and the anticyclonic southeasterlies to the southwestern flank

of the subtropical ridge over the western Pacific. The axis of the subtropical ridge lies at 24-28°N over southeastern China. The convergence zone over the northeastern part of the South China Sea generally extends from low levels to mid levels up to 700 hPa or 500 hPa. Hong Kong will experience strong southeasterly winds when it is right over the convergence zone. Schematic diagram illustrating this type of synoptic pattern which brings strong southeasterly winds to Hong Kong in summer is given in Fig. 6-2(b).

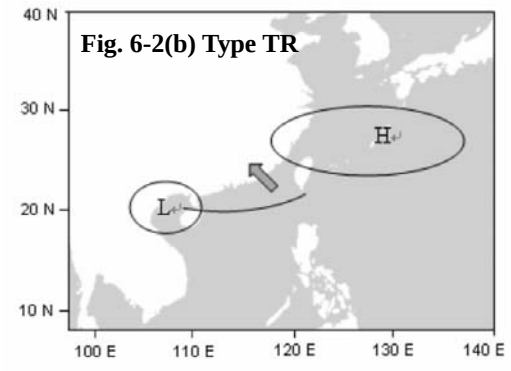

Before the onset of strong southeasterly winds, there is usually a surge of southwesterlies moving across Indochina, further enhancing the low-level convergence over the convergence zone. This signature is most prominent at the 850-hPa level. The trough of low pressure or the monsoon trough over the northern part of the South China Sea becomes sharper and edges closer to the south China coast. There is a significant decrease of baroclinicity in the lower layers as compared with the trough of low pressure in May. The 850-hPa relative vorticity over the region increases rapidly during the onset of strong Southeast Monsoon. Active convections develop over the convergence zone and maintain the strength of the low-level jet. The duration of strong southeasterly winds in Hong Kong of this type ranges from a couple of hours to more than 10 hours.

(iii) Type LR - An area of low pressure or a tropical cyclone near Hainan Island and the subtropical ridge over the western North Pacific

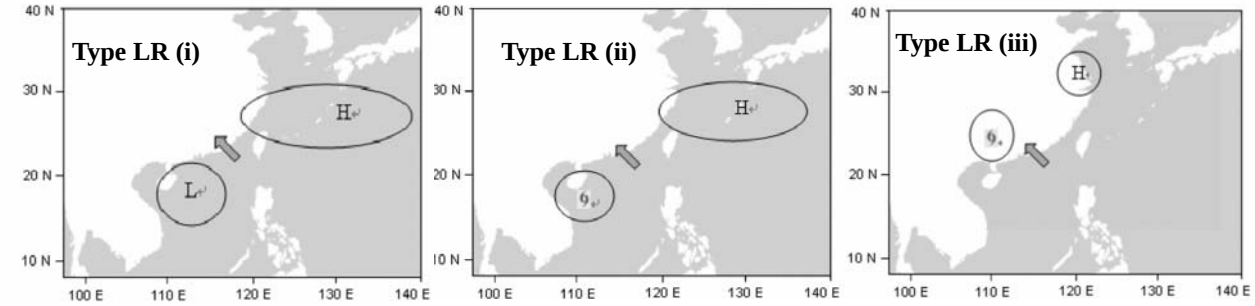

Fig. 6-2(c) Schematic diagrams showing the synoptic pattern Type LR(i), LR(ii) and LR(iii) associated with strong Southeast Monsoon in Hong Kong.

In July and August, low-level southwesterlies crossing Indochina or equatorial anti-cyclone become more active and prevail over the central and southern parts of the South China Sea. The enhancement of southwesterlies increases the horizontal cyclonic shear over the northern part of the South Chin Sea when they encounter southeasterlies to the southwestern flank of the subtropical ridge which has moved northwestwards covering eastern China.

Latent heat released in the precipitation associated with the southwesterly air mass possessing high equivalent temperature warms up the lower atmosphere and a positive feedback mechanism comes

into play. The environmental set-up favours the development of an area of low pressure near Hainan. When the subtropical ridge persists over eastern China or extends further westwards, and the area of low pressure in the vicinity of Hainan intensifies simultaneously, the enhanced convergence between the anticyclonic and cyclonic flows will bring strong southeasterly winds to Hong Kong. A schematic diagram showing this type of synoptic pattern is given in Fig. 6-2(c)(i). The area of low pressure near Hainan Island is relatively persistent. The duration of strong Southeast Monsoon is generally longer in July than in June. For more intense low, the duration of strong winds will be longer. The duration of strong southeasterly winds in Hong Kong of this type ranges from a couple of hours to as long as a day.

The area of low pressure near Hainan in July or August may even intensify into a tropical cyclone with moisture-laden southwesterlies feeding into the low from the Bay of Bengal or cross-equatorial flow between 100°E and 110°E. Strong southeasterlies then prevail over southeastern China. If the size of the tropical cyclone is small enough so that the outermost closed isobar does not cover southeastern China and its adjacent areas, the convergent southeasterlies between the outer circulation of the tropical cyclone and the subtropical ridge constitutes a Southeast Monsoon. A schematic diagram showing this type of synoptic pattern is given in Fig. 6-2(c)(ii). Strong Southeast Monsoon associated with this type is generally more persistent compared with the other types of synoptic pattern. The duration of strong southeasterly winds in Hong Kong usually lasts for 6 hours or more, depending on the movement and strength of the tropical cyclone.

When a tropical cyclone lands over southwestern China while a ridge of high persists over southeastern China, a strong southeasterly airflow will again develop over the convergence zone. The Southeast Monsoon associated with such landfalling tropical cyclones in August is generally short-lived as the cyclone will normally weaken rapidly over inland areas. The duration of strong southeasterly winds in Hong Kong of this type usually lasts for a couple of hours only. A schematic diagram showing this type of synoptic pattern is given in Fig. 6-2(c)(iii).

(iv) Type GR - A monsoon depression over the central part of the South China Sea and the subtropical ridge over the western North Pacific

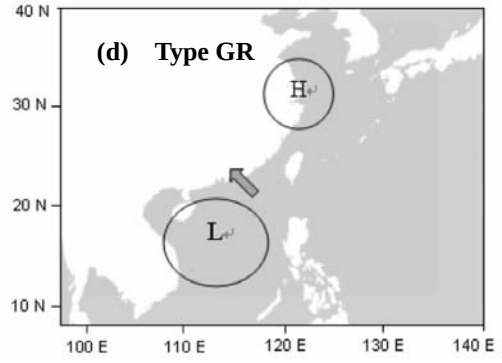

Fig. 6-2(d) Schematic diagram showing the synoptic pattern Type GR associated with strong Southeast Monsoon in Hong Kong.

The subtropical ridge starts to retreat southward in early September. In mid September, the low-level circulation pattern in eastern Asia changes suddenly from cyclonic to anticyclonic. The subtropical ridge reaches 25°N in late September and it retreats to 17°N by late October (Tao and Chen, 1987). Cold anticyclones then frequently invade from the north. The summer monsoon normally ends in August or September. The late season summer monsoon in Hong Kong is usually due to the development of a monsoon gyre over the central part of the South China Sea, bringing

strong southeasterly winds to the region. A schematic diagram showing this type of synoptic pattern is given in Fig. 6-2(d). The convections are mostly concentrated at the outer circulation of the depression as evident from satellite pictures.

A monsoon depression is a tropical cyclonic vortex characterized by (i) its large size, the outermost closed isobar may have a diameter on the order of 1000 km; (ii) a loosely organized cluster of deep convective elements; (iii) a low-level wind distribution which features a 200-km diameter light-wind core that may be partially surrounded by a band of gales; and (iv) a lack of distinct cloud system centre (JTWC, 1994). It may develop from a monsoon gyre. A monsoon gyre is a mode of summer monsoon circulation characterized by (i) a very large nearly circular low-level cyclonic vortex that has an outermost closed isobar with diameter on the order of 2500 km; (ii) a cloud band rimming the southern through eastern periphery of the vortex; (iii) a relatively long life span – initially, a subsidence regime exists in its core and western and northwestern quadrants with light winds and low cumulus clouds, and later the area within the outer closed isobar may fill with deep convective cloud and become a monsoon depression or tropical cyclone or some midget tropical cyclones may emerge from the leading edge of the peripheral cloud band of a monsoon gyre (Lander, 1994). As the South China Sea is surrounded by landmass of China, Vietnam, Borneo and the Philippines, the size of the monsoon gyre over the region will be generally smaller than that over the western Pacific. A monsoon gyre or depression normally progresses westward or northwestward and shrink its size as latitude increases. As far as Southeast Monsoon is concerned, the role played by a monsoon gyre or a monsoon depression is similar. In case of a monsoon gyre, there can be more than one midget low or tropical cyclone developing around the periphery of the gyre.

Some monsoon depressions may develop into a tropical cyclone. The transition to a tropical cyclone structure requires the development of a central region of deep convection and a core of accelerated winds. When there are central convection and gale winds that merge with the outer gales, a tropical cyclone has formed. The tropical cyclone formed in this way is usually larger in size (Elsberry, 2004). Whether a region is affected by the tropical cyclone or Southeast Monsoon requires detailed analysis, taking into account the size and evolution of the tropical cyclone as well as the intensity of the subtropical ridge. If the outermost closed isobar of the tropical cyclone does not cover the region during its life cycle, strong southeasterlies prevailing over the region can be considered as the effect of the Southeast Monsoon.

3. Frequency Analysis of Strong Southeast Monsoon in Hong Kong

A strong monsoon is defined as a surface wind whose hourly mean speed is 11.5 m/s or more that is associated with the summer or winter monsoon. Due to the elevation of the anemometer at Waglan Island (Fig. 6-3), an equivalent wind speed of 14.5 m/s is taken as a surface wind of 11.5 m/s at sea-level in the nearby area (Chin and Leong, 1978). The HKO will issue the Strong Monsoon Signal and special announcements to the public to alert them of the threat of high winds associated with the monsoon with an indication of the direction from which winds are expected to blow and exceed 11.5 m/s near sea level anywhere in Hong Kong. Before 1985, anemometer readings were available from five manned stations in Hong Kong including Waglan Island and Cheung Chau in the offshore areas (Fig. 6-3). A network of automatic weather stations was set up in around 1985. Up to the present, the HKO retrieves data from more than 60 anemometer stations over the territory.

Cases of strong winds associated with monsoons with duration of two hours or more during the period of Strong Monsoon Signal were extracted from all stations. The data period spans from 1951 to 2006. There are 863 cases of Strong Monsoon Signal within a period of 56 years. There

are strong monsoon cases not included in the dataset such as cases with strong winds lasting for less than two hours, and cases with strong winds lasting for two hours or more but somehow the Strong Monsoon Signal was not issued for some reasons.

The frequency distribution for the occurrence of different types of monsoons is analysed and plotted in Fig. C6-4 (COLOUR PLATES). During the 56-year period of study, Northeast Monsoon (wind surge from the East, Northeast or North) amounted to 94.2 % (813 cases) of the strong monsoons,

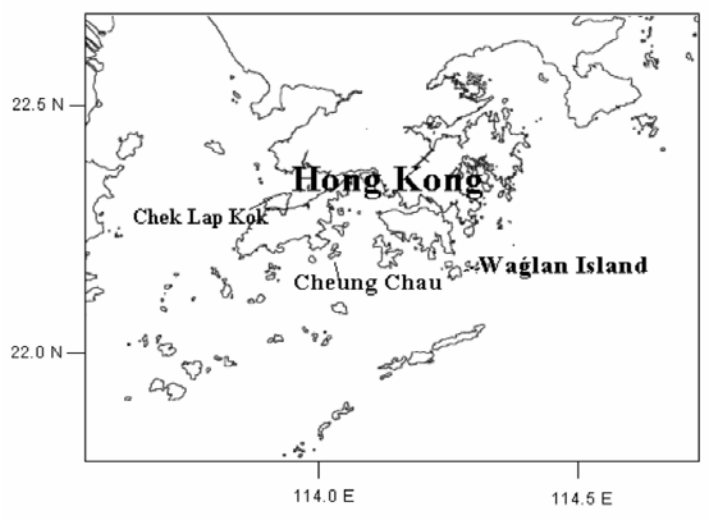

Fig. 6-3
A map showing the location of Hong Kong and the wind stations mentioned in the text.

4.3 % (37 cases) for the Southwest Monsoon (wind surge from the Southwest and South) and 1.5 % (13 cases) for the Southeast Monsoon (wind surge from the Southeast). On average, the Southeast Monsoon attains strong intensity about once every 4.3 years while strong Southwest Monsoon occurs around once every 1.5 years in Hong Kong. Strong summer monsoon is much less frequent than strong winter monsoon which amounts to about 14.5 times a year. It was noticed from Fig. C6-4 that July was the only month that no Strong Monsoon Signal had ever been issued for strong easterly winds. The percentage of strong monsoon signals issued for different wind directions is given in Fig. C6-5 (COLOUR PLATES). Winds at Cheung Chau met the criteria of the Strong Monsoon Signal in all Southeast Monsoon cases while Waglan Island met the criteria in about 25 % of the cases. It should be noted that the statistical analysis in this study is by no means comprehensive and rigorous. The analysed results serve to illustrate in a broad sense the relative frequency of strong monsoons with stratifications in different wind directions and seasons.

Table 6-1 shows the dates and duration of the Strong Monsoon Signal issued in Hong Kong for the Southeast Monsoon. The earliest onset time of strong Southeast Monsoon was in mid April and the latest time of occurrence was in early October. Summer monsoon typically blows from the Southwest (which is the Southwest Monsoon), amounting to 74 % of the total, while the Southeast Monsoon only accounted for 26 % of the summer monsoon. The latest time of occurrence of the Southwest Monsoon was in late August, earlier than that of the Southeast Monsoon. The average duration of the Strong Monsoon Signal for Southeast Monsoon was 13 hours ranging from 1.4 hours to 34.2 hours while that for the Southwest Monsoon was 12 hours. The Northeast Monsoon is generally more persistent with an average duration of about 16 hours. The duration of strong monsoon signals for winter and summer monsoons during the data period is shown in Fig. C6-6 (COLOUR PLATES).

The relative importance of different types of synoptic patterns associated with strong Southeast Monsoon in Hong Kong, which are identified in section 2, can be analysed based on the average duration of strong southeasterly winds recorded and the relative frequency of occurrence for the 13 cases in Table 6-1. Considering that strong winds were recorded at Cheung Chau for all strong Southeast Monsoon cases, the average duration of strong winds recorded at Cheung Chau with different synoptic patterns was taken as a measure of relative importance. The relative frequency of occurrence was also calculated for each type of synoptic pattern. As shown in Table 6-2, Type LR, with the longest average duration of strong winds and the highest frequency of occurrence, is the most important and common type of synoptic pattern associated with strong Southeast Monsoon in Hong Kong. Strong southeasterly winds are generally more persistent in Type LR, which occurs mainly in July and August, and also Type GR in September and October, with an average duration of more than 10 hours. The duration of strong southeasterly winds associated with Type TR varies considerably among cases, albeit with an average duration of more than 10 hours. Type TR, which mainly occurs in June, is also a common pattern associated with strong Southeast Monsoon. The least important pattern is Type MH in which strong southeasterly winds are generally short-lived with an average duration of 2 hours or so in April and May. It should be noted that the dataset may be too small to generate rigorous statistics of Southeast Monsoon. However, the above discussions aim at giving a general idea of the characteristics of strong Southeast Monsoon in Hong Kong.

Start time	Start date	End time	End date	Duration (hours)	Type of SE Monsoon	Rainfall recorded at HKO from start date to end date (mm)
20:30	18 April 2001	1:45	19 April 2001	5.3	MH	7.7
19:15	20 May 2002	23:30	20 May 2002	4.3	MH	7.2
7:55	26 June 2001	16:15	26 June 2001	8.3	TR	73.1
1:30	27 June 2001	23:15	27 June 2001	21.8	TR	136.4
18:50	26 June 1978	5:00	28 June 1978	34.2	TR	53.3
8:30	30 June 2005	10:30	30 June 2005	2.0	TR	47.0
12:10	11 July 2000	15:00	12 July 2000	26.8	LR	37.0
3:00	17 July 2000	9:15	18 July 2000	30.3	LR	104.5
16:10	10 August 2001	19:25	10 August 2001	3.3	LR	20.9
8:25	20 August 2002	9:50	20 August 2002	1.4	LR	14.6
22:25	14 September 2003	14:45	15 September 2003	16.3	GR	186.0
4:45	16 September 2003	16:45	16 September 2003	12.0	GR	23.6
14:30	6 October 1981	19:00	6 October 1981	4.5	GR	13.0

Table 6-1 Dates and duration of strong monsoon signals issued in Hong Kong for the Southeast Monsoon during the 56-year period from 1951 to 2006 in an increasing order of the month. The type of Southeast Monsoon for each case was analysed according to the stratifications in section 2 of the text. Time is specified in Hong Kong local time.

Priority	Type	Common months of occurrence	Average duration of strong southeasterly winds at Cheung Chau on the days with strong monsoon signal (hours)	Percentage of frequency of different types of strong SE Monsoon
1	LR	July, August	15	31 %
2	TR	June	12	31 %
3	GR	September, October	11	23 %
4	MH	April, May	3	15 %

Table 6-2 The characteristics of the four types of synoptic patterns associated with strong Southeast Monsoon in Hong Kong. The priority is in the order of decreasing relative importance of the pattern. Details of the stratifications and the analysis of relative importance can be found in section 2 and section 4 of the text respectively.

4. Case Illustrations of Strong Southeast Monsoon in Hong Kong

Out of the 13 cases of strong southeasterly winds locally with the issuance of the Strong Monsoon Signal from 1956 to 2006, five cases were selected to illustrate the characteristics of each type of synoptic pattern stratified in section 2.

(i) Early Season Case of 20 May 2002 – Type MH

The onset of summer monsoon over southern China in 2002 was in mid May. Low pressure areas developed along the monsoon trough lying across the foothills of the Himalayas in mid May. The trough gradually extended eastwards to southern Taiwan on 17 May. A temperature difference of around three degrees was observed across the trough over the northern part of the South China Sea and it was identified as the Pre-Mei Yu front. Southwesterlies prevailed over the Bay of Bengal, Indochina, northern part of the South China Sea and southern China at 850-hPa level. A southwesterly surge originated from the Bay of Bengal spread to the South China Sea on 20 May. At the same time, the high pressure cell over northern China advanced southeastwards to eastern China with a ridge of high pressure extending along the coast of southeastern China. The southeasterlies prevailed over southeastern China were shallow with a vertical depth of less than 2 km.

In Hong Kong, strong southeasterly winds were recorded at Cheung Chau at 19-21 H on 20 May. Hourly mean winds remained strong for three consecutive hours only. There was a report of very windy conditions resembling a tornado on Chek Lap Kok Island amidst active thunderstorms. The event was captured by the HKO's Terminal Doppler Weather Radar with opposing winds exceeding 90 kilometres per hour detected within one kilometre across at Chek Lap Kok. Fig. C6-7 (COLOUR PLATES) shows the synoptic situation at 00 UTC on 20 May. Satellite imagery showed that the convective activities associated with the trough increased and extended eastwards from Hainan area to the Philippines a couple of days before the onset of strong southeasterlies in Hong Kong and the northward shift of the convective activities towards the south China coast on 20 May (Fig. C6-8 in COLOUR PLATES).

(ii) Summer Case of 26-27 June 2001 – Type TR

Tropical cyclone Chebi developed over the ITCZ running from NW to SE at 10-20°N on 20 June 2001. It tracked northwestwards towards Taiwan along the southwestern periphery of the subtropical ridge over the western North Pacific and then turned northwards to eastern China along the western flank of the subtropical ridge on 24 June. The monsoon trough over the South China Sea shifted northwards and oriented NE-SW following the northward advancement of the southwesterlies associated with Chebi. An area of low pressure developed near Beibu Wan. A mid-level vortex could be identified on 700-hPa and 500-hPa levels over the South China Sea around 5 degrees latitude to the southeast of the surface low pressure area. Strong southerly winds were observed at the confluence zone over the western flank of the subtropical ridge at low to mid levels. Short waves at low to mid levels moved across Indochina feeding energy to the vortex in the strong southwesterlies. With decreasing vertical shear, the mid-level vortex became more aligned with the low-level vortex and intensified rapidly on 25-26 June. Meanwhile, the subtropical ridge oriented E-W at 25-27°N extended westwards towards southeastern China after Chebi dissipated near Shanghai. The westward extension of the subtropical ridge can be visualized as the westward advancement of a reduced cloudiness region on the satellite imagery (Fig. C6-9 in COLOUR PLATES). The confluence zone between the southerlies along the western flank of the subtropical

ridge and those over the eastern periphery of the vortex was situated over southeastern China and the northeastern part of the South China Sea.

In Hong Kong, southeasterlies picked up in the early morning of 26 June, reaching strong force for more than 10 hours at Cheung Chau during 26-27 June. The synoptic situation at 00 UTC 26 June is shown in Fig. C6-10 (COLOUR PLATES). There was no significant difference in surface temperature across the trough. Heavy thundery showers brought more than 200 millimetres of rainfall to the northern part of Hong Kong and 136.4 millimetres of rainfall were recorded at the HKO Headquarters. There were 40 reports of flooding and 8 reports of landslip in Hong Kong.

(iii) Summer Cases of 11 July 2000, 10 August 2001 and 20 August 2002 – Type LR

In the wake of the tropical cyclone Kai-Tak which developed off the west coast of Luzon and tracked northwards towards eastern China, an area of low pressure developed over the northern part of the South China Sea on 10 July 2000. The vortex was most prominent at 500-hPa level before it developed at the low levels. The subtropical ridge over 27°N extended rapidly westwards covering eastern China on 11 July. The convergence zone between the southeasterlies along the southwestern flank of the subtropical ridge and the northeast quadrant of the area of low pressure established over southeastern China. The southeasterlies over the convergence zone were rather deep with a vertical extent to the mid level. Strong and moisture-laden southwesterlies continued to feed to the low pressure area from the Bay of Bengal and the cross-equatorial flow from 100°E and 110°E during 10-11 July. With further westward extension of the subtropical ridge, the region of strong southeasterlies spread to the western part of the south China coastal region and the area of low pressure moved westwards towards northern Vietnam.

In Hong Kong, strong southeasterlies picked up at Cheung Chau in the morning of 11 July and lasted for more than 20 hours. Fig. C6-11 (COLOUR PLATES) shows the synoptic situation at 00 UTC on 11 July. Scattered showers and thunderstorms affected the territory and 37 millimetres of rainfall were recorded at the HKO Headquarters on 11-12 July.

There are some cases that an area of low pressure near Hainan Island develops into a tropical cyclone in July or August. In the case of tropical cyclone Usagi in 2001, it developed about 300 km southeast of Hainan Island on 9 August. It was slow-moving at first but took on a steady westward track on the following day. It started to depart from Hong Kong on the early morning of 10 August and made landfall over Vietnam on 11 August. The outermost closed isobar of Usagi was located about 300 km away from Hong Kong at the closest. Under the combined effect of the ridge of high pressure over southeastern China and Usagi, winds in Hong Kong strengthened from the southeast briefly in the afternoon of 10 August. Strong winds were recorded at Cheung Chau for about 6 hours. As deduced from the synoptic pattern at 00 UTC on 10 August in Fig. C6-12 (COLOUR PLATES), the strengthening of southeasterly winds in Hong Kong was not directly due to the tropical cyclone.

When a tropical cyclone lands over southwestern China while a ridge of high pressure persists over southeastern China, Hong Kong may also experience strong southeasterly winds. The southeast monsoon associated with the landfalling tropical cyclone Vongfong on 20 August 2002 was very short-lived. Vongfong developed about 600 km southeast of Hainan Island on 15 August and took on a northerly track generally towards the coast of western Guangdong. The HKO issued the Standby Tropical Cyclone Signal No.1 on the night of 17 August. Vongfong skirted the

northeastern coast of Hainan, made landfall on the night of 19 August and weakened rapidly afterwards. The Standby Tropical Cyclone Signal No.1 was cancelled in the early morning of 20 August when Vongfong was more than 500 km northwest of Hong Kong (Fig. C6-13 in COLOUR PLATES). The circulation of Vongfong became much smaller as it weakened over land. Strong southeasterlies persisted over Hong Kong though Vongfong was more than 500 km away and was departing. The HKO issued the Strong Monsoon Signal about two hours after the cancellation of the No.1 Signal. As Vongfong weakened rapidly, winds subsided a few hours after the issuance of the Strong Monsoon Signal. This illustrates the situation of the Southeast Monsoon associated with landfalling tropical cyclone to the northwest of Hong Kong with a ridge of high pressure building up or maintaining over southeastern China where the outermost closed isobar of the tropical cyclone is well away from Hong Kong but strong wind persists over the region.

(iv) Late Season Case of 14-16 September 2003 – Type GR

A monsoon depression with a diameter of about 1000 km developed over the central part of the South China Sea on 14 September 2003 (Fig. C6-14(a) in COLOUR PLATES). It moved northwards towards Hainan Island and reduced in size (Fig. C6-14(b)). The convections associated with the monsoon depression were mostly concentrated at its outer circulation (Fig. C6-15(a) in COLOUR PLATES). It was probably due to the fact that regions of significant upper-level divergence were mainly located at the periphery of the monsoon depression (Fig. C6-14(c)-(d)). When the monsoon depression advanced northwards, its central convection increased and its circulation contracted. The convergence zone between the eastern periphery of the monsoon depression and the ridge of high pressure over southeastern China brought strong southeasterly winds to Hong Kong. Southeasterlies strengthened at Cheung Chau on the night of 14 September. Strong winds were rather persistent and they weakened on the afternoon of 16 September after the monsoon depression made landfall over southwestern China. Winds at Waglan Island also once reached strong force for a few hours in the early morning of 15 September. Around 200 millimetres of rainfall were recorded at the HKO Headquarters during 14-16 September.

5. Concluding Remarks

Hong Kong experiences both Southeast Monsoon and Southwest Monsoon in summer. Based on the records of the Strong Monsoon Signal from 1951 to 2006, the earliest onset time of strong Southeast Monsoon was found in mid-April. The Southeast Monsoon accounts for 26 % of the summer monsoon while the Southwest Monsoon accounts for 74 %. The latest time of the occurrence of the Southeast Monsoon is in early October while that of the Southwest Monsoon is in late August. The average duration of the Strong Monsoon Signal for Southeast Monsoon is 13 hours which is comparable to the Southwest Monsoon. Strong winds associated with the winter monsoon are generally more persistent than the summer monsoon in Hong Kong.

The synoptic patterns associated with the Southeast Monsoon in Hong Kong are broadly stratified into four main types in this study, namely

(i) Type MH - A trough of low pressure (pre-Mei-yu front) over the northern part of the South China Sea and a ridge of high pressure over southeastern China;

(ii) Type TR - A trough of low pressure (monsoon trough) over the northern part of the South China Sea and the subtropical ridge over the western North Pacific extending westwards and strengthening;

(iii) Type LR - An area of low pressure or a tropical cyclone near Hainan Island and the subtropical ridge over the western North Pacific;

(iv) Type GR - A monsoon depression over the central part of the South China Sea and the subtropical ridge over the western North Pacific.

The onset of the Southeast Monsoon in May accompanies a trough of low pressure or the pre-Mei-yu front south of Hong Kong and a ridge of high pressure extending from northern China to eastern China. During June to August, the Southeast Monsoon is characterized by the convergence between the cyclonic southwesterlies originated from the Bay of Bengal crossing Indochina or the cross equatorial flow and the anticyclonic southeasterlies to the southwestern flank of the subtropical ridge over the western North Pacific. Along the trough of low pressure or the monsoon trough, an area of low pressure may form near Hainan Island, and the convergence with the subtropical ridge extending westward covering eastern China may trigger Southeast Monsoon to prevail over southeastern China and its adjacent areas. In the late season of September, a monsoon depression or a monsoon gyre may develop over the South China Sea. Together with the southward retreat of the subtropical ridge over eastern China to around 25°N, the convergence zone develops again over southeastern China, and that may bring strong Southeast Monsoon to the region. Due to the relatively large size of the monsoon depression or gyre, and its active convections and high wind regions concentrating at the outer circulation, the Southeast Monsoon may affect Hong Kong even if the monsoon depression or gyre is located more than 1000 km from Hong Kong. A monsoon gyre may develop into a monsoon depression which may in turn develop into a tropical cyclone when intense and persistent convections develop at the centre.

Type LR, with the longest average duration of strong winds and the highest frequency of occurrence, is the most important and common type of synoptic pattern associated with strong Southeast Monsoon in Hong Kong. Strong southeasterly winds are generally more persistent in Type LR, which mainly occurs in July and August, and also Type GR in September and October with an average duration of more than 10 hours. The duration of strong southeasterly winds associated with Type TR varies considerably among cases, albeit with an average duration of more than 10 hours. Type TR, which mainly occurs in June, is also a common pattern associated with strong Southeast Monsoon. The least important pattern is Type MH in which strong southeasterly winds are generally short-lived with an average duration of 2 hours or so in April and May.

Although extensive studies have been carried out by Chinese meteorologists regarding the summer monsoon in China, publications on the Southeast Monsoon are few. This note serves to document the characteristics of the Southeast Monsoon in Hong Kong.

Acknowledgments

The author would like to thank Mr. C.Y. Lam, Dr. M.C. Wong and Mrs. Hilda Lam for their valuable comments. The cloud imagery was originally captured by GMS-5 of the Japan Meteorological Agency.

References

Chen, G.T., and C.-P. Chang, 1980: Structure and vorticity budget of early summer monsoon trough (Mei-Yu) over southeastern China and Japan. *Mon. Wea. Rev.*, **108**, 942-953.

Chen, B.L., G.R. Qian, Z.H. Yu, and Z.Z. Yu, 1981: The preliminary analysis of the summer monsoon and the rainy season in the Zhejiang Province. *Proceedings of the Symposium on the Summer Monsoon in South East Asia, 15-21 August 1981, HongZhou, China*. People's Press of

Yunnan Province, 227-228 (in Chinese).

Chin, P.C., and H.C. Leong, 1978 : Estimation of wind speeds near sea-level during tropical cyclone conditions in Hong Kong. Hong Kong Observatory Technical Note No.45, 35 pp.

Elsberry, R.L., 2004: Monsoon-related tropical cyclones in East Asia. *East Asian Monsoon*, C-.P. Chang, Eds., World Scientific Series on Meteorology of East Asia, 463-498.

He, H., J.W. McGinnis, Z.S. Song and M. Yanai, 1987: Onset of the Asian summer monsoon in 1979 and the effect of the Tibetan Plateau. *Mon. Wea. Rev.*, **115**, 1966-1994.

Hsu, H.-H., C.-T. Terng and C.-T. Chen, 1999: Evolution of large-scale circulation and heating during the first transition of Asian summer monsoon. *J. Climate*, **12**, 793-810.

JTWC, 1994 : *Annual Tropical Cyclone Report*, Joint Typhoon Warning Center, 425 Luapele Road, Pearl Harbor, HI 96860-3130, 337 pp.

Johnson, R.H., Z. Wang, and J.F. Bresch, 1993: Heat and moisture budgets over China during the early summer monsoon. *J. Meteor. Soc. Japan*, **71**, 137-152.

Lander, M.A., 1994: Description of a monsoon gyre and its effects on the tropical cyclone in the western North Pacific during August 1991. *Wea. Forecasting*, **9**, 650-654.

Lau, K.M., and S. Yang, 1997: Climatology and interannual variability of the southeast Asian summer monsoon. *Adv. Atmos. Sci*., **14**, 141-162.

Matsumoto, J., 1992: The seasonal changes in Asian and Australian monsoon regions. *J. Meteor. Soc. Japan*, **70**, 15-32.

Pan, Y.H., 1984 : Typhoon, monsoon in Asia and sea surface temperature in the equatorial Pacific ocean. *Proceedings of the Beijing International Symposium on Climate, 30 Oct.-3 Nov, 1984, Beijing, China. The Climate of China and Global Climate*, Y. Duzhen, C. Fu, J. Chao and M. Yoshino, Eds., 157-166.

Tang, M.M., and S.S. Huang, 1981: On the advance and retreat of the summer monsoon of eastern China in 1979. *Proceedings of the Symposium on the Summer Monsoon in South East Asia, 15-21 August 1981, HongZhou, China,* People's Press of Yunnan Province, 15-30 (in Chinese with English abstract).

Tao, S.Y., 1978 : East Asian Monsoon. *Knowledge on Synoptic Meteorology*, Institute of Atmospheric Physics, Chinese Academy of Sciences, Eds., 105-114 (in Chinese).

Tao, S.Y., and L. Chen, 1987 : A review of recent research on the East Asian Summer Monsoon in China. *Monsoon Meteorology*, C.P. Chang and T.N. Krishnamurti, Eds., Oxford Univ. Press, 60-92.

Wu.G., and Y. Zhang, 1998: Tibetan Plateau forcing and the timing of the monsoon onset over South Asian and the South China Sea. *Mon. Wea. Rev.*, **126**, 913-927.

Zhu, K.Z., 1934: The enigma of southeast monsoon in China. *Acta Geographica Sinica*, **1**, 1-27 (in Chinese).

Comparison of Manual Observations and Instrumental Readings of Visibility at the Hong Kong International Airport

P.W. Chan and C.M. Shun, Hong Kong Observatory, Hong Kong, China

1. Introduction

Instrumental measurements with properly maintained sensors have the advantages of being objective and consistent at all times. There is a global trend to use instrumental readings, either as an aid to or as a substitute for manual meteorological observations. In step with this trend, a dense network of six forward scatter sensors (locations in Fig. 7-1) was installed along the two runways of Hong Kong International Airport (HKIA) in 2002, for measuring the visibility in various sectors. A similar sensor has also been installed at Central Pier in 2006 for visibility measurement in the Victoria Harbour. It is envisaged that more will be set up in other parts of Hong Kong in the coming years.

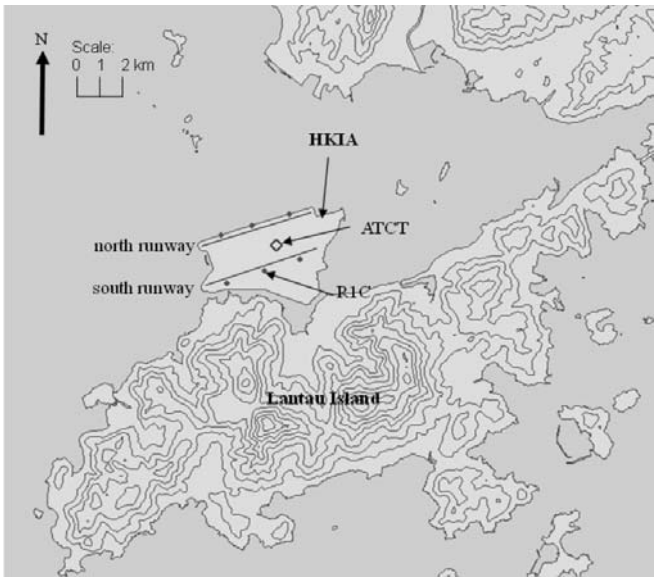

Fig. 7-1
Locations of the airport weather office (spade) and the forward scatter sensors (grey dots) at HKIA. Height contour: 100 m.

Manual observations by trained meteorological observers at the Air Traffic Control Tower (ATCT) near the middle of the airport (location in Fig. 7-1) have been used for official visibility reporting at HKIA since March 1997. In line with changes in the requirements of International Civil Aviation Organization (ICAO), the forward scatter readings were made available to observers for reference in making visibility reports provided to aircraft starting from late November 2004.

To establish the continuity of the climatology of visibility in the transition from manual observation to instrumental measurement, this paper compares the manual observations and instrumental measurement data sets over a 2-year period at HKIA. The construction of a continuous time series of reduced visibility at the airport before and after the introduction of the instrumental data is also explained.

2. Instrumental visibility readings vs. manual observations

Between the two means of visibility measurement, there are fundamental differences, viz. (a) in the sampling volume (atmospheric conditions in all directions for manual observation vs. a limited

sampling volume of 0.1 litre for the forward scatter sensor in use at HKIA) and (b) the averaging period (nearly instantaneous observation by the weather observer vs. 10-minute mean from the sensor). The readings derived from the two methods would inevitably differ from time to time. It is thus important to conduct a statistical comparison through parallel runs. Following the guidelines of WMO (2007), for the transition from manual observations to instrumental readings, the continuity of climatological records has to be assured by parallel collection of data for at least two years. The data of parallel run compared in this paper cover the period January 2003 to December 2004.

Among the six forward scatter sensors at HKIA, the one near the middle of the south runway (R1C, location in Fig. 7-1) is situated near the middle of the airfield and close to ATCT where the visibility observations by human observers are made. Following the WMO standard of visibility measurements (WMO, 2006), 10-minute mean values of the meteorological optical range (MOR) provided by the forward scatter sensor were analyzed.

The analysis method used by the Royal Netherlands Meteorological Institute (KNMI) in the transition from human observations to forward scatter data for visibility climatology applications was adopted in this study (KNMI, 2003). The following analyses have been performed:

(a) contingency matrix of the observed (by the human observer) and the measured (by the forward scatterer sensor) visibility readings in various visibility classes;

(b) box plot of the ratio of the measured to the observed visibility in these visibility classes.

The results are shown in Fig. 7-2.

Manual observation	R1C 10-minute mean MOR										
	NA	<100m	<200m	<500m	<1km	<2km	<5km	<10km	<20km	>=20km	all
NA	0	0	0	0	0	0	0	0	0	0	0
<100m	0	0	0	0	0	0	0	0	0	0	0
<200m	0	0	0	0	0	0	0	0	0	0	0
<500m	0	0	0	1	0	0	0	0	0	0	1
<1km	0	0	0	1	3	7	0	0	1	0	12
<2km	0	0	0	0	3	42	47	1	1	0	94
<5km	22	0	0	0	0	25	786	352	8	1	1194
<10km	234	0	0	0	0	0	298	4853	738	45	6168
<20km	231	0	0	0	0	0	3	1390	4591	882	7097
>=20km	70	0	0	0	0	0	0	1	233	2674	2978
all	557	0	0	2	6	74	1134	6597	5572	3602	17544

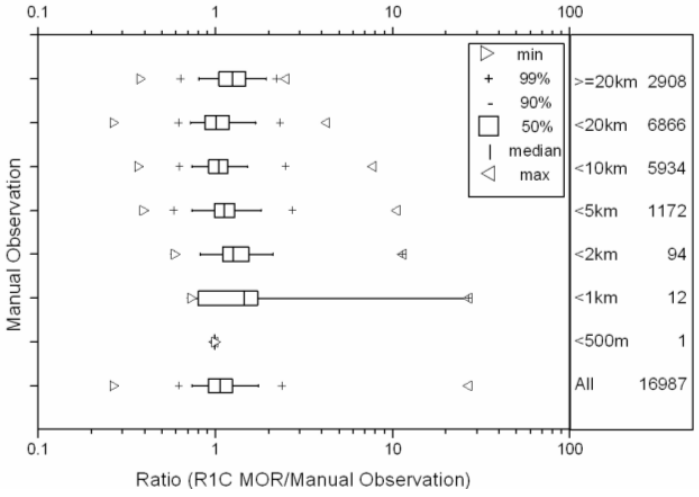

Fig. 7-2
Contingency matrix (upper) and box plot (lower) based on the observed and the measured visibility values in the period Jan 2003 to Dec 2004

In the contingency matrix, about 76.2% of the data lie on the diagonal, i.e. the observed and the measured visibilities are in the same visibility class. The proportion of data within one visibility class is 99.6%.

In the box plot, the mean and the median of the ratio are 1.13 and 1.07 respectively, with a standard deviation of 0.42. The 50% ratio limits are 0.91 and 1.24, and the 90% ratio limits are 0.74 and 1.75. The mean and the median ratios in the "<10 km" category are 1.09 and 1.05 respectively.

The above results are generally comparable with those reported in KNMI (2003). It is considered that the measured and the observed visibility values at HKIA have good overall statistical agreement. It supports the transition from human observations up to 2004 to R1C MOR data starting from 2005, for the purpose of constructing a continuous climatology of visibility at HKIA.

3. Time Series of Reduced Visibility

The climatology of visibility could be expressed in terms of the percentage of reduced visibility (PRV). The threshold of reduced visibility in haze is taken to be 8 km (Cheng and Koo, 1986). The PRV is derived from the hourly visibility readings (observed by the human observer or measured by the forward scatterer sensor) excluding weather conditions when fog, mist or precipitation is reported or when the relative humidity (RH) is 95% or above, following Chang and Koo (1986).

The time series of PRV at HKIA constructed based on the manual observations in 2004 and before and that based on the 10-minute mean MOR readings from R1C forward scatter sensor in 2004 and later is shown in Fig. 7-3. In the year of overlap, that is, 2004, the PRV values based on manual observations and R1C MOR data are within 3%.

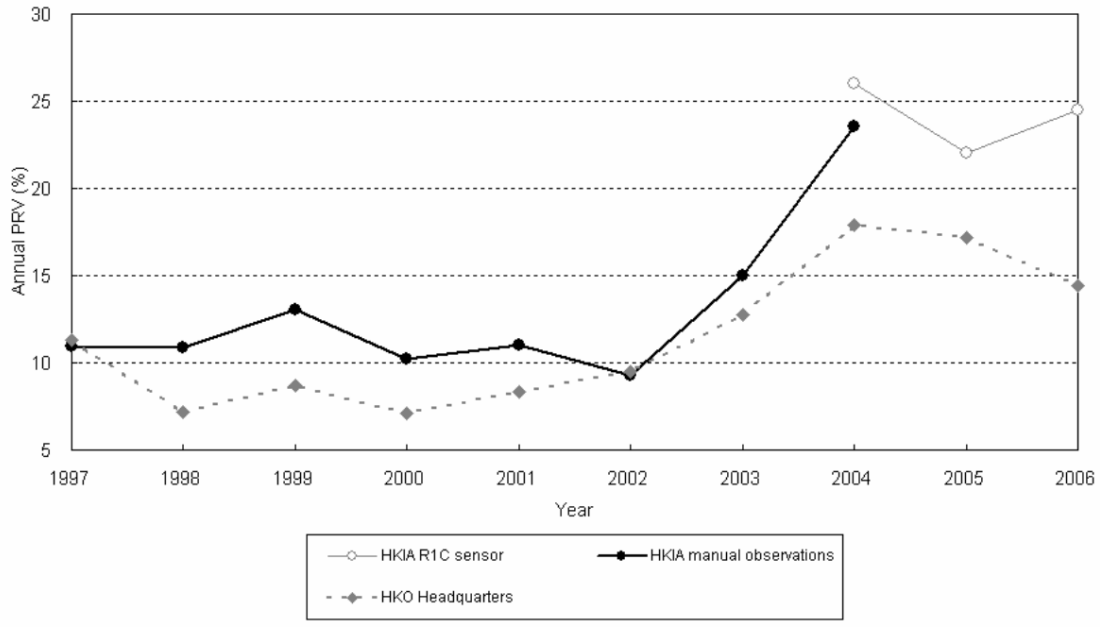

Fig. 7-3 Time series of annual percentage of reduced visibility at HKIA and HKO Headquarters

Fig. 7-3 also shows the time series of the annual PRV based on human-observed visibility at the Hong Kong Observatory (HKO) Headquarters. Broadly speaking, the trend of annual PRV at HKIA is generally consistent with that at HKO Headquarters. In a couple of years, different trends were apparent between HKIA and HKO, which could be attributed to regional differences.

Fig. 7-3 also reveals that the annual PRV at HKIA is generally higher than that at HKO Headquarters over the years. The more frequent occurrence of haze at HKIA in comparison to the urban areas is consistent with the findings of past studies on the meteorological conditions of the airport site in the early 1980s (Lam, 1981a and 1981b). This regional difference in turn could be a result of the local sea breeze circulation pattern. For example, under the influence of the west to northwesterly sea breeze wind over the western part of Hong Kong, it is common to have lower visibility at HKIA than that at the Victoria Harbour. An example is shown in Fig. 7-4, which also illustrates the presence of a confluence zone favouring the accumulation of particulate matter.

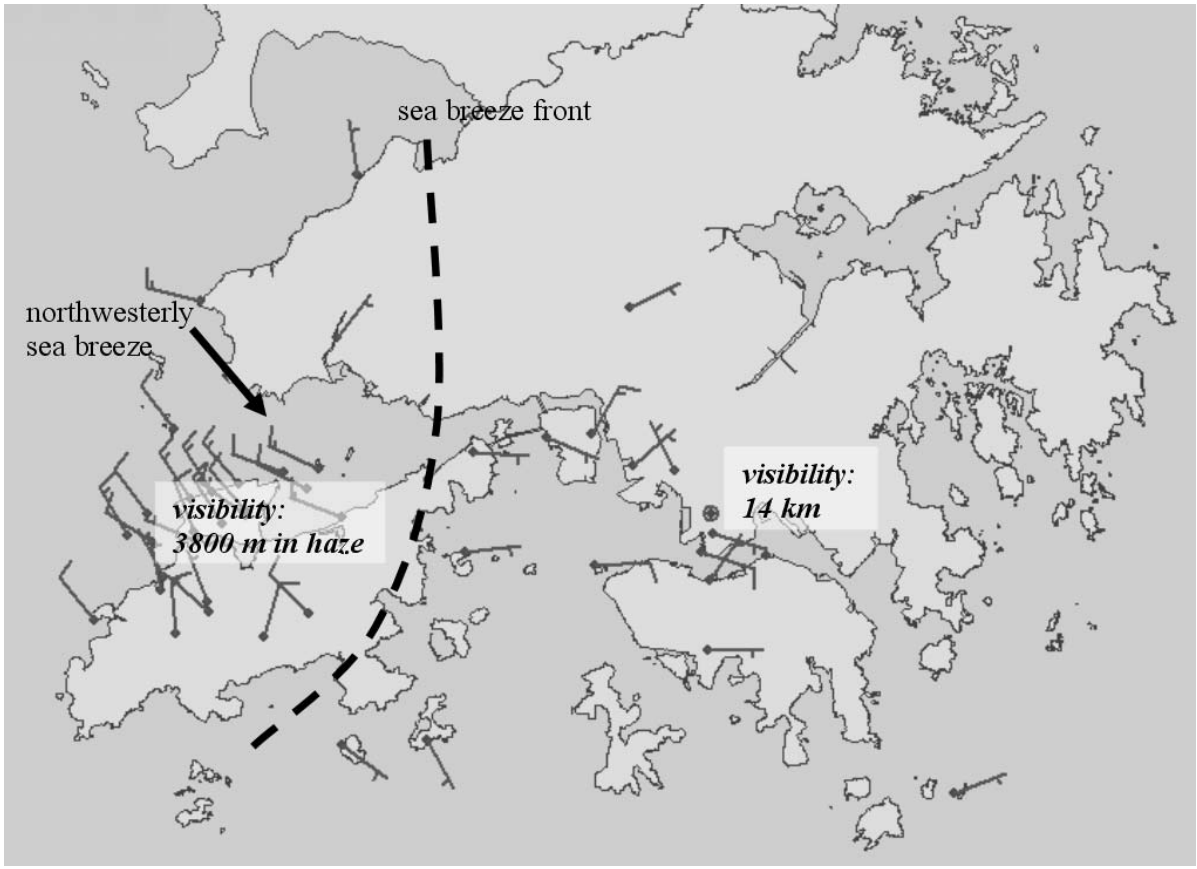

Fig. 7-4 Wind and visibility distribution in Hong Kong at 2 p.m., 29 October 2006

4. Conclusions

The 10-minute mean MOR reading at middle of the south runway (R1C) of HKIA is shown to be in good statistical agreement with the manually observed visibility, in accordance with WMO standards and overseas meteorological practices. The continuity of visibility climatology at HKIA is preserved in the transition from human observations to instrumental readings.

For long-term trend studies, the time series of PRV based on manual observations up to 2004 together with that based on R1C MOR data in 2005 and after may be adopted. This time series could be compared with the time series for other locations in Hong Kong with instrumental readings as forward scatter sensors are set up in more regions in the future.

Acknowledgement

The authors would like to thank useful discussions with Dr. Wiel Wauben of KNMI on the experience in automated visibility observations. Special thanks also go to Ms. S.H. Wong of HKO for performing the analysis of HKIA data and Mr. C.Y. Lam for his advice regarding the manuscript.

Reference

Chang, W.L., and E. Koo, 1986: A study of visibility trends in Hong Kong (1968-1982). *Atmo. Environ.*, **20**, 1847-1858.

KNMI, 2003: Comparison of visibility measurements with routine visual observations in the Netherlands. *3rd International Conference on Experiences with Automatic Weather Stations*, Torremolinos, Spain, 19 – 21 February 2003.

Lam, C.Y., 1981a: Meteorological Conditions at Chek Lap Kok. Occasional Paper No. 42, Royal Observatory, Hong Kong.

Lam, C.Y., 1981b: Meteorological Conditions at Chek Lap Kok, Second Report. Occasional Paper No. 44, Royal Observatory, Hong Kong.

WMO, 2006: Guide to Meteorological Instruments and Methods of Observation-No. 8, Seventh edition.

WMO, 2007: Guide to the Global Observing System, WMO-No. 488, Third edition, 170 pp.

The Tropical Cyclone Warning Systems During the Years of Modern Hong Kong, 1945-2004

Mickey Man-Kui Wai, Plum Rain Solutions, Tallahassee, FL 32303, USA

Abstract

The development of tropical cyclone warning systems, according to the local and non-local approaches, is traced between 1945 and 2004.

This study does not support the common belief that the warning system has been laid down exclusively for the mariners. Since 1903, the local warning system has provided the gale information to the visiting mariners, the boat population, and the local residents in the territory.

Confusion with the gale signals similar to 1930s and Irregular gale signals still persist. Despite the Observatory is modernized; the benefits from modernization have not generated similar dividends from the tropical cyclone warning system because of the use of signals. In a recent study of the Hong Kong typhoons (2001), Wai discussed an alternative warning system that would not use warning signals.

Associated with the warning system is the closure of Hong Kong when a gale signal has been displayed. Arguments of irregular gale signals and their adversary impact on the public kept recurring at the Legislative Council in the past forty years.

From these records, the governmental departments appear to adopt better communication, new guidelines, new equipment, and technology as the chief mechanisms to avoid the recurrence of these incidents and to improve individual departmental services. Such approaches of following its own policy and its own things are not good problem solving methods. To manage the passage of a typhoon, Wai (2001) outlined such a model along with an alternative tropical cyclone warning system.

The examination of these two approaches has provided some insight not just into the rationale of the warning system but also into the science of the tropical cyclone. As the study of the tropical cyclone warning system began with the British settlement in Hong Kong, we also learn a brief history of the Hong Kong Observatory. The assessments of the local and non-local warning systems and the public's reaction are also included.

1. Introduction

The use of signals to inform the Hong Kong public about the approach of a typhoon has a long history. Numerous revisions of the warning system and the introduction of new warning system were made. The rationale of these changes that led to the present tropical cyclone warning system, that is evidently unsuitable for the current demographic condition and diverse economic bases and land uses (Wai, 2001), was rarely discussed.

Moreover, as early as in 1877, a black drum was hoisted and a typhoon gun was fired as the means to warn the local residents and mariners about an approaching typhoon. The signals were meant for the probable local bad weather condition. Yet, throughout the early years, the core of the tropical cyclone warning system was meant for non-local purposes. The basis for using the non-local signals was not

well documented and understood.

Furthermore, the current condition to display a gale signal has been based on either the observed or expected gales inside the Victoria Harbour since 1973. Therefore, such a condition has led the public to believe that the warning system is aimed to serve the mariners. However, the use of gales inside the harbour, or perhaps the warning system, is meant to serve the mariners exclusively has never been substantiated.

Consequently, Wai (2004) followed the development of tropical cyclone warning systems according to the local and non-local approaches over four historical periods since the establishment of Hong Kong in 1841. The examination of these two approaches will provide some insight not just into the rationale of the warning system but also into the science of the tropical cyclone. It will also clarify if the present warning system is indeed designed for the mariners exclusively. As the study of the tropical cyclone warning system began with the British settlement in Hong Kong, we also learn a brief history of the Hong Kong Observatory.

One can find the discussions of the tropical cyclone warning systems during 1841-1899 (Wai, 2004), during 1900-1919 (Wai, 2005), and also during 1920-1939 (Wai, 2006). During the early years, there was no organized typhoon warning. The warning of a typhoon came only from those mariners who had knowledge of atmospheric signs of an approaching typhoon, or who had experience in working with a barometer on board. It was not until 1870 when Thomsett provided the mariners in port some useful precursory signs of approaching storms in the form of a notice. When it was a clear indication that a storm approached Hong Kong, Thomsett hoisted a black drum and firing of a typhoon gun inside the harbour to warn the mariners in 1877.

By 1880, Hong Kong, as an entrepot, no longer served primarily as a way station for the triangular trade between Britain, China and India. The trade areas of Hong Kong expanded into Japan, Korea, Southeast Asia, Australia, and United States. The increased shipping led to the establishment of Hong Kong Observatory in 1884. The goal was to instruct the shipmasters on the subject of marine meteorology and terrestrial magnetism necessary for navigating the China Sea and how to avoid the track of approaching typhoons. Therefore, Doberck introduced a non-local tropical cyclone warning system in May 1884. To assist navigation, an outpost lighthouse was built on Gap Rock in 1892. For the local warning, Doberck fired a typhoon gun whenever the local gales would be expected. Between February 1, 1897 and January 28, 1898, Doberck used the modified FitzRoy's system to warn the local residents of local gales. Then the warning system reverted to the system of 1884 at the request of the Hong Kong Chamber of Commerce.

In order to meet the demand of shipping in the early 1900s, the Observatory introduced two sets of warning code. In the first set, the Observatory continued to use a system of drum and ball in providing the probable location of a storm to the residents in the territory and also mariners who were about to leave the harbour. In the second set, the Observatory adopted the China Coast Codes of the Zi Ka Wei Observatory. The China Coast Codes would indicate the approximate location, movement, and intensity of a storm over the China Seas. By using the China Coast code in Hong Kong, the original proposal of 1881 was fulfilled such that the ports along the China coasts would use one uniform set of warning codes.

Both sets of code did not indicate that bad weather would be immanent upon the territory. The Observatory used an urgent signal to warn the public whenever local gales would be expected.

The hoist of red signals frequently interrupted shipping work inside the harbour as the native mariners ran for the shelter as soon as the red signals were hoisted. Therefore, the Chamber of Commerce urged the Government to abolish the red signals on several occasions.

The storm in September 1906 and the subsequent inquiry led to several positive changes. First, it compelled the Observatory to seek new ways to improve the local warning. The use of wireless telegraphy to exchange the meteorological information instantly between the Observatory and vessels made it possible to allow some realistic lead time when local gales would arrive. Therefore, in 1917, the Observatory introduced a new local warning system for the local residents and those who were in the harbour. Contrarily to the local warning system in 1902, the signals now indicated directions of gales over the territory. The system of local warning signals in 1917 marked the origin of the current warning system.

To serve the mariners in the Far East, the Observatory sought a new era of cooperation with other observatories in the Far East, and the new cooperation would lead to consider a new uniform system of warning codes for the entire Chine Seas. To provide a safe haven to the floating population during the typhoon in the territory, the public and government began to finance the construction of typhoon shelters in various locations in the territory in order to deal with however a short notice of the typhoon warning might be; consequently sufficient time would always be given to boats to proceed safely to a refuge.

During the inter-war years, the Observatory had a remarkable success in the cooperation with other observatories in the Far East. At the request of the Chamber of Commerce on June 1, 1920, the Observatory adopted the China Seas Storm Signal Code of the Zi Ka Wei Observatory. The new non-local code was intended for the entire China Seas.

Then in 1930, Claxton was asked to hold a conference of Directors of Far Eastern Weather Service. The main agenda of this conference was to address the uniform codes for local and non-local visual storm warning signals for the Far East and also a uniform code for the transmission of daily weather reports by cable in the Far East.

On December 10, 1930, new sets of local and non-local storm codes were introduced and were recommended for use in the Far East Weather Services. It turned out that the non-local storm warning system differed little form the China Seas Storm Signal Code. The local storm signal code now consisted of 10 signals.

While the China Seas Storm Signal Code was used for shipping, the local codes were primarily used to warn the local residents of the local gales. Because the severity of local gales was given by the progression of signal numbers, confusion began to occur as the public thought that gales signified by signal No. 8 were more severe than the gales signified by signal no. 5. In addition, the public and some government officials either misunderstood the meaning of the signals or misinterpreted how the signal should be used, as shown in the case of passing the Public Reclamations Validation and Clauses Ordinance, 1936. The difficulty stemmed from the indefinite nature of the language in the signal and was also fed by the press's inaccurate comments of the signal. Despite the Observatory put great efforts to correct the public about the proper meaning of the signals and how the signals should be used, the confusion of the signals and misconception of the signal will not go away in the public.

This objective of this article continues to investigate the tropical cyclone warning system between

1945-2003 as Hong Kong marches to become a modern cosmopolitan city. Similar to Wai's previous three studies (2004, 2005, 2006), the discussions of the tropical cyclone warning system in Hong Kong are presented according to various eras, during which either a major revision in the tropical cyclone warning system or a new tropical cyclone warning system was introduced. The assessments of the local and non-local warning systems and the public's reaction are also included. Finally, the article will be ended with a conclusion.

2. Sources of Documentary Data

Most of the sources used in this article concerning the Hong Kong tropical cyclone warning systems are based on three public records. The first is the Colonial Office Records: Series CO 129, Governor's Dispatches and Replies from the Secretary of State for the Colonies. The second is the Hong Kong Government documents, including Sessional Papers, Administrative Reports, Hong Kong Hansard (reports of Legislature Council Meetings), Hong Kong Government Gazettes, and the Director's Departmental Annual Reports of the Hong Kong Observatory. The third includes several historical newspapers, which are used to provide additional information on the historical typhoons mentioned in the article.

In brevity, the biographical information of the historical and current characters involved in the events will not be given in the article. However, a brief biographical note of each of these historical and current characters is given in Appendix II.

3. Hong Kong Storm Warning Systems

a. 1945 – 1949

After the war, the Observatory became a joint Naval and Royal Air Force forecasting center. The Observatory staff returned to duty on May 1, 1946. Unlike the early years, the scope of the meteorological service of the Observatory was widened in early 1948 in order to meet the requirements of the general public, merchant marine, Royal Navy, civil aviation, Royal Air Force, and Government departments.

On June 15 1947, the main forecasting and synoptic centers, administered by the Royal Air Force, were re-located to Kai Tak Meteorological Office at the Kai Tak Airport. The Observatory was maintained as administrative headquarters, climatological and training centers. It was not until August 1, 1948 that the Observatory staff began to take over the Kai Tak Meteorological Office from the Royal Air Force.

In these few years of reconstruction, the immediate concern was to restore the weather service, in particular the storm warning system. During the war, the lighthouse on Gap Rock was severely damaged. When the Observatory resumed regular observations, weather observations had not been possible to resume at Gap Rock. With the help of the Royal Navy, the Chinese government re-established the meteorological station on Pratas in May 1946.

Beside surface observations, upper air observations with pilot balloons resumed, but the daily meteorological flights returned on February 1 1947. However, the daily meteorological flights were discontinued in late 1949 when flights of radiosondes began. Additional weather reports from overseas weather stations included Singapore, Bangkok, Saigon, Tokyo, Manila, Shanghai, and Guam.

After consulting with the shipping companies and Royal Navy, the Observatory established the Weather Service for Merchant Shipping (WSMS) on May 1, 1947. WSMS would produce forecasts in the following eleven areas: Shanghai and Foochow, Formosa Strait, Hong Kong, South China Coastal waters, Gulf of Tonkin, Luzon, China Sea north of latitude 100 N, Luzon Strait to Riukius, Eastern Sea, South of Japan, and Yellow Sea.

i. Non-local warning system

The non-local warnings were of the system of 1935, but they were distributed by radio instead of cable. To benefit the marine captains who remained in port, the Observatory continued to display the non-local warning signals on Blackhead Hill.

During typhoon season, warnings were broadcasted whenever a storm center was located within these eleven areas of the Observatory's responsibility, roughly covering the entire South China Sea bounded by latitudes 100 and 300 N and longitudes 1050 and 1250 E. Forecasts (also known as General Situation) for these areas were broadcast twice daily from Cape D'Aguila.

ii. Local warning system

The Observatory continued to use the same set of pre-war local storm signals of 1935. The warnings were also prepared for the Radio Hong Kong and the press whenever a typhoon threatened Hong Kong.

iii. The first phase of reconstruction

Because of the unique geographic location of Hong Kong and the political turmoil in China, it was becoming increasingly clear that the Observatory would be expected to provide a wider field in the region beside the primary service of providing storm warnings for the citizens of Hong Kong and shipping and aircraft using the port. Therefore, the Observatory took every effort to seek cooperation with the regional and international weather services and obtain new technology and equipment in order to provide reliable forecasts and warnings in the region.

Subsequently, the Observatory became a member of the International Meteorological Organization (later known as World Meteorological Organization) in 1948. Soon the Observatory was requested to establish a radiosonde and radar wind-finding station. Therefore, the Observatory received a grant in February 1949 for the establishment of a radiosonde and radar wind-finding station. On November 1 1949, routines of daily ascent of radiosonde began, and the daily meteorological flights were discontinued.

It turned out that the Observatory was not a suitable location for the launch of radiosonde; the government started the construction of a new station at King's Park for the work of radiosonde.

b. 1950 – 1972

The representatives of the Weather Services in the Far East met in Manila in May 1949 addressing the uniform storm warning procedures (Anonymous, 1956). The revised non-local and local storm signals became effective on January 1, 1950. The principle of non-local warning signals remained the same, but more information was allowed in location, direction, and speeds of the storms.

The only major change in the local storm signal was the introduction of the international signal warning signal for strong winds. Several years later, the local storm signal codes were revised again with effective from April 1, 1956.

Beginning in 1956, the tropical cyclones were classified to four classes according to the intensity.

(1)Tropical Depression	up to 33 knots (force 7)
(2)Tropical Storm	34 to 47 knots (force 8-9)
(3)Severe Tropical Storm	48-63 knots (force 10-11)
(4)Typhoon	64 knots (force 12) or above

i. Non-local warning system

The revised non-local storm signal code remained to be known as the China Seas Storm Signal Code, which still used the 10 symbols as in the year of 1930. However, to be consistent with the new classification of tropical cyclone intensity, the meanings of the code were modified accordingly.

The first was the time signal of observations (9 signals); each signal was expressed by 1 symbol (numeral). The first 8 signals (numeral 1 to 8) corresponded to time, hour in GMT, at every 3- hour interval. For instance, the time signal no. 8 referred to 0000 or 2400 hours. Signal no. 9 referred to a position that was deduced from supplementary information since last warning.

The second was the signal of speed and direction of motion; each signal was made of two symbols. There were four series of speed of motion, each of which consisted of 16 direction codes (corresponding to 16 compass points). For instance, a speed of 10 knots consisted of codes 01 to 16; a speed of 15 knots consisted of codes 17 to 32; a speed of 20 knots consisted of codes 33 to 48, and finally a speed of 25 knots or more consisted of codes 49 to 64. The signal 08 would indicate that the typhoon would move south at 10 knots. The signal 60 would indicate that the typhoon would move west at 25 knots or more.

The conditions were marked by two symbols from codes 65 to 99, representing various movements of the tropical cyclones, such as curving, or filling.

The intensity of the tropical cyclone was given by one symbol from code 1 to 9, which was divided into three groups of three. The first group, code 1 to 3, indicated tropical depression. The second group, code 4 to 6, indicated tropical storm, and the third group, code 7 to 9, indicated typhoon. Code 0 indicates uncertain position and intensity.

In 1953, the Weather Service for Merchant Shipping was renamed as the Marine Weather Service. In addition to the China Seas Weather Bulletin, the Observatory began the hourly China Seas Storm Warning broadcast in 1957. These warnings were transmitted on the ‘emergency’ frequency from Cap D’Aguilar during typhoon.

To provide better services to shipping, the Observatory replaced the eleven areas by sixteen new areas in 1967, which roughly covered the South China Sea: Chusan, North Taiwan, Ryukyu, East Taiwan, Taiwan Strait, Kwangtung, Tonkin, Danang, Paracel, Pratas, Bashi, Balintang, Scarborough, Mindoro, Nansha, and Varella. The names of these areas reflected the internationally known

geographical features.

The usefulness of the China Seas Storm visual signals in Hong Kong had gradually became limited because the warnings were widely distributed by radio. The visual signals were retained for the benefits for the marine captains who remained in port and might not be maintaining a radio watch. When the China Seas Storm visual signals were hoisted, it also served as a reminder that there was a tropical cyclone somewhere in the South China Sea or the China Coastal areas. Finally in June 1962, the hoist of non-local signals was discontinued.

ii. Local warning system

When a tropical depression passed to the south of Hong Kong on June 28 1950, the Observatory used the strong wind signal to warn the native vessels of the onset of strong winds which were not expected to reach gale force. The frequency in the use of strong wind signal increased in the following years in order to avoid the unnecessary hoist of signal no. 1, which led to disruption of work in the harbour, as far as possible.

Towards the end of 1955, it was decided that the international strong wind signal would be used only as a warning of strong monsoon winds. A new signal No. 3 was introduced as the strong wind signal. Signal No. 1 was then redefined as a depression of typhoon existed (centered within 400 nautical miles of Hong Kong) which might affect the territory. The local storm signals, that became effective on April 15, 1956, are shown in Fig. 8-1. Unlike the local storm signals of 1930s, the local warning signals were designed to convey a more definite warning of gales. For instance, signal no. 3 would expect a strong wind of 22-33 knots. Similarly, signals no 5 to no.8 would refer to a gale of having a mean speed of 34 knots and upward from the four cardinal quadrants, and signal no. 10 would expect a mean typhoon wind speed of 64 knots.

In 1959, the Observatory established 10 signal stations and 16 supplementary signal stations. By 1972, the total number of typhoon signal stations climbed to the maximum of 42. These typhoon signal stations covered the entire Hong Kong territory.

iii. Law of storms

Prior to 1950, the knowledge of tropical cyclone came primarily from mariners and ship data, which were centered on the surface wind-pressure field and distribution of clouds in the sky. While the mechanical and thermal theories helped to explain the formation of a tropical cyclone, no one knew quite sure how the theories worked in nature.

The study of the three-dimensional structure of a tropical cyclone probably started in late 1950 when NHRP (National Hurricane Research Project) research aircraft flew over four days in observing Hurricane Daisy. The objectives of these flights were to answer two questions: how the latent heat of condensation is released in tropical cyclones; how the latent heat produces the inner warn region of the cyclone and drives its transverse and horizontal circulations. Malkus and Riehl (1960) introduced a concept of ‘narrow warn towers’, or later known simply as ‘hot towers’, in which cumulonimbus clouds could transport heat upward from the surface of the ocean into upper troposphere against the mean gradient of moist static energy. Moreover, the calculation of budgets of heat, moisture, kinetic energy and momentum showed that the concept of hot tower could describe the intensification and maintenance of Hurricane Daisy (Riehl and Malkus, 1961).

Fig. 8-1 Hong Kong Storm Signal Code (Local), 1959

Signal No.	Day Signal	Night Signal	Meaning
1	T	White White White	A depression or typhoon exists (centered within 400 nautical miles of Hong Kong) which may affect the locality.
3	⊥	Green White Green	Strong wind (mean wind speed 22-33 knots) expected.
5	✠	White Green Green	Gale (mean wind speed 34 knots and upwards) expected from the NW quadrant
6	✡	Green White White	Gale (mean wind speed 34 knots and upwards) expected from the SW quadrant
7	✠ ∃	Green Green White	Gale (mean wind speed 34 knots and upwards) expected from the NE quadrant
8	✡ %	White White Green	Gale (mean wind speed 34 knots and upwards) expected from the SE quadrant
9	♎	Green Green Green	Gale expected to increase
10	♋	Red Green Red	Hurricane or typhoon wind (mean wind speed 64 knots and upwards)any direction

Signals Used at Supplementary Stations

Red T	Red Green	No. 1 hoisted in Hong Kong Harbour
Red ✠	Red Red	Nos. 3, 5, 6,7,8,9,or 10 hoisted in Hong Kong Harbour

The work of Reihl and Malkus began a new era of the study of a tropical cyclone: the formulation of a new mathematical theory, such as conditional instability of the second kind (CISK); numerical modeling of a tropical cyclone, and field experiments such as the Barbados Oceanographic and Meteorological Experiment (BOMEX) in 1969, and the Global Atmospheric Research Program (GRAP) Atlantic Tropical Experiment (GATE) in 1974, and more recently SPECTRUM, and TYPHOON-90. Subsequently, the scientific attention has now focused on various features and processes in a tropical cyclone (Anthes 2003), such as large-scale environmental factors, ocean-atmosphere interaction and boundary layer processes, stratiform clouds and precipitation, and radiation.

iv. Reorganization of the Forecasting Office

The rapid growth in the Observatory was largely to meet the demanded services in aviation. By 1955, the senior staff at the Observatory began to realize that the demands of aviation had largely dictated the operation of the Observatory. Therefore, the Observatory either reduced or postponed other legitimate activities of the Observatory. The re-location of the forecasting office to the Kai Tak Airport in order to satisfy the aviation needs inevitably was accomplished at the expenses of the

Observatory. For instance, more staff was assigned from the Observatory to the Forecasting Office. Furthermore, the forecasters were continually interrupted at the forecasting office; the conditions were not suitable for accurate forecasting. Ramage indicated that the forecast for the public, including local typhoon warning, and for shipping had suffered.

A re-organization of the Observatory began in 1955. A Central Forecasting Office, located at the Observatory, would provide the meteorological information and forecasts for the public including local typhoon warning, the Armed Services, shipping, in addition to the meteorological information and weather analyses for the Aviation Forecasting Office at the Kai Tak Airport. The re-organization was completed by May 1 1957.

After May 1, 1957, the Kai Tak Forecast Office would issue forecasts solely for aviation and dealt exclusively with aviation inquires.

v. Acquisition of data, equipment and technology

During the early part of 1949, the Observatory received a limited number of weather reports from China. Toward the end of 1949, no information came from the Chinese mainland and Manchuria. Over the South China Sea, the Observatory received reports from Pratas, Macau, Manila, Paracels, and Indo-China. Additional meteorological information from Formosa and adjacent islands were intercepted in August 1952. It was not until June 1, 1957 when the Chinese Government commenced weather broadcasting. To the south, the surface observations at Pratas ceased to send reports directly to the Observatory starting on May 1, 1959.

The transfer of radiosonde and pilot balloon from the Observatory to King's Park occurred on June 1 1951. Because Hong Kong was the only upper air station in the South China Coast, the Observatory started a pilot program by loaning pilot balloon to a Hong Kong steam ship, Hin Sang, in 1954. Observations of upper level winds were taken from the pilot balloon during Hin Sang's en route between Hong Kong and Borneo. The ascent of pilot balloon on Hin Sang ended in just two years. In January 1969, rawinsonde was added to the upper air observations.

To have access to the weather data in the Southeastern Asia, the Observatory completed a circuit between Bangkok-Hong Kong-Tokyo point-to-point circuits on June 8, 1970. These circuits enabled the Observatory to receive quickly and reliably the majority of the weather data in the regions required for the weather forecasting.

In 1961, USAF began reconnaissance flights when a tropical disturbance existed in the Northwest Pacific. On these occasions the Observatory intercepted the radio-teleprinter broadcast of the earliest available information from reconnaissance flights made by the USAF from Guam.

The demands in shipping and rapid development in aviation allowed the Observatory to purchase new instruments and be equipped with new methods of observations. For instance, the installation of radar in 1959 and reception of satellites imageries in 1964 helped with the typhoon forecasting.

vi. Improvement of forecasting techniques

To aid forecasting, the forecasting office plotted cross-sectional charts and weather charts at various pressure levels except for 200 mb. Therefore, one could not apply modern techniques and was compelled to rivet attention on the surface charts, supplemented by time section. Subsequently,

typhoon forecasting has become largely empirical and extrapolatory (Anonymous, 1955).

In 1959, the Observatory began to plot the 200 mb air contour at 1000 and 1200 GMT in addition to the reception of the prognostic charts of 200 mb air contour from a USAF station in Japan. In late 1966, the Observatory regularly intercepted radio-facsimile broadcast of upper air prognostic charts and the northern hemisphere analytic and prognostic charts from USAF in Fuchu, and also from the Japan Meteorological Agency in Tokyo.

To assist the empirical and extrapolatory approaches in typhoon forecasting, Heywood (1950), Starbuck (1951), Thompson (1951), Chin (1958, 1972), Tse (1966) among others contributed a great deal in this effort. Another important contribution was to re-evaluate the British Standard Code of Practice under the typhoon situation, in particular, the pressure of typhoon wind on building and engineering structure (Heywood, 1950). A more precise wind loading and better building design (Faber and Bell, 1963-1964) would give a strong building code that would provide a safe home for the citizens during typhoon even though the gale signal caused irregularities.

vii. Dissemination of warnings

Towards the beginning of 1970s, many citizens were becoming more aware of usefulness of the meteorological services, and more critical of the form and presentation of warning and forecasts. The demand for information by the public and the mass media during typhoon was tremendous. To avoid disruption and detraction during critical moments when a typhoon approached Hong Kong, the Observatory decided to channel typhoon warning bulletins and messages to various media organizations through the Information Services Department. To deal with requests by the public for information on the typhoon, the Observatory utilized the Information Center of the Secretariat for Home Affairs.

Despite a significant improvement in weather services, warnings and forecasts were often misinterpreted similar to those of 1930s. Moreover, the greater use of Chinese and the difficulties of translating unfamiliar technical terms also created difficulties. Therefore, considerable effort was devoted to making the tropical warnings more effective and easily understood. The Observatory concluded that there was a need for some guidance material for the public, closer liaison with the press and careful monitoring of weather broadcasts.

viii. Irregular gale signals

Recall that in the local warning system of 1930, gale-warning signals were not displayed unless *it is tolerably certain that a gale (40-45 mph by the Dines anemometer) will occur at Hong Kong or Gap Rock, or when a typhoon is sufficiently bear to warrant a danger signal, although the occurrence of a gale is by no means certain.*

The loss of observations at Gap Rock during the war and the termination of direct link between the Observatory and Pratas in 1959 left just one vague condition for the display of gale signals: *a gale will occur at Hong Kong*. Such an indefinite condition undoubtedly caused difficulties and irregularities. The study of Hong Kong typhoons by Heywood with the assistance of Starbuck in 1950 appeared to help resolve the difficulties and reduce the irregularities of the condition for hoisting the gale signal, at least temporary. Heywood's results showed that all but 11 of 74 gales first set in from the NE quadrant, and all but 12 of 74 gales the wind veered in direction during the passage of the typhoon. The wind will back when the typhoon passes to the N or NE of Hong Kong,

and will veer when it passes to the S or SW. The wind at the height of typhoon is from the easterly quarter in the majority of cases. While these findings were based on winds at the Observatory, Heywood (1950) concluded that the behavior of gales probably would apply reasonably accurately to the central area of the Victoria Harbour.

A recent, quantitative study of warning signals (Wai, 2001) indeed re-confirmed Heywood's conclusion that the surface winds inside the Harbour are basically easterly in most cases, as indicated by the stations along the waterfronts. However the wind speeds inside the Harbour are significantly lowered than the speed signified by the signals, as indicated by the wind speeds at the stations along the waterfronts and at the Observatory. One must recognize that Heywood's wind records were obtained during the years that the winds at the Observatory were not significantly affected by the local urban development. For instance, Wai (2001) illustrated that the wind speeds recorded at the Observatory showed a continuous downward trended during the post-war years.

Before the war and shortly after the war, the daily routines of public and private businesses were concentrated along the waterfronts of the harbour. Heywood did not anticipate that the Hong Kong Government would establish the Territory Development Department in 1973 that marked the beginning of the new town development. After 30 years since the inception of the Territory Development Department, the demography of Hong Kong, the landscape, and economical bases do not resemble any of those of 1950s. Consequently, the applicability of Heywood's results has become very limited in recent years.

c. 1973 – 2004

i. Local warning system

On January 1 1973, the Observatory replaced signal nos. 5, 6, 7, and 8 with signal no. 8 NW, signal no. 8 SW, signal no. 8 NE, and signal no. 8 SE respectively (Fig. 8-2). The changes were made in order to avoid misinterpretation of changes in the wind intensity when the inter changing of signals among nos. 5, 6, 7, and 8. As early as 1975, additional meanings were added to each signal (Chin, 1977).

Signal No. 1*: a tropical cyclone is centered within about 400 nautical miles of Hong Kong, and it might affect Hong Kong. Hong Kong is placed in a state of alert because the tropical cyclone is a potential threat and may cause destructive wind later.*

Signal No. 3: *strong wind expected or blowing, with a sustained speed of 22-33 knots and gusts which may exceed 60 knots. The timing of the hoisting this signal is aimed to give about 12 hours advance warning of a strong wind in Victoria Harbour.*

Signal No. 8: *gales or storm expected or blowing, with a sustained wind speed of 34-63 knots from the quarter indicated and gusts which may exceed 100 knots. The time of the replacement of the strong wind Signal No. 3, by the appropriate one of these four signals is aimed to give about 12 hours advance warning of a gale in Victoria Harbour but the sustained wind speed may reach 34 knots within a shorter period over more exposed waters. Expected changes in the direction of the wind will be indicated by corresponding changes of these signals.*

Signal No. 9: *gale or storm expected to increase significantly in strength. This signal will be hoisted when the sustained wind speed is expected to increase and come within the range 48-63 knots during*

the next few hours.

Signal No. 10: *Hurricane force wind expected or blowing, with sustained speed reaching upwards from 64 knots and with gusts that may exceed 120 knots. This signal is hoisted as soon as there are definite indications that the sustained wind speed anywhere near sea level in Hong Kong is likely to exceed 63 knots.*

Fig. 8-2 Hong Kong Tropical Cyclone Warning Signals, 1975

Signal No.	Day Signal	Night Signal	Meaning
1	T	White White White	A tropical cyclone is centered within about 400 nautical miles of Hong Kong and later affect Hong Kong . Hong Kong is placed in a state of alert because the tropical cyclone is a potential threat and may cause destructive winds later.
3	⊥	Green White Green	Strong wind expected or blowing, with a sustained speed of 22-33 knots and gusts, which may exceed 60 knots. The timing of the hoisting of this signal is aimed to give about 12 hours advance warning of a strong wind in Victoria Harbour
8 NW	✠	White Green Green	Gales or storm expected or blowing, with a sustained wind speed of 34-64 from the quarter indicated and gusts which may exceed 100 knots. The timing of replacement of the strong wind signal No. 3 by the appropriate one of these four signals is aimed to give about 12 hours advance warning of a gale in Victoria Harbour but the sustained wind speed may reach 34 knots within a shorter period over more exposed waters. Expected changes in the direction of the wind will be indicated by corresponding changes of these signals.
8 NE	✠ ∃	Green Green White	
8 SW	✡	Green White White	
8 SE	✡ %	White White Green	
9	⏏	Green Green Green	Gale or storm expected to increase significantly in strength. The signal will be hoisted when the sustained wind expected to increase and come within the range 48-63 knots during the next few hours.
10	⍾	Red Green Red	Hurricane force wind expected or blowing, with sustained speed reaching upwards from 64 knots and with gusts that may exceed 120 knots. The signal is hoisted as soon as there are definite indications that the sustained wind speed anywhere near sea level in Hong Kong is likely to exceed 63 knots.

Signals Used at Supplementary Stations

Red T	Red Green	No. 1 hoisted in Hong Kong Harbour
Red ✠	Red Red	Nos. 3, 5, 6,7,8,9,or 10 hoisted in Hong Kong Harbour

Another common misconception related to the wind direction remained; wind direction is not the

same as the direction of a tropical cyclone movement.

When the metric system was fully used on January 1, 1986, the wind speed in each storm signal was converted from knots to km per hour. The meaning of each signal is also simplified (Anonymous, 1992). For instance, signal no. 8 is defined as

Gale or storm force wind, with a sustained speed of 63-117 km/h from the quarter indicated (NW, SW, NE, or SE), is expected or blowing in the Victoria Harbour; and gusts may exceed 180 km/h.

ii. Building a network of meteorological data

To acquire the best information on the earliest state of a typhoon in the Northwest Pacific, Bell led a delegation of his staff to visit the Joint Typhoon Warning Center (JTWC) in Guam in 1972. The delegation sought cooperation with JTWC in receiving their reports of early information of typhoon available from US reconnaissance aircraft.

As a member of the ECAPE Typhoon Committee, the Observatory found it extremely valuable when the committee successfully established a radiosonde and radar station on Pratas Island. Upper air and radar wind observations started to come in February 1973.

In October 1976, Bell and his delegation were invited to visit the Central Meteorological Service of the People of Republic China concerning the establishment of Peking to Hong Kong circuit of the World Meteorological Organization Global Telecommunication System. The link was open on December 20, 1975.

iii. Arrival of a computer era

The acquisition of a computer system in 1973 allowed the Observatory to begin new eras of numerical weather prediction (NWP) from a simple, balanced barotropic model in 1979, to the limited area model in 1988, and currently a regional spectral model in 1999. Besides, the Observatory also received NWP products from other weather services.

Moreover, the lack of observational data needed to ascertain the location of a typhoon over the South China Sea has been resolved with the reception of the Japan's Geostationary Meteorological Satellite beginning in 1977. A new weather radar system, which provided high resolution of the weather features, was installed at Tai Mo Shan in 1999. Currently, the in-house super-computer helps to process these remote sensing data on the real time basis.

The development of in-house NWP and the acquisition of new equipment and technology along with the new networks of meteorological data have made typhoon forecasting no longer largely empirical and extrapolatory.

As the World Wide Web became the global means of electronic exchange of information, the Observatory launched the observatory web pages on the Internet in 1996. The web pages allow the public to have access to numerous educational resources and various categories of the Observatory services and weather products including typhoon warnings. In addition to the media, the public frequently obtains the information on the typhoons electronically. Moreover, the skyward commercial and apartment buildings along the waterfronts make the typhoon signals largely invisible to the majority of the public, not to mention the current demography of population. The visual

typhoon signals have lost its purpose. Consequently, the Observatory closed the last typhoon signal station, Chung Chau, on January 1, 2002.

iv. Dissemination of warnings

Entering the late 1970s and early 1980s, the Observatory continued to put great efforts in correcting the public misconception of the severity of signal number by massive distributing booklets, signal cards, and also by giving interview in the media.

When the warning signals were displayed, the representative of Information Center for the Secretariat for Home Affairs helped to deal with the public request for general information on the warning signals. Beginning 1974, the Home Affairs Department and the Information Services Department assigned their translators to the Observatory in order to expedite the dissemination of warnings in both Chinese and English during the approach of a typhoon. When a warning signal no. 8 or above was displayed, warnings in Chinese were broadcast from a broadcasting studio in the Observatory Headquarters and relayed by Radio Television Hong Kong and by Commercial Radio.

v. Law of storms

The launch of polar-orbiting satellites in April 1960 and operational meteorological satellites in 1966 revolutionized the methods on tracking and ascertaining the center of a tropical cyclone. The usefulness of twelve-point rule in the "law of storms" has largely left to the sailing community.

The modern "law of storms" focuses on what governs the life history of a tropical cyclone. The studies of tropical cyclones by observational, mathematical, and numerical approaches have shown the complexities of the life history of a tropical cyclone. Moreover, there are diverse views on the importance of the physical processes.

The popular theory, CISK, was unable to explain or predict the major features of a tropical cyclone (Emanuel, 2003). Furthermore, several diagnostic studies showed that the intensity of a typhoon as a function of sea surface temperature alone does not generate concrete evidence that other factors are not important (Merrill, 1988; Evans, 1993; Baik and Paek, 1998).

Numerical studies on the formation of a tropical cyclone gave ambiguous conclusions. For instance, Holland (1987) pointed out that the axisymmetric analytic and numerical models, described by Ooyama (1969), Carrier et. al. (1971), Yamasaki (1977), Chala and Pfeffer (1980), and Emmanuel (1986), produced 'realistic' tropical cyclone structure, but each of these models contained different explicit physics. Moreover, observational studies found consistent environmental interactions associated with changes in the tropical cyclone structure; yet most numerical models developed tropical cyclones without including such environmental interactions.

In a recent review of the skills of numerical forecast of typhoon tracks and intensity, the results were mixed. In the typhoon tracks, only the GFDL (Geophysical Fluid Dynamics Laboratory) model overtook statistically the skills of statistical methods (Emanuel, 2003). However, in the typhoon intensity, no numerical models have yet produced the forecast better than statistical methods except at a longer time period (72 hrs).

The genesis of a tropical cyclone, and its subsequent movement, intensity, coupling process between a typhoon and ocean/land surface, and its interaction with the atmospheric environment are active

research topics. For an overview, one may refer to the global perspective on tropical cyclone (WMO, 1995), the progress in the understanding of the hurricane (AGU, 2003), and the intensity changes of typhoons over the South China Sea (Wai, 2000).

4. The Warning System for the Mariners: A Myth

This study does not support the common belief that the warning system has been laid down exclusively for mariners. Prior to 1884, the signals were indeed intended for the visiting mariners and local boat population. Between 1884 and 1896, the signals were used for shipping and navigation. In 1897, the signals were used for both local residents and mariners. From 1898 to 1903, the signals reverted to the shipping and navigation.

Starting in 1903, specific uses of non-local and local signals were introduced. The non-local signal codes, such as China Coast Codes (1903-1919) and China Sea Storm Signal Code (1920-1962), were used for shipping indicating the distant storms in the South China Sea. The local codes provided meteorological information to local residents, boat population, and visiting mariners about the location of a typhoon from the territory.

Beginning in 1917, the meaning of the local signals changed from the location of a typhoon with respect to Hong Kong to the direction of gales that the Hong Kong citizens would expect from. In order to hoist the gale signals, it must satisfy that the gale force was force 8 on Beaufort scale, or a mean 40-45 mph by the Dimes Anemometer was recorded at either Gap Rock, Waglan Island, or at Hong Kong. A further modification of the rule was made in 1930: a gale (40-45 mph by the Dines Anemometer) would occur at Hong Kong, or at Gap Rock, or when a typhoon is sufficiently bear to warrant a danger signal, although the occurrence of a gale is by no means certain.

The loss of the lighthouse and observational instruments on Gap Rock during the war and the termination of direct link between the Observatory and Pratas in 1959 would leave one condition for hoisting the gale signal: gales occurred at Hong Kong.

In 1975, to correct the indefinite nature in the rule for hoisting the gale signal, the Observatory used the gale inside the Victoria Harbour. The new rule was apparently derived from the conclusion of Heywood's study of Hong Kong typhoons, and it has remained that way ever since.

Since 1903, the local warning system really has not just provided the gale information to the visiting mariners but also the boat population and the local residents in the territory.

5. Confusion and Persistence of Irregular Gale Signals

As the twenty-first century approached, the confusion over the gale signals in the public and irregular gale signals still persist. For instance, one can found incidences of the confusion over the gale signals similar to those in 1930s in the weather discussion forum at a local popular website.

On September 2 1999, the subject of the discussion was that if a gale signal should be hoisted. One participant stated that

The definition of no. 9, according to HKO, is that wind will significantly increase to gale or storm force. The explanation, given by HKO, simply equated signal no. 9 with storm force winds. Then, I think that it is better for HKO to redefine signal no. 9.

On September 2 2003, a courageous weather fan predicted that the signals would be hoisted and lowered in the following order:

2215 Signal no. 1 last night

1100 Signal no. 3 this morning

1700 Signal no. 8 this evening

1930 Signal no 9 this evening

2330 Signal no 10 tonight

0530 Signal no. 8 tomorrow morning

0900 Signal no 3

1200 Lower of signal no 3

On July 18, 2004, one participant said:

During a typhoon passage, even though it is weaken, usually it can maintain a S. T. S. strength. Storm force is likely to be blown in the territory and therefore No. 9 is often issued during the typhoon passage.

On July 19, 2004, one contributor made a statement such as:

From the age I know what TCs and TC signals are, I always think that No. 9 is a transitional signal from No. 8 to 10. It was a surprise to me when I found that No. 9 can serve as a stand alone signal in 1997 when I was in US.

On the same date, another participant explained:

In 1970s, the definition of No. 9 signal stated that sustained winds of storm force (88-117 km/h) would blow over Hong Kong within 3 hours after the hosting of this signal.

However, this definition is no longer used today. I think the rationale behind this change is that HKO wants to use the No. 9 signal for marginal typhoons but not any storm of EXPECTED STS strength.

When the typhoon is inactive in the Western North Pacific, most Hong Kong citizens tend to forget the adversary effects of previous irregular gale signals probably because of short memory. However, irregular gale signals can become an issue if the typhoons are becoming extremely active in the Western North Pacific.

During 1999-2001, Hong Kong entered a period of very active typhoons as compared to the years 1998 and 2002. For instance, the number of hours required the Observatory to hoist signal no. 1 and above were 517.9 (1999), 327.4 (2000), 253.6 (2001) as compared to 188.6 (1998) and 144.4 (2002). In term of frequency that gale signals and above were displayed, there were zero in 1998, 12 times in 1999, zero in 2000, 5 times in 2001, and 1 time in 2002.

During these three years, the problem of irregular gale signal resurfaced in front of the public. Such incidents due to irregular gale signals attracted public, unfriendly scrutiny on the warning system and the Observatory. For instance, a column about Typhoon Leo appeared in the Hong Kong Standard on May 4 1999; the correspondent stated that the Observatory insisted that hoisting signal no. 8 was a right decision. Safety of the public is the paramount concern, which will not be affected by other factors. Only nine days later in another column in the Hong Kong Standard on May 13, 1999, the correspondent reported that the Observatory had apologized for inconvencing the Hong Kong people. The blame for the inconvenience was the lack of equipment that could not accurately predict the effect of typhoon Leo after it suddenly changed course and strength. Continuing in the same column there was the reason for hoisting of gale signal no. 8:

At that day, the Observatory has recorded a wind speed of 90 km per hour off Waglan Island. Provided that wind speed exceeds 63 km, typhoon signal no. 8 has to be hoisted. At that moment, there was a need to hoist typhoon signal no. 8.

More recently, on July 28, 2001, Tien questioned the Director of the Observatory how the decision was made when the gale signal was hoisted during typhoon Yutu. Also, what circumstances had put Hong Kong under the gale signal for 19 hours?

In replying to Tien, a representative of the Observatory stated the reason as:

The forecast track would take Yutu to within 150 km of Hong Kong. As gale force winds (67-117 km/h) were observed on the Observatory's Doppler radar to affect areas within 160 km of Yutu, and during the previous 3 hours. Yutu had been intensifying with maximum winds increasing from 120 km/h to 150 km/h. there was a high probability that Hong Kong would be affected by gale force winds. The No. 8 signal therefore hoisted at 0030 hours on 25 July 2001.

Enclosed with the reply was a map showing the affected area by the gale force winds during the passage of Typhoon Yutu. Using the data obtained from the Doppler radar, the Observatory showed that the affected area covered the open water to the south of 22^0 N, Chung Chau, and the windward sides of mountains along the southwestern – southeastern Lantau Island.

The circumstances put Hong Kong under gale signals were:

(1) Gale force winds were already affecting parts of Hong Kong, practically at the doorstep of Victoria Harbour where the criteria of wind speed for signal 8 is based;

(2) All objective forecasting tools at the time still indicated a possible change of course to more west-northwest, edging Yutu closer and the gale force winds further into the territory;

(3) Yutu was still an intense typhoon with no signs of weakening. It has been slowing down and would be within 200 km of Hong Kong for a prolonged period of time.

Remote observations during the early hours of July 25, 2001 did not support the notion that Yutu showed no sign of weakening. First, the 36-hr forecast of JTWC, made at HKTime, 23:00 on July 24, 2001, indicated that Typhoon Yutu would dissipate to become a tropical storm. The time used here in the case of Typhoon Yutu is the Hong Kong time. The warning remarks, made by JTWC at 23:00 on July 24, 2001, indicated that Typhoon Yutu had intensified based on the animated satellite imagery (from the past 12 hours). For the next 24 hours, the warning remark did not indicate that

Typhoon Yutu would continue to intensify. Second, remote observations from microwave imager at 18:00 on July 24, 2001 depicted decay convection in the consolidating eyewall south of the system. The eye of Typhoon Yutu became irregular by 05:00 on July 25, 2001, and filled with clouds by 16:00, July 25, 2001.

During the period when Typhoon Yutu slowed down, Typhoon Yutu was weakened. The closest point between Hong Kong and Typhoon Yutu occurred around 06:00 on July 25, 2001 before Typhoon Yutu turned more northwestward. While Typhoon maintained a course of roughly between 280-295 degrees, Typhoon Yutu actually inched away from Hong Kong.

The examination of the life history of Typhoon Yutu will be presented elsewhere. However, one can obtain useful guidance by applying the results of changes of intensity of typhoons after penetrating into the South China Sea (Wai, 2001). Using the typhoon data (1954 -1999) that affected Hong Kong, Wai catalogued five types of intensity changes after typhoons entered the South China Sea. In Type 2, when a typhoon enters the South China Sea with the intensity less than 60 kts and moves along the southeast-northwestern direction, the typhoon will intensify within 24 hours and then weaken. In Type 2, only one typhoon takes another 24 hours to reach its peak intensity.

Let us briefly examine the intensity change of Typhoon Yutu. Tropical storm (TS) Yutu entered South China Sea through the Bashi-Ballintang Channel (at 02:00 on July 24, 2001) with the intensity of about 35 kts. Moving along a weak southeast-northwestern direction, TS Yutu intensified and became a typhoon within 24 hours and reached an intensity of 85 kts (at 20:00 on July 24, 2001). During the next 12 hours (until 08:00 on July 25, 2001), the intensity of Typhoon Yutu did not change. The Observatory issued the gale signal at 00:30 on July 25, 2001. Beginning at 08:00 on July 25, 2001, the intensity of Typhoon Yutu began to weaken while Typhoon Yutu changed its course from southwestward (260 degrees at 0800 hours on July 25, 2001) to slightly more northwestward (285 degrees at 14:00; 290 degrees at 20:00; and 280 degrees at 02:00, July 26, 2001). The actual typhoon track was further west of the forecast track and moved away from Hong Kong slowly.

The changes in the intensity of Typhoon Yutu agree quite well with those in Type 2. Although one typhoon in Type 2 takes 48 hours to reach its maximum intensity, one can conclude that Typhoon Yutu will not intensify because Typhoon Yutu has reached its maximum intensity within 24 hours after entering the South China Sea.

To improve the service, the Observatory pleaded that the staff would work on two fronts: new technique in forecasting and better communication with the public and other government departments. In the area of communication, the Observatory proposed:

(1) The public is informed in advance of likely changes in warning status, as far as possible,

(2) More information is supplied to the public through more frequent media briefings and a diversity of other means including the Internet.

(3) Closer liaison with public transport operators and other government departments are made to enable them to act promptly in changing situations.

It is doubtful that such proposed procedures in communication will remove any irregular gale signals for several reasons. First, the solutions to the numerical weather predication models are not

deterministic. Therefore, the numerical solutions always carry a certain amount of uncertainly. Recall that in the typhoon tracks, only the skills of GFDL model overtook statistically the skills of statistical methods; in typhoon intensity, no numerical models have yet produced the forecast better than statistical methods except at a longer time period (72 hrs). Second, when the new communication procedures are used, even together with the correct forecast of the position and intensity of typhoon Yutu, the circumstances put Hong Kong under the gale signal for 19 hours did not change during Typhoon Yutu because of the use of signal unless the Observatory followed the rule of using the gale inside the Victoria Harbour.

Two months later on September 21, 2001, Cheng wrote to Tsang expressing the concern of the Hong Kong General Chamber of Commerce on the reliability and the effectiveness of the typhoon warning system. Furthermore, the Chamber believes that the community needs to find a more reliable and effective signal system. In closing his letter, Cheng said it well:

While we believe in 'safety first' and accept economic losses due to serious weather condition, we should not accept economic losses due to too-conservative or out-dated grading of typhoons or inaccurate interpretation of scientific data.

Despite the Observatory is equipped with advanced remote observational systems and receptors, a super-computer system, in house numerical weather prediction models, a dense local surface observational network, and a regional – international data exchange network, the benefits from the modernization have not generated similar dividends from the tropical cyclone warning system because of the use of signals, which is inherent in the current tropical cyclone warning system.

In a recent study of the Hong Kong typhoons, Wai (2001) concluded that the use of signals in the current tropical cyclone warning system is not suitable for Hong Kong. Wai discussed an alternative warning system that would not use warning signals.

Associated with the warning system is the closure of Hong Kong when a gale signal has been displayed. The subjects of irregular gale signals and their adversary impact on the public kept recurring on the agenda at the Legislative Council in the past forty years. For instances, several known incidents are summarized in Table 8-1.

Table 8-1. Subjects of Debate related to gale signals on the agenda at the Hong Kong Legislative Council Meeting

March 10, 1966	Traffic disruption
July 23, 1986	Traffic chaos
July 30,1986	MTR and passengers
October 21, 1993	Traffic congestion
August 30, 1999	HYF service
October 13, 1999	Traffic chaos
July 17, 2001	Airport chaos
July 7, 1971	Closure of school/examination
June 29, 1983	Closure of schools
July 23, 1986	Closure of schools
July 15, 1992	School examination
July 23, 1986	Hoist of gale signals
December 6, 2000	Hoist of gale signals

From these records, it appeared that the governmental departments adopted a standard procedure to avoid the recurrence of these incidents and to improve the departmental services. For instance, the first step is to improve the communication between the governmental department and the Observatory, or the public. The second step is to state how to improve individual departmental services to the public by means of new guidelines, new equipment, and technology.

The defect in the technique of problem solving with this approach had been pointed out by Wong, who addressed the problem of flooding at a Legislative Council meeting on October 21, 1993:

At present, flood emergency mechanism is improvised during real emergencies. There is no well-laid planning. When it is time to act, each department will follow its own policy and its own things.

During the passage of a typhoon, the practice of "when it is time to act, each department will follow its own policy and its own things" would bring many ill effects, such as in the case of Typhoon Utor, or in the case of Typhoon Yutu.

In early years, shipping was the cause and reason of existence of Hong Kong. Therefore, the Observatory was given a prime responsibility to issue the warning to the shipping community. The hoist of red signals often led to the pre-mature closure of the harbour, subsequently affecting largely the shipping work in the harbour. As Hong Kong enters the twenty-first century, shipping is no longer the only cause and reason of existence of Hong Kong, but the tourisms, aviation, shipping, finance, and real estates are. The hoist of gale signals does not just close the Victoria Harbour but also the entire Hong Kong, essentially affecting every Hong Kong citizens, interfering the visitors, and interrupting distant partners in dealing with public affairs and global business that will bring ill effects to Hong Kong. Therefore, to manage the closure of Hong Kong and re-open of Hong Kong in the post typhoon period require the collective efforts of all essential governmental departments and co-coordinating the operations of these essential governmental departments. To manage the passage of a typhoon, Wai (2001) outlined such a model along with an alternative tropical cyclone warning system.

Acknowledgements

I am grateful to Irene Shieh, the Law Librarian of Lui Che Woo Law Library, Hong Kong University, for directing me to various sources of Hong Kong Government documents including those available at the Hong Kong University (HKUL Digital Initiatives).

I thank Mabel Cheung, the Government Counsel, Law Drafting Division, Hong Kong Department of Justice, for replying to the enquiry about the current legal status of the Public Reclamation Validation and Clauses Ordinance, 1936.

The Index to the CO 129 documents, compiled by Dr. Elizabeth Sinn, of the Center of Asian Studies, Hong Kong University, has made the research easier. Dr. Louis Ha, of the Hong Kong Catholic Society, also provided the author additional insight into the database of the CO 129 documents.

My appreciation will also go to Hoi -To Poon, of the Hong Kong Observatory, Man-Keung Wai, of the Chinese University of Hong Kong, and the staff at the Resources Center, Hong Kong Observatory, for helping to fulfill the requests for needed publications for this study.

Finally, Y.- K. Chan has provided invaluable suggestion and editorial assistance making the

manuscript into the final form suitable for publication. Thank you, Y. K.

Appendix I. Biographical Notes

Bell, G. J., Director (1965 –1981), Royal Observatory, Hong Kong.

Cheng, C., Chairman (2001), The Hong Kong General Chamber of Commerce, Hong Kong.

Ramage, C. S., Acting Director (1955), Royal Observatory, Hong Kong.

Tien, J. P.-C., Legislative Council Member (1989-1990, 1994-present), Panel Chairman (2001), Economics Services, Hong Kong.

Tsang, D. Y.-K., Financial Secretary (1996-1999), Chief Secretary for Administration (2001- present), Hong Kong.

Wong, Z. W.-Y., Unofficial Legislative Council Member (1992-1997), Hong Kong.

References

AGU (2003) *Hurricane! Coping With Disaster*. R. Simpson, Editor, American Geophysical Union. Washington, DC. 359 p.

Anonymous (1992) *Typhoon*. Second Edition. Hong Kong Government Printer. 64 p.

Anonymous (1956) Storm and Monsoon Warning Service. Occasional papers No. 7. Royal Observatory. 9 p.

Anonymous (1955) *Hong Kong Forecasters' Manual*. C. S. Ramage, Editor, Royal Observatory Technical Note No. 10, Royal Observatory, Hong Kong.

Anthes, R. A. (2003) Hot towers and hurricanes: early observations, theories, and models. In *Cloud System, Hurricanes, And The Tropical Rainfall Measuring Mission (TRMM)- A Tribute To Dr. Joanne Simpson*. W.- K. Tao and R. Adler, Editors. Meteorological Monograph No. 23, Amer. Meteor. Soc. 234p.

Baik, J. J., and J. S. Paek (1998) A climatology of sea surface temperature and the maximum intensity of western North Pacific tropical cyclones. *J. Meteor. Soc. Japan*, **76**, 129 -137.

Carrier, G. F., A. L. Hammond, and O. D. George (1971) A model of mature hurricane. Part I. *J. Fluid Mech*., **47**, 145-170.

Challa, M., and R. L. Pfeffer (1980) Effects of eddy fluxes of angular momentum on model hurricane development. *J. Atmos. Sci*., **37**, 1603-1618.

Chin, P. C. (1977) *The Life History Of A Tropical Cyclone*. General Publication No. 4, Royal Observatory, Hong Kong. 43p.

Chin, P. C. (1972) Tropical cyclone climatology for the China Sea and Western Pacific from 1883 to 1970, Vol. 1: Basic data. Royal Observatory Tech. Memoirs No. 11. Royal Observatory, Hong Kong. 207 p.

Chin, P.C. (1958) Tropical cyclones in the Western Pacific and Chin Sea area 1884-1953. Royal Observatory Tech. Memoirs No. 7. Royal Observatory, Hong Kong. 89 p.

Emamuel, K. A. (2003) A century of scientific progress. In *Hurricane! Coping With Disaster*. R.

Simpson, Editor, American Geophysical Union, Washington, DC. 177-204.

Emanuel, K. A. (1986) An air-sea interaction theory for tropical cyclones. Part I. *J. Atmos. Sci.*, **43**, 585-604.

Evans, J. (1993) Sensitivity of tropical cyclone intensity to sea surface temperature. *J. Climate*, **6**, 1133-1140.

Faber, S. E., and G. J. Bell (1963-1964) Typhoons in Hong Kong and building design. Proceedings of the Engineering Society of Hong Kong, **17**.

Heywood, G. S. P. (1950) Hong Kong Typhoons. Royal Observatory Techn. Memoirs No. 3, Royal Observatory, Hong Kong.

Holland, G. J. (1987) Mature structure and structure change. In *A Global View Of Tropical Cyclones*, R. L. Elsberry, Editor, Office of Naval Research, Arlington, VA, 13-52.

Malkus, J. S., and H. Riehl (1960) On the dynamics and energy transformation in steady-state hurricanes. *Tellus*, **12**, 1-20.

Merrill, R. T. (1988) Environmental influences on hurricane intensification. *J. Atmos. Sci*., **45**, 1678-1687.

Ooyama, K. (1969) Numerical simulation of the life-cycle of tropical cyclones. *J. Atmos*. *Sci*., **26**,3-40

Riehl, H., and J. S. Malkus (1961) Some aspects of Hurricane Daisy, 1958. *Tellus*, **13**, 181-213.

Starbuck, L. (1951) A statistical survey of typhoons & tropical depressions in the Western Pacific & China Sea from observations & tracks recorded at the Royal Observatory Hong Kong from 1884-1947. Royal Observatory Techn. Memoirs No. 4. Royal Observatory, Hong Kong.

Thompson, B. W. (1951) The upper-level flow structure near typhoons. *Quart. J. Roy. Meteoro*. Soc., **77**, 272-282.

Tse, S. Y. W. (1966) A new method for the prediction of typhoon movement using the 700 mb chart. *Quart. J. Roy. Meteor. Soc*., **92**, 239-253.

Wai, M. M. - K. (2006) The tropical cyclone warning systems during the inter –war years of Hong Kong, 1920-1939. *Bull. Met. Hong Kong Soc.,* **16**, 28-48.

Wai, M. M. - K. (2005) The tropical cyclone warning systems in the early twentieth century of Hong Kong, 1900-1919. *Bull. Met. Hong Kong Soc.,* **15**, 3-31.

Wai, M. M. - K. (2004) The early tropical cyclone warning systems in Hong Kong, 1841-1899. *Bull. Met. Hong Kong Soc.*,**14,** 54-87.

Wai, M. M. - K. (2001) Is there any hope for the use of signals in the tropical cyclone warning system in Hong Kong? *Bull. Met. Hong Kong Soc*., **11**, 24 - 44.

Wai, M. M. - K. (2000) Changes in the characteristics of typhoons affecting Hong Kong, Part I: Typhoon Intensity in the South China Sea. *Bull. Met. Hong Kong Soc.*, **10**, 17-45.

WMO (1995) *Global Perspective On Tropical Cyclones*. Tropical Cyclone Programme. WMO/TD-No. 693. R. L. Elsberry, Editor, World Meteorological Organization. Switzerland.

Yamasaki, M. (1977) A preliminary experiment of the tropical cyclone without the effects of cumulus Convection. *J. Meteor. Soc. Japan*, **55**, 11-31.

HONG KONG METEOROLOGICAL SOCIETY

INFORMATION FOR CONTRIBUTORS TO THE BULLETIN

Technical or research articles, as well as reviews and correspondence of a topical nature are welcome. In general contributions should be short, although exceptions may be made by prior arrangement and at the sole discretion of the Editorial Board. Copyright of material submitted for publication remains that of the author(s). However, any previous, current, or anticipated future use of such material by the author must be stated at the time of submission. All existing copyright materials to be published must be cleared by the contributor(s) prior to submission.

Manuscripts must be accurate and preferably in the form of a diskette containing an electronic version in one of the common word processing formats. WORD is preferred but others are also acceptable. Whether or not an electronic version is submitted, two complete manuscript copies of the articles should be submitted. These should be preceded by a cover page stating the title of the article, the full name(s) of the author(s), identification data for each author (position and institution or other affiliation and complete mailing address). An abstract of about 150 words should be included. Manuscripts should be double-spaced, including references, single-side only on A4 size paper with a 2.5 cm margin on all sides, and be numbered serially. All references should be arranged in alphabetical and, for the same author, chronological order. In the text they should be placed in brackets as (Author'(s) name(s), date). In the reference list at the end the Author'(s) name(s) and initials followed by the date and title of the work. If the work is a book this should be followed by the publisherís name, place of publication and number of pages; or, if a journal article, by the title of the periodical, volume and page numbers.

Submission of electronic versions of illustrations is encouraged. Originals of any hardcopy illustrations submitted should be in black on tracing material or smooth white paper, with a line weight suitable for any intended reduction from the original submitted size. Monochrome photographs should be clear with good contrasts. Colour photographs are also accepted by prior arrangement with the Editorial Board. Originals of all illustrations should be numbered consecutively and should be clearly identified with the authorí(s) name(s) on the back. A complete list of captions printed on a separate sheet of paper.

All submitted material is accepted for publication subject to peer review. The principal author will be sent comments from reviewers for response, if necessary, prior to final acceptance of the paper for publication. After acceptance the principal author will, in due course, be sent proofs for checking prior to publication. Only corrections and minor amendments will be accepted at this stage. The Society is unable to provide authors with free offprints of items published in the Bulletin, but may be able to obtain quotations from the printer on behalf of authors who express, at the time of submission of proofs, a desire to purchase a specified number of offprints.

Enquiries and all correspondence should be addressed to the Editor-in-Chief, Hong Kong Meteorological Society Bulletin, c/o Hong Kong Observatory, 134A, Nathan Road, Kowloon, Hong Kong.

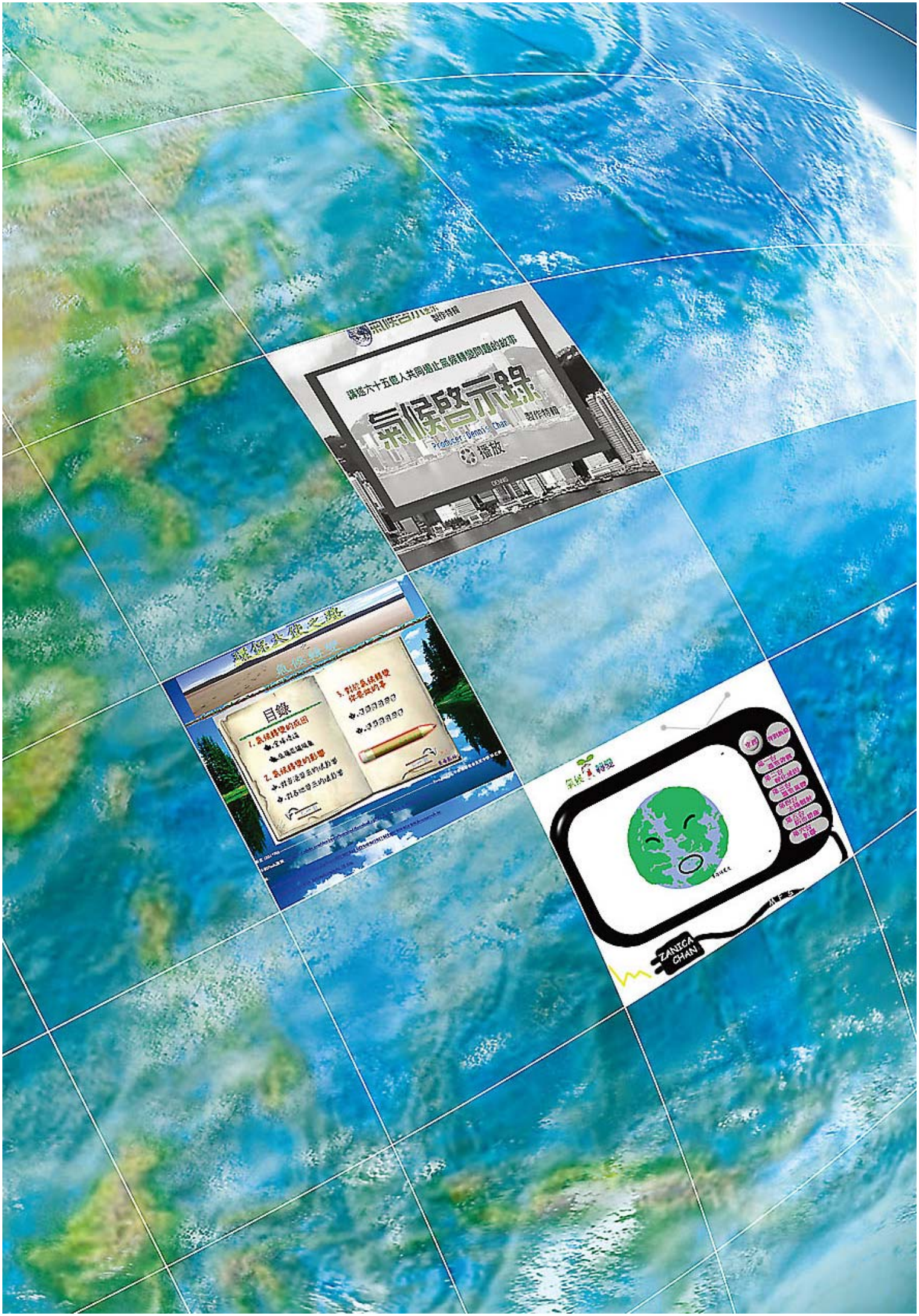
講述六十五億人共同遏止氣候轉變問題的故事
氣候啟示錄
Producer: Dennis Chan
製作特輯
播放
目錄
1. 系統轉變的成因
2. 系統轉變的影響
3. 對於系統轉變
作出的行動
氣候轉變
ZANICA CHAN